

**DEVELOPMENT OF FIBRE OPTIC SENSORS FOR DYE
CONCENTRATION MEASUREMENT**

CHONG SU SIN

**FACULTY OF ENGINEERING
UNIVERSITI MALAYA
KUALA LUMPUR
2016**

**DEVELOPMENT OF FIBRE OPTIC SENSORS FOR
DYE CONCENTRATION MEASUREMENT**

CHONG SU SIN

**THESIS SUBMITTED IN FULFILMENT OF THE
REQUIREMENTS FOR THE DEGREE OF DOCTOR OF
PHILOSOPHY**

**FACULTY OF ENGINEERING
UNIVERSITY OF MALAYA
KUALA LUMPUR**

2016

UNIVERSITY OF MALAYA
ORIGINAL LITERARY WORK DECLARATION

Name of Candidate: CHONG SU SIN

Registration/Matric No: KHA 120029

Name of Degree: DOCTOR OF PHILOSOPHY

Title of Project Paper/Research Report/Dissertation/Thesis (“this Work”):

DEVELOPMENT OF FIBER OPTIC SENSORS FOR DYE CONCENTRATION
MEASUREMENT

Field of Study: ADVANCED MATERIAL AND TECHNOLOGY

I do solemnly and sincerely declare that:

- (1) I am the sole author/writer of this Work;
- (2) This Work is original;
- (3) Any use of any work in which copyright exists was done by way of fair dealing and for permitted purposes and any excerpt or extract from, or reference to or reproduction of any copyright work has been disclosed expressly and sufficiently and the title of the Work and its authorship have been acknowledged in this Work;
- (4) I do not have any actual knowledge nor do I ought reasonably to know that the making of this work constitutes an infringement of any copyright work;
- (5) I hereby assign all and every rights in the copyright to this Work to the University of Malaya (“UM”), who henceforth shall be owner of the copyright in this Work and that any reproduction or use in any form or by any means whatsoever is prohibited without the written consent of UM having been first had and obtained;
- (6) I am fully aware that if in the course of making this Work I have infringed any copyright whether intentionally or otherwise, I may be subject to legal action or any other action as may be determined by UM.

Candidate’s Signature

Date:

Subscribed and solemnly declared before,

Witness’s Signature

Date:

Name:

Designation:

ABSTRACT

The quality of industrial effluent needs to be monitored to prevent environmental pollution. Continuous development in non-invasive sensing technologies is expected to improve the efficiency and precision of various types of sensors for detecting chemical species in various industrial processes. Among the existing sensors, fibre optic sensors are widely accepted because of their minute size and non-destructive characteristics, which offer considerable advantages under diverse conditions compared to traditional sensors. In this work, three fibre optic sensors: tapered plastic optical fibre sensors (TPOF), core-mismatch interferometer fibre optic sensors (CMFOS) and non-adiabatic tapered fibre optic sensor (NATFOS) were developed in order to measure various concentrations of Remazol Black B (RBB) dye solutions. TPOF is based on the intensity modulation while NATFOS and CMFOS are based on the wavelength modulation approach. Optimizing fiber configuration can improve the sensitivity of a sensor. The performance of the sensors in terms of sensitivity, regression coefficient values, standard deviation, limit of detection and linearity was evaluated. Cross sensitivity due to temperature variation and the presence of other contaminants in the analyte were also investigated as they could affect the measurement accuracy of the developed sensors. Two methods were used to overcome the cross-sensitivity issue: multi-parameter sensing approach, as demonstrated in CMFOS and compensation of the cross-sensitivity effect, as demonstrated in TPOF and NATFOS respectively. Predictive models for the preliminary stage of designing a structure for RBB dye concentration detection were also developed. The results showed that the developed sensors could be potentially used for online monitoring of wastewater quality in the future. Soft computing techniques, including multiple linear regression, central composite design and adaptive neuro-fuzzy inference system (ANFIS) were used as support tools for analyzing data to predict RBB concentrations. In addition, a new approach for analyzing

dye concentration by combining two typical responses – absorption and spectral shift, was also introduced to infer RBB dye concentrations using NATFOS. Eventually, the objectives of the research were achieved. The developed sensors had different sensitivities and detection limits. TPOF could measure dye concentration of as low as 7.80 ppm while CMFOS and NATFOS could measure dye concentration of up to 800ppm. The sensing errors caused by the cross sensitivity effect were minimized and the accuracy of the sensing capability was improved by the established predictive models.

Universiti Malaya

ABSTRAK

Kualiti efluen perindustrian perlu dipantau untuk mengelakkan pencemaran alam sekitar. Pembangunan secara berterusan dalam teknologi sensor dalam bentuk bukan invasif dijangka akan meningkatkan kecekapan dan ketepatan sensor untuk mengesan spesies kimia dalam pelbagai industri process. Di antara sensor-sensor tersebut, sensor gentian optik mempunyai potensi yang cerah disebabkan saiz yang amat kecil dan bersifat tidak binasa, telah menawarkan kelebihan yang amat besar jika berbanding dengan sensor-sensor traditional. Tiga jenis sensor gentian optik: sensor gentian optic plastik (TPOF) yang ditirus, sensor gentian optik teras tidak sepadan (CMFOS) dan sensor gentian optik sensor bukan adiabatik (NATFOS) telah diterokai dalam kajian ini untuk mengukur pelbagai kepekatan Remazol Black B (RBB). TPOF beroperasi berdasarkan modulasi keamatan cahaya manakala CMFOS dan NATFOS beroperasi berdasarkan modulasi penganjakan gelombang. Sensitiviti sensor dapat ditingkatkan dengan mengoptimumkan konfigurasi serat dan prestasi sensor dari segi kepekaan, nilai pekali regresi, sisihan piawai, had pengesanan dan kelinearan telah dinilai. Kesan sensitiviti silang (*cross sensitivity*) disebabkan oleh perubahan suhu dan kehadiran bahan cemar lain dalam analit turut disiasat kerana ia boleh menjejaskan ketepatan pengukuran. Dua kaedah telah digunakan untuk mengatasi isu tersebut, iaitu mengesan pelbagai parameter, seperti yang ditunjukkan dalam CMFOS dan pampasan kesan merentas sensitiviti, seperti yang ditunjukkan masing-masing dalam TPOF dan NATFOS. Model ramalan untuk pengesanan kepekatan pewarna RBB juga telah dibangunkan. Teknik pengkomputeran, termasuk regresi linear berganda (MLR), reka bentuk komposit berpusat (CCD) dan penyesuaian rangkaian-neuro inferens sistem (ANFIS) telah digunakan untuk menganalisis data dan membuat ramalan terhadap kepekatan pewarna RBB. Model-model ramalan ini menunjukkan ketepatan yang tinggi terutamanya model ANFIS. Di samping itu, pendekatan baru diperkenalkan untuk menganalisis kepekatan

pewarna dengan menggabungkan kedua-dua experiment respons - penyerapan dan perganjakan gelombang dan disahkan melalui data eksperimen Akhirnya, objektif kajian telah dicapai. Setiap sensor yang dibangunkan mempunyai sensitiviti dan had pengesanan yang berbeza. Misalnya, TPOF boleh mengukur kepekatan pewarna serendah 7.80 ppm manakala CMFOS dan NAFOS boleh mengukur kepekatan pewarna sehingga 800ppm. Kesilapan pengesanan yang disebabkan oleh kesan sensitiviti silang telah dikurangkan dan ketepatan keupayaan penderiaan telah bertambah baik dengan model ramalan ditubuhkan. Hasil kajian menunjukkan bahawa sensor-sensor yang dibangunkan, berpotensi digunakan untuk memantau kualiti air pada masa akan datang.

Universiti Malaysia

ACKNOWLEDGEMENT

I wish to express my heartfelt indebtedness and deep sense of gratitude to my supervisor Prof. Ir. Dr. Abdul Aziz Abdul Raman and Prof. Dr. Sulaiman Wadi Harun. Words are inadequate to place my gratitude to them for their valuable suggestions and many fruitful discussions to fulfill this work. My appreciation also goes to Prof. Dr. Hamzah Arof for sharing his expertise and offered invaluable assistance which greatly contributed to this work.

Many thanks to the members of the Unit Operation Lab especially Raja Shazrin, Kai Shing, Farhana, Izzudin, Hooi Wen, Archina, Tiam You, Shima, Anam, Nizam and Mustaq, You have made the lab most enjoyable to work despite the many challenges we have to put up with. I would also like to thank to Abang Fauzan, Kak Malathy, Kak Asiah, Kak Arni, Somayeh, Ninik, Rafis and Dr. Lim for providing help in conducting experiments at the Photonic Research Center. Not forgetting to my best friends who always been there.

My deepest thanks got to my mother and family for their understanding and endless love. I would also like to convey thanks to the University of Malaya High Impact Research Grant HIR-MOHE-D000037-16001 which financially support the work

TABLE OF CONTENTS

Abstract	iii
Abstrak	v
Acknowledgement	vii
Table of Contents	viii
List of Figures	xii
List of Tables	xv
List of Symbols	xvi
List of Abbreviations	xvii
List of Appendices	xviii
CHAPTER 1: INTRODUCTION	1
1.1 Research Background	1
1.2 Fibre Optic Sensor	1
1.3 Research Problem	3
1.4 Aim of Research	4
1.5 Novelty of Research	4
1.6 Scope of Research	4
1.7 Research Objectives.....	4
1.8 Research Outline	5
CHAPTER 2: LITERATURE REVIEW	9
2.1 Dye Concentrations Monitoring	9
2.2 Fibre Optic Sensors	10
2.3 Applications of Tapered Fibre Optic Sensors	12
2.3.1 Intensity and wavelength modulation based FOS	13

2.4	Recent Development in Optical Fibre Based Sensors	15
2.5	Sensor Performance Evaluation	16
2.5.1	Soft Computing Technique for Modeling Design	18
2.5.2	Evaluation Prediction Model.....	21
2.6	Summary of Literature Review	22
CHAPTER 3: RESEARCH METHODOLOGY		24
3.1	Introduction	24
3.2	Plastic Optical Sensor	24
3.2.1	Tapered Plastic Optical Fibre Sensor Preparation.....	24
3.2.2	Working Principle of Tapered Plastic Optical Fibre Sensor	25
3.2.3	Experimental Setup for TPOF Sensing System.....	26
3.3	Silica-based Fibre Optic Sensors.....	27
3.4	Core Mismatch Fibre Optic Sensor	28
3.4.1	Preparation for Core Mismatch Optical Fibre Sensor	28
3.4.2	Working Principle of Core Mismatch Optical Fibre Sensor	28
3.4.3	Experimental Setup for CMFOS Sensing System.....	30
3.5	Non-adiabatic Tapered Optical Fibre Sensor	31
3.5.1	Preparation for NATFOS	31
3.5.2	Working Principle of Non-adiabatic Tapered Optical Fibre Sensor	31
3.5.3	Experimental Set Up for NATFOS Sensing System	32
3.6	Precaution Steps	32
3.7	Sensing Medium Preparation	33
3.8	Summary	35
CHAPTER 4: TAPERED PLASTIC OPTICAL FIBRE SENSOR.....		36
4.1	Introduction.....	36

4.2	Experimental Set-up	37
4.3	Performance of the TPOF Sensor	39
4.4	Cross Sensitivity	41
4.4.1	Effects of Temperature.....	42
4.4.2	Effects of pH.....	47
4.5	Predicting Using Soft Computing Techniques.....	48
4.5.1	Multiple Linear Regression Model.....	49
4.5.2	Central Composite Design Model	51
4.5.3	Adaptive Neuro-Fuzzy Interference System Model	55
4.5.4	Evaluation of Model Performances	59
4.6	Summary	61
 CHAPTER 5: TAPERED FIBRE OPTIC SENSOR BASED ON CORE-MISMATCH STRUCTURE.....		63
5.1	Introduction.....	63
5.2	Dye Concentrations Measurement Using CMFOS	63
5.2.1	Experimental Set-up.....	64
5.2.2	Response Surface Methodology	65
5.2.3	Effects of the Variables on Sensing Efficiency	66
5.2.4	Estimate the Prediction Accuracy of the Model.....	71
5.3	Measurement of Dye Concentrations and Temperature	74
5.3.1	Experimental Set-up.....	75
5.3.2	Dye Concentrations Measurement.....	76
5.3.3	Temperature of Dye Solution Measurement	78
5.3.4	Validation of RBB Concentration Measurement Results	81
5.4	Summary	83

CHAPTER 6: NON-ADIABATIC TAPERED FIBRE BASED SENSOR.....	85
6.1 Introduction.....	85
6.2 Dye Concentration Determination with Cross Sensitivity Compensation.....	85
6.2.1 Experimental Set-up.....	90
6.2.2 Preparation.....	90
6.2.3 Remazol Black B Concentration Measurement	92
6.2.4 Effect of pH.....	96
6.2.5 Effect of Suspended Solid On Sensing Efficiency	98
6.2.6 Effect of Temperature on Sensing Efficiency	99
6.2.7 Development of a Temperature Compensation Model.....	101
6.3 Dual Output Approach in Dye Concentrations Determination	105
6.3.1 Preparation.....	106
6.3.2 Absorption Characteristics	107
6.3.3 Wavelength shift Characteristics	108
6.3.4 Coupling the Two Responses and Validation	110
6.4 Summary.....	114
CHAPTER 7: CONCLUSIONS AND RECOMMENDATIONS FOR FUTURE	
 WORK.....	116
7.1 Conclusion	116
7.2 Knowledge Contribution to the Field	119
7.3 Recommendations for Future Work.....	119
REFERENCES	121
LIST OF PUBLICATIONS AND PAPERS PRESENTED.....	131
APPENDIX A	133
APPENDIX B.....	134
APPENDIX C	135

LIST OF FIGURES

Figure 2.1: Extrinsic FOS	11
Figure 2.2: Intrinsic FOS	11
Figure 2.3: ANFIS structure.....	20
Figure 3.1: Three tapered POF based sensors with waist diameter (a) 0.65 mm (b) 0.45 mm and (c) 0.35 mm.	25
Figure 3.2: The tapered POF based sensor system for RBB concentration measurement	27
Figure 3.3: The propagation of modes of the proposed MZI with (a) experimental setup and (b) tapered MMF structure	30
Figure 3.4: (a) Experiment setup for dye concentrations sensing. (b) Non-adiabatic tapers for fundamental order core modes transfers'	33
Figure 3.5: Absorption spectra of the RBB aqueous solution for concentrations range from 50 ppm, 80 ppm to 100 ppm.	34
Figure 3.6: The change in RBB dye concentration from 50 to 300 ppm corresponds to a change in refractive index where refractive index of distill water as a reference point.	35
Figure 4.1: The tapered POF based sensor system for RBB concentration measurement	38
Figure 4.2: The variation of the output intensity ratio with tapered fibre diameters $d = 0.65$ mm, 0.45 mm and 0.35 mm for RBB at various concentrations	40
Figure 4.3: Responses of sensors toward temperature increment at (a) 50 ppm and (b) 100 ppm analyte.	43
Figure 4.4: Responses of sensor toward pH variation at 50 ppm.....	47
Figure 4.5: Cross-correlation of empirical and predicted values of $IRBBIdw$ for multiple linear regression model	51
Figure 4.6: Plots for Response surface and contour of the effects of diameter of POF and concentration of RBB on the output intensity ratio sensing	54
Figure 4.7: Cross-correlation of the empirical and predicted output of central composite design model	55

Figure 4.8: Response surface contour plots to estimate the responses surface of fibres with different diameters for various RBB concentrations	57
Figure 4.9: Scatter plots of the predicted value compared to experimental value using the ANFIS model.....	59
Figure 5.1: Transmission spectrum of the SMF ₁ -MMF-SMF ₂ sensor with MMF diameter, $d=27.7 \mu\text{m}$, $23.2 \mu\text{m}$ and $19.5 \mu\text{m}$	65
Figure 5.2: Response surface plot for intensity ratio interact with independent variables.	69
Figure 5.3: Response surface plot for wavelength shift interact with independent variables.	69
Figure 5.4: Propagation constant at various ambient RI using tapered MMF with $d=27.7 \mu\text{m}$	70
Figure 5.5: Cross-correlation the actual and predicted RBB dye concentration using given responses of the sensor: intensity ratio only, wavelength shift only and combination of the two outputs.....	72
Figure 5.6: Input and output ASE spectra to/from the tapered CMFOS measured at wavelength range from 1545 nm to 1560 nm	76
Figure 5.7: Transmitted spectra of CMFOS device in different concentrations of RBB solution.....	77
Figure 5.8: Delineating curves of the measured wavelength shift as a function of concentration of RBB	78
Figure 5.9: Transmitted spectra of CMFOS device in various temperatures with constant concentration 100 ppm of RBB solution.	79
Figure 5.10: The measured wavelength shift for temperature of analyte sensing with fixed concentration of RBB.....	79
Figure 5.11: Cross correlation of actual and predicted values of RBB dye concentrations ranged 50 ppm to 1000 ppm of which operated under controlled room temperature. ...	82
Figure 5.12: Cross correlation of actual and predicted values of RBB solutions temperature when the RBB concentrations are fixed at 200 ppm and 300 ppm.	83
Figure 6.1: Output spectra responses for untapered fibre (dotted line), non-adiabatic tapered fibre in air medium (solid line) and non-adiabatic tapered fibre immersed into distilled water (dashed line), respectively.....	91

Figure 6.2: The experimental data and its best-fit curve for RBB concentration 0 ppm and 800 ppm based on the value of $I_{\text{core}}=0.28$ and $I_{\text{clad}}=0.26$ where $n_{\text{eff}}=1.3337$ and 1.2866 respectively.	93
Figure 6.3: Measured wavelength shifted to right as a function of difference refractive indices of RBB solution.	95
Figure 6.4: Measured wavelength shifted to right as a function of concentration for two different runs with increasing and decreasing RBB concentrations.	95
Figure 6.5: Plot showing the stability of the sensor during repeats measurement of analyte in 100, 200 and 300 ppm respectively over pH ranged 2.51 to 11.35.	97
Figure 6.6: The performance of the proposed sensor at various ambient temperatures when the RBB dye concentration is fixed at 400 ppm (a) output wavelength and (b) wavelength shift.	100
Figure 6.7: Responses of wavelength shift for the RBB with different concentrations which operate in temperature ranged from room temperature up to 70 °C.	101
Figure 6.8: A temperature correction factor model developed from various sensitivity of sensor towards temperature in different concentrations of solution.	102
Figure 6.9: Cross-correlation of the actual and predicted dye concentration by taking the temperature effects of cross sensitivity into account.	104
Figure 6.10: Cross-correlation of the actual and predicted dye concentration from mixture solution (RBB and KHP) by taking the temperature effects of cross sensitivity into account.	105
Figure 6.11: Delineating curves of the absorbance for analyte sensing with different concentrations of RBB.	108
Figure 6.12: Measured attenuation wavelength shifted to right as a function of concentration of RBB.	110
Figure 6.13: Cross-correlation of actual and predicted values of RBB dye concentrations in three approaches.	111
Figure 6.14: Scatter plots of the actual value compared to predicted value for average of both outputs using NATFOS-2.	113

LIST OF TABLES

Table 2.1: Conventional methods for color detection	9
Table 2.2: Wavelength dependence of attenuation for a silica fibre	16
Table 4.1: Performance of tapered POF with three different diameter, $d = 0.65$ mm, 0.45 mm and 0.35 mm, respectively.	41
Table 4.2: Model validation of the developed TPOF sensors.....	46
Table 4.3: The variation of the output intensity ratio for tapered fibre with diameters of 0.65 mm, 0.45 mm and 0.35 mm for RBB at various concentrations	50
Table 4.4: Statistical results obtained from the MLR analysis	50
Table 4.5: Operating conditions and results for the sensing process.....	52
Table 4.6: Estimated regression coefficients and significance level	53
Table 4.7: Computed error measure criterion for ANFIS functions.....	56
Table 4.8: ANFIS rule structure.....	58
Table 4.8: Performance indices (RMSE, MAPE and R^2) for models.....	60
Table 5.1: ANOVA for the response surface models.	68
Table 5.2: Performance Indices for Predictive Models	73
Table 5.3: Performance of sensor.....	81
Table 6.1: Selected previous studies resolved cross-sensitivity issue.	88
Table 6.2: Overall performance of the developed sensor.	96
Table 6.3: Performance of NAFOS with two different predictive models	110
Table 6.4: Performance indices (R^2 , RMSE and MAPE) for models using two different NATFOS.	113

LIST OF SYMBOLS

n_2	:	Refractive index of passive cladding
n_1	:	Refractive index of fibre core
ϵ	:	Extinction coefficient
C	:	Concentration of analyte
l	:	Sensing region
d	:	Diameter of tapered plastic optical fibre
D_{waist}	:	Diameter of non-adiabatic tapered fibre optic sensor
I_{core}	:	Light intensity in the core mode
I_{clad}	:	Light intensity in the dominant low-order cladding mode
$\Delta\phi_{MF}$:	Phase shift of the microfibre
β	:	Propagation constant of the light
λ	:	Wavelength of the input light
n_{eff}	:	Effective index of the core and the cladding modes
Δ	:	Relative error between the reference values and experimental responses
I_{RBB}/I_{dw}	:	Output intensity ratio between RBB and distill water
$\Delta\lambda$:	Wavelength shift
γ	:	Thermal expansion coefficient of the fibre
δ	:	Thermo-optic coefficient of the modal index difference
ΔT	:	Changes of incident temperature

LIST OF ABBREVIATIONS

ANFIS	:	Adaptive neuro-fuzzy inference system
ASE	:	Erbium amplified spontaneous emission
CCD	:	Central composite design
CMFOS	:	Core mismatch optical fibre sensor
DOE	:	Department of Environmental
FSR	:	Free spectral range
LOD	:	Limit of detection
MAPE	:	Mean absolute percentage error
MLR	:	Multiple linear regression
MMF	:	Multimode fibre
MZI	:	Mach-Zehnder interferometer
NATFOS	:	Non-adiabatic tapered fibre optic sensor
OSA	:	Optical spectrum analyzer
POF	:	Plastic optical fibre
RBB	:	Remazol Black B
RI	:	Refractive index
RMSE	:	Root mean square error
RSM	:	Response surface methodology
SMF	:	Single mode fibre
TFOS	:	Tapered fibre optic sensors
TPOF	:	Tapered plastic optical fibre
VAF	:	Value accounted for

LIST OF APPENDICES

Appendix A: MATLAB script using matrix commands for multiple linear regression analysis.....	132
Appendix B: The experimental data of the interference spectrum with its best-fit theoretical curve.....	134
Appendix C: Published works.....	135

Universiti Malaya

CHAPTER 1: INTRODUCTION

1.1 Research Background

While the industrial revolution was the cause of positive change for the economic growth, there is no question that it has started to affect the environment with its severe downside problems. One of the challenges of industrialization is the effects of wastes by-products on the environment, of which wastewater from industrial activities is a major contributors to water pollution due to the copious amount of chemicals used in the processes. Such wastewaters are abundant with chemical residue containing heavy metal and colouring. According to a Malaysia Department of Environmental (DOE) report, within 2012 (D.O.E, 2012) to 2013 (D.O.E, 2013), approximately 1.6 million tons of wastewater was discharged from various industries. Monitoring of wastewater quality parameters is currently a subject of growing concern in internationally. Indeed, Malaysia regulatory measures and recommendations, such as the Environmental Quality (Industrial Effluent) Regulations 2009, have put pressure on the water and wastewater treatment industries with respect to discharge requirements. In order to mitigate the effects of the compromised environment and comply with stringent government legislation, close performance monitoring of each of the treatment plant needs to be done on a regular basis since wastewater effluent quality can change rapidly in the event of treatment plant performance failure.

1.2 Fibre Optic Sensor

Spectroscopic techniques have been acknowledged as the most compelling spectrum analysis techniques since the 1990s. They have the advantages of being relatively inexpensive, having short test times and not requiring reagents or sample preparation. In addition, their ability to measure directly makes them suitable for on-site

determination. A breakthrough in optical fibre spectroscopy research using tapered fibre reveal that light which is guided through along the tapered section of the fibre, the evanescent field will leak from the core into the surrounding. The leaked wave optically interacts with surfactant molecules near the fibre surface, while propagating through the sensing region along the fibre with repeating reflections (Rahman et al., 2011). The portion of light that leaks travels and interacts with the ambience outside the fibre and is called the evanescent wave (Janunts, Babajanyan, Margaryan, & Nerkararyan, 2004). This finding enables tapered fibre to be used in sensing applications. Essentially, tapered fibre optic sensors (TFOS) work like other electrical sensors except that the TFOS uses a plastic or glass fibre instead of copper wire and light instead of electricity which can be resistant to harsh (chemical) environments as well as impervious to electromagnetic interference. The devices are also inherently safe because of the absence of electric current and low optical power is required at the sensing point (Thyagarajan & Ghatak, 2007). Technology has since taken optical fibre to new heights of innovation of sensor and proffered an outstanding solution for chemical sensing application where it can be become a competitive alternative to the conventional sensors (Ahmad, 1994). The use of TFOS is leading to the construction of reagent-less methods for chemical or pollutant monitoring has rapidly gained attention. Recent reports offer some potential incorporation solutions including trace cobalt in seawater (Paleologos, Prodromidis, Giokas, Pappas, & Karayannis, 2002); in-situ monitoring of aromatic hydrocarbons in contaminated groundwater was also investigated by Bureck et al. (Buerck, Roth, Kraemer, Scholz, & Klaas, 2001). TFOS are well developing on sensing application owing to their ease configuration, cost effective, minute in size, fast response and high sensitivity. These remarkable characteristics that make them particularly suitable use for contaminant water measurement and process analysis. This dissertation is concerned with the development of a simple of tapered FOS for

selected environmental parameters measurement. The performance of the system is investigated based on the experimental results. Also, predictive models are suggested as an efficient technique for improving the capability of the sensing system.

1.3 Research Problem

Dyes contained in wastewater that are not completely removed by treatment and are later discharged into drains are potentially carcinogenic due to their benzidine content and high compositional variability (Alves de Lima et al., 2007). At present, the automation of wastewater systems is not as developed as other process industries, mainly because of the hostile environment in which sensors have to be located. Limited space within the sewer system and its separation from the laboratory are also one of the factors to constrain continuous water quality monitoring unit operation at the wastewater treatment plant. Regrettably, the standardized laboratory based techniques which involve scheduled sampling and chemical analysis are costly and time consuming. Furthermore, the results obtained through laboratory measurements only provide snapshots of moments in time, which are insufficient to provide a meaningful and high resolution picture of the nature of, and variation in wastewater quality. Thus, reliable of the developed alternative sensor in aspect of sensitivity, accuracy, reproducibility and minute in size is required and has to be prioritized to measure concentrations of dye in solution. Tapered fibre optic sensors offer a better alternative since it well-fit the mentioned requirements of which optical signal do not suffer from interference by electromagnetic fields. Tapered FOS is commonly used for monitoring physical quantities and less common but potentially deployed for wastewater quality measurement with the intention of open the possibility to replace expensive and bulky instruments in measuring concentration of dyestuffs.

1.4 Aim of Research

The aim of this research is to develop a simple, minute, sensitive and accurate fibre optic sensor for environmental parameters measurement.

1.5 Novelty of Research

The novelty of this research is to develop a sensor capable of measuring dye concentration under the influence of noises, such as temperature.

1.6 Scope of Research

Since there are numerous dyes that are present in the wastewater, it has always been a challenge to determinate dyes concentration in a single step. Therefore, this study was designed and it was the first attempt to determine dye concentration in solution as a whole instead of by distinguished types of dye. In the current research, three types of tapered fibre optics sensors: tapered plastic optical fibre sensor, core mismatch fibre optic sensor, and non-adiabatic tapered fibre optic sensor were fabricated for Remazol Black B dye concentrations measurement.

1.7 Research Objectives

On the basis of stated problems, four key objectives were set in order to address the aim of research:

1. To develop optimum configuration of tapered fibre optics sensors. There are three types of tapered fibre optics sensors are selected:-
 - a) Tapered plastic optical fibre sensor, will be discussed later in the Chapter 4
 - b) Core mismatch fibre optics sensor, will be discussed later in the Chapter 5
 - c) Non-adiabatic tapered fibre optics sensor, will be discussed later in the Chapter 6

2. To investigate the feasibility of using tapered fibre sensor to measure concentrations of RBB dye in aqueous medium which based on two optical transduction mechanisms:-
 - a) Intensity-based modulation measurement, OR
 - b) Wavelength shift-based modulation measurement
3. To investigate the practicability of tapered fibre to measure monitor dye concentrations by cross-sensitivity consideration. Two approaches are devoted to resolve this issue:-
 - a) Compensation approach, OR
 - b) Multi-parameters sensing approach
4. To develop the predictive models for the preliminary stage of designing a structure for RBB dye concentrations detection. There are:-
 - a) Soft computing technique, OR
 - b) Dual output approach by combining the predicted dye concentrations of absorption and wavelength shift with equal weightings

1.8 Research Outline

The report is divided into seven chapters, each of which is then subdivided into sections and subsections. The chapters are arranged in the following sequences. A diagram is illustrated as in Figure 1.1 that summarized the work described in this thesis.

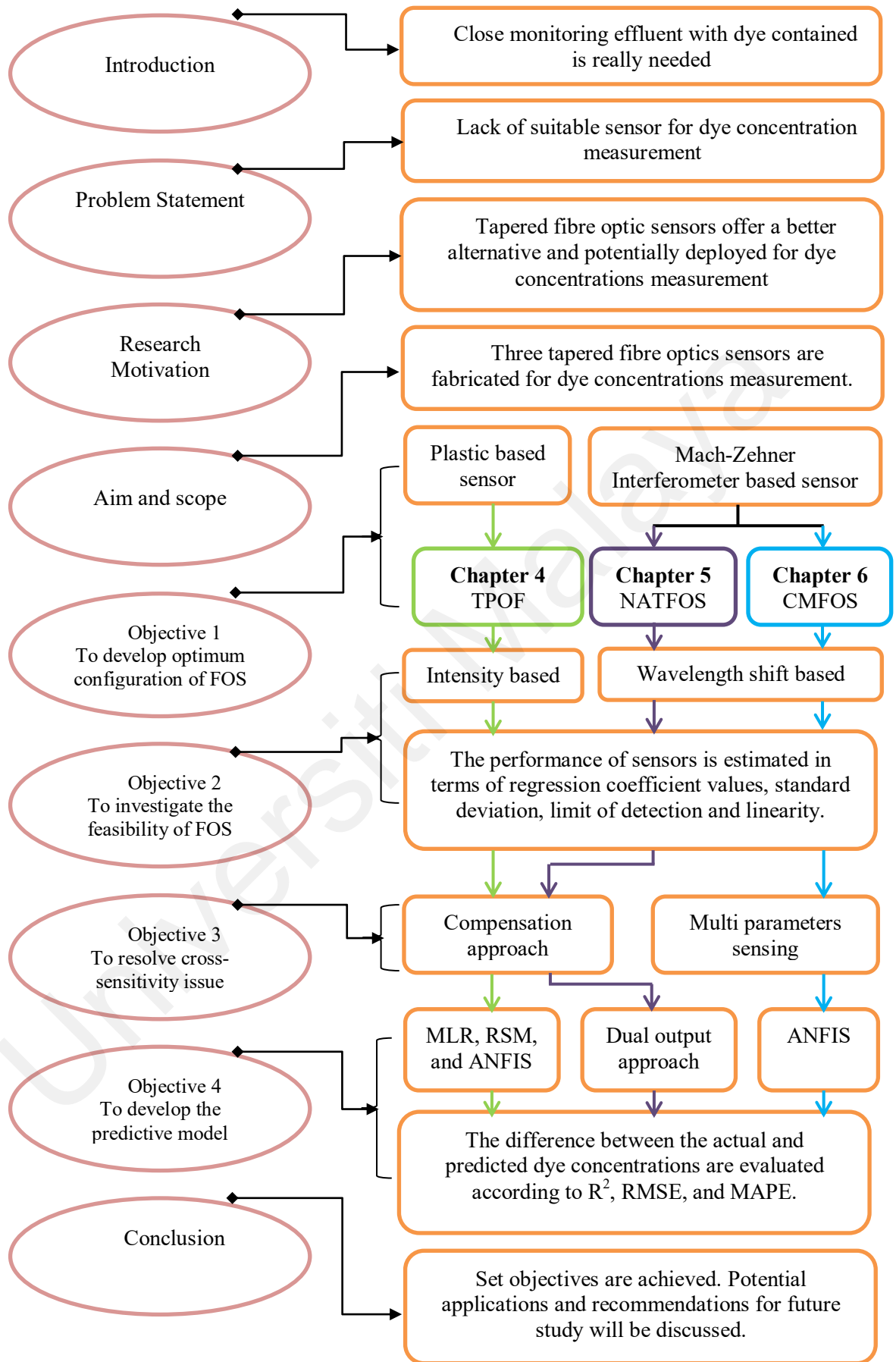


Figure 1.1. Overview of the thesis.

Chapter 1: Introduction

This introductory chapter briefly highlights the growing problem of wastewater and states the need for developing a reliable sensor to measure the quality of wastewater, especially dye-contained solution. Thus, here the objectives of this research work are presented along with the scope of the research.

Chapter 2: Literature review

This chapter is reviews existing methods to determine coloured wastewater characteristics. Furthermore the role of establish an accuracy tapered fibre optic sensor in improving the capability of dye concentrations sensing is also discussed.

Chapter 3: Research Methodology

In this chapter, the sensor preparation, working principle, and experimental setup of sensing system for three miniaturized microfibre: tapered plastic optical fibre sensor, core mismatch fibre optic sensor, and non-adiabatic tapered fibre optic sensor for Remazol black B dye concentrations measurement are demonstrated and discussed.

Chapter 4: Tapered Plastic Optical Fibre Sensor

This chapter is dedicated to present the feasibility of using tapered optical fibre sensor to measure the concentration of Remazol Black B dye in aqueous medium. In addition, soft computing techniques are used as a support tool for analyzing data and making prediction.

Chapter 5: Tapered Fibre Optic Sensor Based on Core-Mismatch Structure

This chapter demonstrates the construction of a tapered fibre optic sensor based on core mismatch structure to apply in Remazol Black B dye concentrations measurement for achieving the research objectives. In addition, it is also demonstrates for multi-parameter measurement of dye concentration and temperature using similar type of sensor.

Chapter 6: Non-adiabatic Tapered Fibre-Based Sensor

In this chapter, non-adiabatic tapered optical fibre sensors are fabricated and use to measure the dye concentration of an analyte. A corrective measure for temperature bias is also carried out. In extended experiment, a new predictive model was formulated by to infer the dye concentrations of analyte.

Chapter 7: Conclusion

This is the last chapter for this research and here the conclusions have been drawn. Moreover, knowledge contribution and recommendations for the future work in particular their implications for the fields have been addressed.

Universiti Malaysia

CHAPTER 2: LITERATURE REVIEW

2.1 Dye Concentrations Monitoring

The wastewater, especially textile waste which contains approximately 20% to 40% of synthetic dyes remain in the effluent (Inaloo et al., 2011). The concentration of dyestuffs found in the environment can cause environmental risks due to its inherent eco-toxicology. In order to mitigate the effects of the compromised environment and comply with stringent government legislation, close performance monitoring of each of the treatment plant needs to be done on a regular basis. Conventionally, various methods have been used to evaluate dye concentration and monitor wastewater quality in a laboratory (Guwy et al., 1999). These methods have been summarized in Table 2.1.

Table 2.1: Conventional methods for color detection

Method	Description	References
Visual comparison	The sample is visually evaluated by comparing to the standard	(American Public Health Association, 1992)
Spectrophotometric	The sample quality is determined by its optical transmission characteristics	(American Public Health Association, 1992)
Tri-stimulus filter	A limited number of wideband spectral energy readings are taken along the visible spectrum	(American Public Health Association, 1992; Ohno & Hardis, 1997)
ADMI tri-stimulus Filter Method (3 and 31 wavelength ADMI)	An extension of tri-stimulus method. It is based on the use of the Adams-Nickerson chromatic value formula	(C. M. Kao, Chou, Fang, Liu, & Huang, 2001)

Results obtained through these methods are insufficient for sampling the highly changeable quality of effluent. Thus, simple, minute in size, and accurate monitoring by the industry has to be prioritized (Pelaez-Cid, Blasco-Sancho, & Matysik, 2008). Continuous wastewater quality monitoring at the plant provides real time recognition of changes in order to alert the plant operators if the quality of effluents matches up with the established criteria.

2.2 Fibre Optic Sensors

Indeed, dye concentrations can be characterized by the analysis of the absorption or transmission spectrum by means of optical spectroscopy (Blanco et al., 2000). Spectrophotometry methods with a broad wavelength range have been chosen due to the fact the colour absorption band is highly correlated with the dye concentration in the substrate. This allows the synchronized and expeditious determination of the dyes studied, as demonstrated in (Abbott, Batchelor, Smith, & Moore, 2010; Şahin, Ülgen, Kekeç, & Gökmen, 2004). However, the use of optical sensor for determining dye concentration is requiring a large number of experiments and analysis that involve scheduled sampling and use of cuvettes. These limitations impede their widespread use in rapid monitoring application. Therefore, a less cumbersome alternative is necessary needed (Saratale, Saratale, Chang, & Govindwar, 2011).

An optical fibre based spectroscopic research is initiated by Kao and Hockham (K. C. Kao & Hockham, 1966) when they revealed that light could be guided through a thin flexible dielectric fibre with a low loss. Fibre optic sensor (FOS) can be categorized into two groups: intrinsic and extrinsic (Udd, 1995). Figure 2.1 and Figure 2.2 show a basic construction of extrinsic and intrinsic FOS, respectively. Extrinsic fibre-optic devices are where the optical fibre is used to couple light. The light beam transmits and passes out of fibre to the exposed environment effect. Then the light coupled back to the

fibre again. Consequently, the light beam to and from the fibre region are influenced by the analyte. So-called intrinsic devices rely on a light beam propagating through the fibre and interaction occurs within the environmental effect and the optical fibre itself (Grattan & Sun, 2000). The latter one was chosen as a device model owing to their unique characteristics, which are susceptibility to linear and non-linear environmental effects to enable distributed sensing. An optical fibre sensing system is basically composed of a light source, optical fibre (a sensing element or transducer) and a detector. So, to achieve optimum performance to a given analyte, a detailed system design which matches the system to the environment is necessary. However, there is a wide variation in package designs and configurations because there are no existing standards for FOS. The choice of proper sensors and the configuration depend on the types of wastewater.

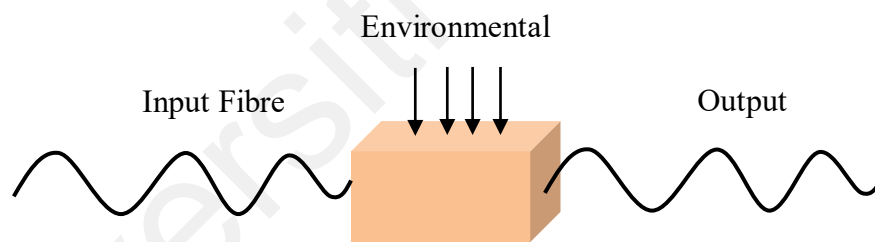


Figure 2.1: Extrinsic FOS

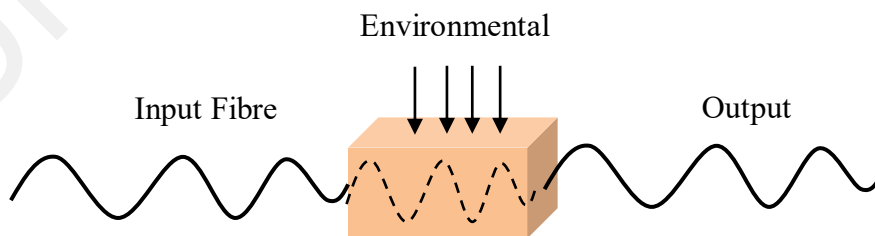


Figure 2.2: Intrinsic FOS

2.3 Applications of Tapered Fibre Optic Sensors

The basic optical fibre structure consists of a core surrounded by some cladding material of a lower refractive index and both are transparent dielectric cylindrical. Light propagating along the optical fibre has a mechanical attenuation under all anticipated operational conditions without performance degradation (Ahmad, 1994). Light propagating along a tapered fibre is not confined to the core region but penetrates into the surrounding cladding region. This taper fibre creates the evanescent field, resulting a light scattering phenomenon on the optical fibre structure. When radiation losses increase, the transmitted light decreases along the fibre (Elosua, Matias, Barriain, & Arregui, 2006). The main point of a tapered fibre is the fact that it can enhance the power fraction in the cladding, and this increases its sensitivity to environmental changes. Therefore, many works have been reported on the possibility of determining the concentration of analytes using a fibre optic sensor (Hang-Zhou, Xue-Guang, Ali, Islam, & Kok-Sing, 2014; Su & Huang, 2007).

Designing evanescent field absorption based sensor requires knowledge of certain parameters because these design parameters play a crucial role in determining the sensitivity and dynamic range of FOS. The degree of penetration of evanescent field into the medium of low refractive index is very important, so-called 'evanescent wave penetration depth', d_p . This is defined as if the incident angle measured from the normal of core-cladding interface, the evanescent wave will transmit along the vertical axis and decline exponentially. The magnitude of the penetration depth derived as in Equation (2.1),

$$d_p = \frac{\lambda}{2\pi \sqrt{n_{core}^2 \sin^2 \theta - n_{clad}^2}} \quad (2.1)$$

where λ is the wavelength of the light propagating along the fibre, n_{core} is the refractive index of the fibre core, n_{clad} is the refractive index of fibre cladding and θ is the angle of incidence at the core-cladding interface. In the tapered region, the evanescent field increases with increasing number of modes, V_{taper} in a fibre which have a larger distribution of optical power in the evanescent area. In this case, the entire tapered region of the fibre acts as the core while the external sensing medium plays the role of a passive cladding. V_{taper} can be expressed as Equation (2.2) where $r_{\text{tot}}(z)$ is the radius of tapered fibre in function of z while n_{core} , n_{clad} , and λ represent refractive index of core fibre, refractive index of cladding (external sensing medium acts as a passive cladding), and wavelength propagating along the fibre respectively. According to Equation (2.2), it is apparent that radius of tapered fibre and characteristic of external sensing medium affect the number of V_{taper} . Therefore, variation in external sensing medium can be monitored by measuring the changes in transmitted power with different tapered fibre diameters.

$$V_{\text{taper}} = \frac{2\pi r_{\text{tot}}(z)}{\lambda} \sqrt{n_{\text{core}}^2 - n_{\text{clad}}^2} \quad (2.2)$$

2.3.1 Intensity and wavelength modulation based FOS

Optical transduction mechanisms of tapered fibre based FOSs are always related to absorption or refractive index changes when the propagating light interact interacts with the target analyte (Yeo, Sun, & Grattan, 2008). Attenuation of light will occur when there is absorption of optical energy during the propagation of light through a sensing medium. Various parameters can be sensed by measuring the change in output intensity arising from the evanescent field of light in the sensing region. The relation between input and output light intensity of the incident radiation which leads to the

analysis of the chemical species follows the Beer-Lambert's law, as described in the Equation (2.3) (Yin, Ruffin, & Yu, 2008).

$$I_{dye} = I_0 e^{-\varepsilon Cl} \quad (2.3)$$

where I_0 denoted the incident light intensity, ε is the extinction coefficient, C is the concentration of analyte and l is the sensing region. Based on this law, the output intensity, I_{dye} of the incident light, I_0 which propagates through a homogeneous solution decreases exponentially as the concentration increases.

An evanescent wave based sensor could also be used for evaluating the refractive index changes based on wavelength shift approach. Any change in the optical or structural characteristic of the chemical provokes a change in the effective refractive index of the optical fibre, thus changing its transmission properties (Khalil, Bansal, & El-Sherif, 2004). There is great interest in these types of sensor since they offer high sensitivity and broad measuring ranges (Jha, Villatoro, & Badenes, 2008). The refractive index of the passive cladding, n_2 (sensing medium) can be considered in two situations: (a) having a lower refractive index than the fibre core, n_1 and (b) having a higher refractive index than the fibre core, n_1 . If the passive cladding, n_2 has a lower refractive index than fibre core ($n_2 < n_1$), the incident ray bends away from normal and greater than the critical angle. Then the total reflection condition is met (Thyagarajan & Ghatak, 2007). Moreover, if the passive cladding has a higher refractive index than the fibre core ($n_2 > n_1$), the incident ray bends towards to normal and less than the critical angle. A portion of the propagated light is refracted into the cladding, and another portion is reflected back into the core (Elosua et al., 2006). The latter condition being the one showing in this studied.

2.4 Recent Development in Optical Fibre Based Sensors

The use of silica optical fibres for photonic sensing has attracted the interest of many researchers and opened up a variety of new applications (Minkovich, Monzón-Hernández, Villatoro, & Badenes, 2006). One of the popular structures used to construct the sensor probe is Mach-Zehnder interferometer (MZI) that is based on core mismatch (Nguyen, Hwang, Moon, Moon, & Chung, 2008; Wu, Semenova, Wang, & Farrell, 2011), non-adiabatic fibre tapers, or photonic crystal fibres (Choi, Kim, & Lee, 2007). MZI sensors have also been widely used for monitoring physical quantities like acoustic vibration (Xu et al., 2012), strain and temperature (Muhammad, Jasim, Ahmad, Arof, & Harun, 2013) and other physical parameters. They can be used to monitor biological processes and chemical compounds such as antimicrobial activity (Mohammad Ismail Zibaii, Latifi, Saeedian, & Chenari, 2014), α -amino acids in aqueous (M I Zibaii et al., 2010) and can even operate in magnetic fluid (Layeghi, Latifi, & Frazao, 2014). With some modifications, MZI sensor can also be deployed for water quality monitoring to replace expensive and bulky instruments. In this study, two MZI sensor based core mismatch structure and non-adiabatic tapered fibre optic sensor are developed to measure environmental parameters. The attenuation of an optical beam power due to absorption may affect the performance of the sensor. Table 2.2 shows the representative wavelength dependence of attenuation for a silica fibre. Notice that the lowest attenuation is attained at 1,550 nm. For wavelengths longer than 1,550 nm, the attenuation increases as a consequence of the absorption of infrared light by the silica molecules themselves (Ghatak & Thyagarajan, 2004; Thyagarajan & Ghatak, 2007). Thus, an Erbium amplified spontaneous emission (ASE) source with operated wavelength range from 1520 nm to 1560 nm was selected as input light signal in this study.

Table 2.2: Wavelength dependence of attenuation for a silica fibre

Wavelength (nm)	Loss due to impurity (dB/km)
850	1.70
1,300	0.35
1,550	0.15
1,625	0.21

The use of plastic optical fibre (POF) for sensing applications has also attracted many interests in recent years. For instance, a number of applications of tapered POF sensor have been reported such as for salinity detection (Lu, Chen, Xie, & Chen, 2012; Rahman et al., 2011), refractive index measurement (De-Jun, Guan-Xiu, Xi-Lu, Ming-Shun, & Qing-Mei, 2014), liquid level monitoring, humidity level assessment (Ribeiro, Canedo, Werneck, & Kawase, 2002) and remote flood monitoring (Kuang, Quek, & Maalej, 2008). Tapered POF have attracted increasing interest for sensing deployment owing to higher mechanical strength if compared with silica optical fibre (Bilro, Alberto, Pinto, & Nogueira, 2012). From study (Peters, 2011a), break down strain of POF is around 30%, whereas the silica-based optical fibres are fragile and will fail under a strain of 5%. The ease of use related to simple end preparation and achieving low cost implementations, makes POF a suitable material to apply on dye concentrations sensing and no special coating is needed in this research. POF is made from materials that have lower absorption at shorter wavelengths, so red light at 650 nm is commonly used with POF.

2.5 Sensor Performance Evaluation

Assessment of sensor performance was a cross-cutting issue in order to develop reliable sensors that accurately measure key environmental parameters. The sensor

performances can be evaluated in terms of sensitivity, linearity and limit of detection of sensor system. The sensitivity is a measure describing the response of the sensor in the parameter being measured. It can be determined by the slope of a linear calibration curve with constant magnification (Loock & Wentzell, 2012). The linearity measures the maximum deviation in the output signal value of a linear transfer function. Linearity is measured using the correlation coefficient, R which is a measure of the reliability of the linear relationship between the input and output parameter values. The linear reliability increases as R approaches 1. R can be determined using Equation (2.4).

$$R = \frac{n(\sum_{i=1}^n y'_i \cdot y_i) - (\sum_{i=1}^n y'_i) \cdot (\sum_{i=1}^n y_i)}{(n(\sum_{i=1}^n y_i'^2 - (\sum_{i=1}^n y'_i)^2)) \cdot (n(\sum_{i=1}^n y_i^2 - (\sum_{i=1}^n y_i)^2))} \quad (2.4)$$

where n, y and y' are the number of data points, input and output parameter values, respectively. Typically, an assay is simply not capable of accurately measuring analyte concentrations down to zero. Sufficient analyte concentration must be present to produce an analytical signal that can be distinguished from the signal produced in the absence of analyte, so-called limit of detection (LOD). LOD is the lowest analyte concentration distinguished from the blank sample and describes the smallest change in a quantity being measured (Armbruster & Pry, 2008). The use of different types of fibre configurations affects these features.

Differences in sensor design may respond differently in similar conditions. In order to achieve reliable measurement, an accurate and precision calibration curve should be established for the sensing system where it will be used. Precision specifies the closeness of agreement between measured quantity values obtained by replicate measurements on the similar objects under specified conditions. A good sensor will always produce the same output for the same input. However, some type of sensors

might exhibit hysteresis which tends to read low with an increasing signal and high with a decreasing signal or vice versa. Therefore, a reversibility test is required in this study in order to show the sensor can produce precise readings with increasing or decreasing the concentrations of analyte. Most of the measurement systems are subject to cross sensitivity to some degree. Measurement system effected by cross sensitivity will have problem making repeatable and accuracy measurements. The application of these techniques into practicability conditions requires a cross sensitivity compensation model due to unwanted loss changes induced by temperature effects, pH and other contaminants. As such, some efforts have put forward to overcome these issues by compensating the cross-sensitivity effect or realizing multi parameters and will be discussed in Chapter 4, 5 and 6 respectively.

2.5.1 Soft Computing Technique for Modeling Design

The use of empirical methods for determining dye concentration does not account for multiple factors involved which are time-consuming and require a large number of experiments and analysis. These limitations impede their widespread use in real applications. Reliable predictive models that could correlate the sensed output with the relevant input parameters in a quick and nondestructive manner are useful at the preliminary stage of designing a structure. In this work, soft computing technique involved multiple linear regression (MLR), central composite design (CCD) and adaptive neuro-fuzzy inference system (ANFIS) are used as a support tool to improve the data analysis and prediction of the dye concentration.

Multiple linear regression (MLR) analysis involves exploring the linear relationship between a dependent variable and two or more independent variables. A general MLR model is usually written as in Equation (2.5).

$$y_i = \alpha_0 + \alpha_1 X_{i1} + \dots + \alpha_n X_{in} + \epsilon_i, \quad i = 1, 2, \dots, k \quad (2.5)$$

where y_i is the dependent variable, X_i are the independent variables, α_0 is a constant, α_1 and α_n are coefficients of the independent variables and ϵ_i is the error term (Tiryaki & Aydın, 2014). Central Composite Design (CCD) is a useful statistical-based experimental design tool which has been widely used to identify and optimize the performance of complex systems (Ghafari, Aziz, Isa, & Zinatizadeh, 2009; Nosrati, Jayakumar, & Hashim, 2011). CCD models allow researchers to visualize interaction among independent factors under different experimental conditions. Compared to the conventional approach which considers an individual parameter separately, CCD is able to evaluate the interaction of a few parameters simultaneously. Besides that, it can also yield good estimations of output variable with the help of the established model.

Another common modeling tool is neural network type called adaptive neuro-fuzzy inference system (ANFIS). ANFIS is a hybrid intelligent system that possesses good learning and prediction capabilities to deal with uncertainties in many different systems (Ghose, Panda, & Swain, 2013; Rezaeianzadeh, Tabari, Arabi Yazdi, Isik, & Kalin, 2014). This tool has been used by researchers for identification and real-time prediction of various engineering systems due to its adaptability to a wide range of uncertainties. It has the capability of mapping input and output variables in mathematical form. With an appropriate training scheme, ANFIS was capable of associating the input values with the target values accurately. To generate fuzzy IF-THEN rules, the first-order Takagi-Sugeno system was used with two inputs: the diameter of POF and concentration of RBB. This inference system model can be defined as in Equation (2.6).

$$\text{if } x \text{ is } A \text{ and } y \text{ is } B, \text{ then } f_1 = p_1x + q_1y + t_1 \quad (2.6)$$

where p_1 and q_1 represent premise parameters. The structure of the ANFIS model is shown in Figure 2.3. It consists of five layers and the designated nodes are described below.

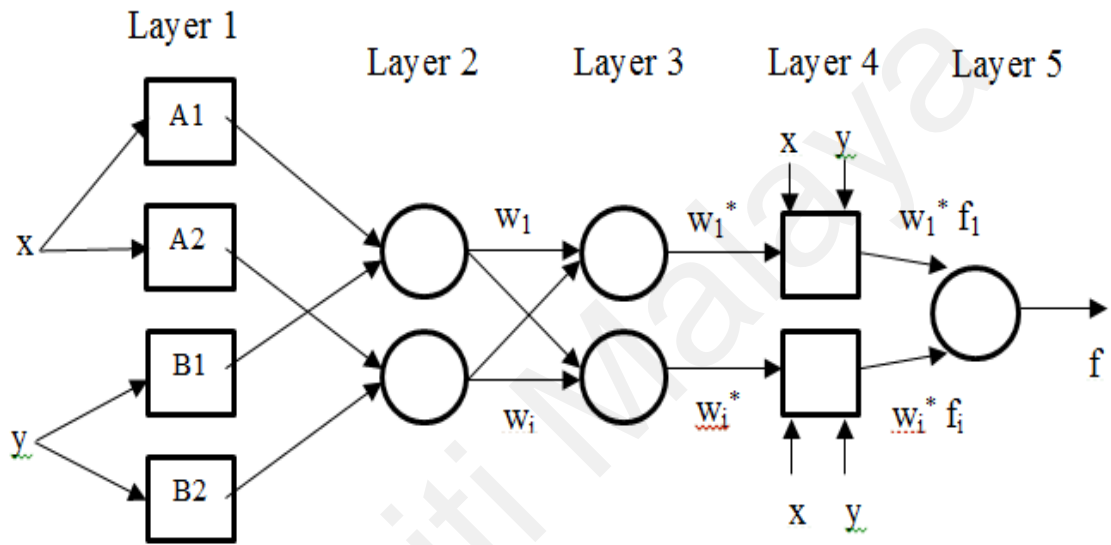


Figure 2.3: ANFIS structure.

Layer 1: This layer supplies the input values to the next layer. Parameters in this layer are called premise parameters. The node function can be defined as in Equation (2.7).

$$O = \mu(x)_i \quad (2.7)$$

where $\mu(x)_i$ are is the membership function (MF). Every node is an adaptive node.

Layer 2: This is a membership layer which checks the weights of each MF. It collects the inputs from the first layer and multiplies the incoming signal before exporting the output, as in Equation (2.8).

$$w_i = \mu(x)_i * \mu(x)_{i+1} \quad (2.8)$$

Each node's output, w_i , symbolizes the firing strength of a rule or weight.

Layer 3: The third layer is a rule layer. Every node in this layer generates the ratio of the rule's firing strength to the sum of activation degrees of all rules like Equation (2.9). The outputs of this layer are expressed as normalized firing strengths or normalized weights.

$$w_{i*} = \frac{w_i}{w_1 + w_2} \quad (2.9)$$

Layer 4: The fourth layer is called the defuzzification layer. Parameters in this layer are referred as consequent parameters. It generates the output values resulting from the Layer 3. The node function can be defined as in Equation (2.10).

$$O_i^4 = w_i^* x f = w_i^* (p_i x + q_i y + r_i) \quad (2.10)$$

where p_i, q_i, r_i is the parameter set.

Layer 5: The fifth layer is called the output layer. The node computes the overall output with sums up all the incoming signals from the fourth layer, as shown in Equation (2.11).

$$O_i^5 = \sum_i w_i^* x f = \frac{\sum_i w_i f}{\sum_i w_i} \quad (2.11)$$

2.5.2 Evaluation Prediction Model

Accuracy of the prediction model is evaluated the difference between the actual and predicted dye concentrations by measuring the correlation coefficient (R^2), root mean square error (RMSE) and mean absolute percentage error (MAPE), as stated in Equation (2.12), (2.13) and (2.14), respectively. The model achieves the best prediction

with the highest R^2 (maximum equal to 1) and the lowest RMSE and MAPE (minimum equal to 0).

$$R^2 = \frac{n(\sum_{i=1}^n y'_i \cdot y_i) - (\sum_{i=1}^n y'_i) \cdot (\sum_{i=1}^n y_i)}{\sqrt{(n(\sum_{i=1}^n y_i'^2 - (\sum_{i=1}^n y'_i)^2) \cdot (n(\sum_{i=1}^n y_i^2 - (\sum_{i=1}^n y_i)^2))}} \quad (2.12)$$

$$RMSE = \sqrt{\frac{1}{N} \sum_{i=1}^N (y_i - y'_i)^2} \quad (2.13)$$

$$MAPE = \frac{1}{N} \sum_{i=1}^N \left| \frac{y_i - y'_i}{y_i} \right| \times 100 \quad (2.14)$$

where y_i and y'_i are the predicted and actual values, respectively.

2.6 Summary of Literature Review

Demands for real-time measurements techniques to meet environmental regulation and treatment compliance are increasing. In this chapter, conventional techniques to determine dye concentrations have been thoroughly reviewed. However the conventional techniques, which involve scheduled sampling and chemical analysis can be expensive and time consuming. Therefore cheaper and simple alternative to monitor wastewater characteristics are required as alternatives to conventional methods. The review confirms that with appropriate configuration, calibration and fibre features the parameters can be determined with accuracy comparable to conventional method. In spite of the progress in the optical fibre sensors, there are still some limitations that need to be addressed. For example, they are not widely used in the detection of dye

concentration and affected by susceptibility to surrounding variations, e.g., pH, turbidity, and temperature. Further study to improve the effectiveness of sensing capability can be initiated especially on improving the sensitivity and accuracy of FOS. For this purpose, author will develop three types of tapered fibre sensor in this research by using silica and polymer optical fibre in conjunction with chemical sensor application. A methodology to prepare the three tapered fibre optic sensors, necessary materials and sample preparation will be discussed in the next chapter.

Universiti Malaya

CHAPTER 3: RESEARCH METHODOLOGY

3.1 Introduction

Tapered fibre optics sensors have a big potential for many applications including liquid concentration measurements. This thesis focuses on the development of three types of tapered optical fibre sensors for dye concentrations measurement since simple, sensitive and accurate measurement of the concentration of chemical compounds in liquid is essential for many industries. These sensors are designed based on both methods; intensity modulation mechanism by employing a tapered plastic fibre optic sensor probe and wavelength shift modulation mechanisms by using silica fibre based probes for dye concentrations measurement. Core-mismatch fibre optic sensor and non-adiabatic tapered fibre optic sensor are used as the silica fibre sensing probe. In this chapter, the working principle and the experimental procedures for the tapered fibre optic sensors are discussed.

3.2 Plastic Optical Sensor

3.2.1 Tapered Plastic Optical Fibre Sensor Preparation

The plastic optical fibre (POF) used in this study was obtained from Edmund Optics (Model 02-534, USA) and it has an overall diameter of 1 mm, with refractive indices of 1.492 and 1.402 for the core and cladding, respectively. It was tapered using acetone, de-ionized water, and sand paper (Gold Cattle, 800 grit size) in accordance with chemical etching techniques (Batumalay, Harith, et al., 2014; Merchant, Scully, & Schmitt, 1999). First, a cotton bud was dipped in the acetone and used to wipe the surface of the POF. The acetone reacted with the outer surface of POF cladding to form a whitish layer. Then, the entire whitish layer was then wiped out using a sand paper. The POF was inspected under a microscope to ensure that the entire turned white

surface of the target area had been polished by sand paper. This process was repeated until the desired diameter was obtained. Finally, total length of the tapered section (approximately 10 mm) was neutralized and cleaned by using deionized water. The tapered region and waist diameter, d of the POF were measured using a micrometer (Model 103-137, Mitutoyo, Japan) with a measuring range of 0.00–25.00 mm. The finished taper appears symmetrical enough under microscope (Model CT-2200, CT BRAND, China) inspection. Of course, a better way is to use the flame-brushing technique, which is more costly and complicated. Three TPOFs with $d = 0.65$ mm, 0.45 mm, and 0.35 mm were prepared. The axial profile of a tapered fibre is shown in Figure 3.1, wherein a ruler with a scale of 0.5 mm was inserted for comparison purpose.

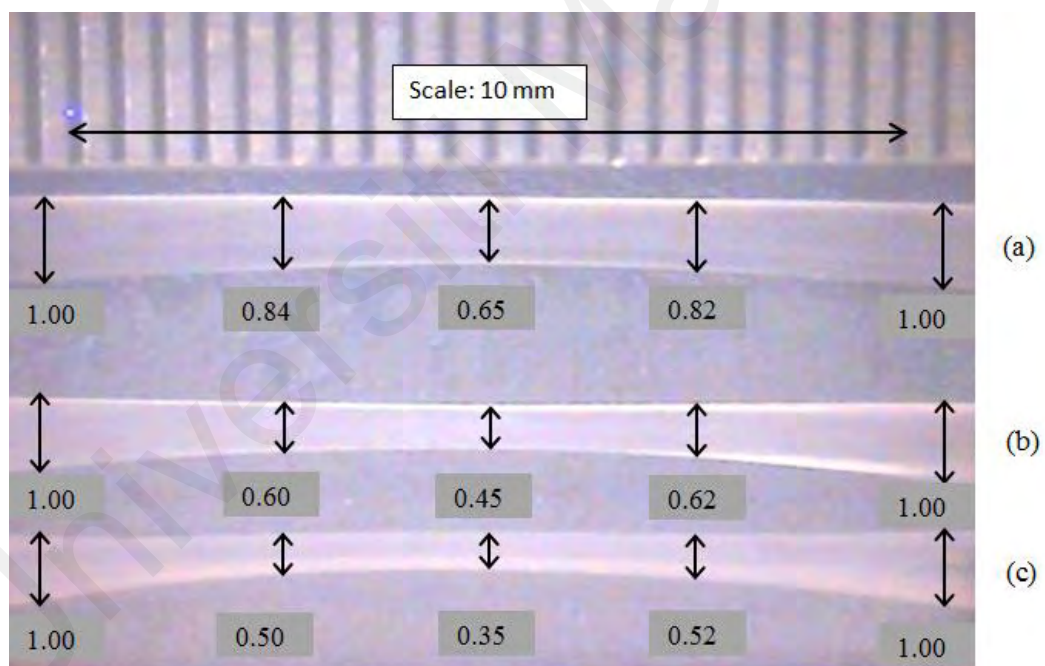


Figure 3.1: Three tapered POF based sensors with waist diameter (a) 0.65 mm (b) 0.45 mm and (c) 0.35 mm.

3.2.2 Working Principle of Tapered Plastic Optical Fibre Sensor

Tapered plastic optical fibre sensors (TPOF) have been used in many physical, biological, and chemical sensing applications. They have high sensitivity, fast response,

immunity to electromagnetic interference, and compact size. The interaction between the evanescent wave of POF and the surrounding can be used in different ways to achieve a distributed sensing effect. When the sample has a distinctive absorption spectrum, changes in the spectrum can be detected by TPOF through the transmitted signal. The sensitivity and level of interaction between the TPOF sensor and the surrounding environment also rely on the physical configuration of the sensors (Potyrailo, Hobbs, & Hieftje, 1998). For sensors that employ tapered fibre probe, the amount of evanescent field produced can be influenced by the diameter of the tapered section. By adopting thinner fibre, a stronger evanescent field is made available which in turn increases the probe's sensitivity (Batumalay, Rahman, et al., 2014).

3.2.3 Experimental Setup for TPOF Sensing System

The experimental setup of the sensing system is depicted in Figure 3.2. A He-Ne laser (HRP050, Thorlabs) operates at a wavelength of 633 nm with an average output power of 5.5 mW is used as light source. An optical chopper is stably rotating to modulate the intensity of the light beam and filter the harmonics from the power line. The He-Ne light source is launched into the TPOF, which is placed in a container filled with RBB solution. The output light is sent into the highly sensitive silicon photodiode detector (818 SL, Newport) to be converted into electrical signal. Then, the electrical signal together with the reference signal from the optical chopper is sent to the lock-in amplifier (SR-510, Stanford Research System) which is used to improve the signal-to-noise ratio. Finally, the output signal from the lock-in amplifier is analyzed. The reference signal from the chopper is matched with the input electrical signal from the photodiode detector. The coupling of these two signals will remove the noise generated by the laser source, photo-detector and the electrical amplifier in the photo-detector. Eventually, the output signal from the lock-in-amplifier is analyzed by a personal

computer. This setup is used to detect various concentrations of the dye solutions and the result will analyze and presented in the next chapters.

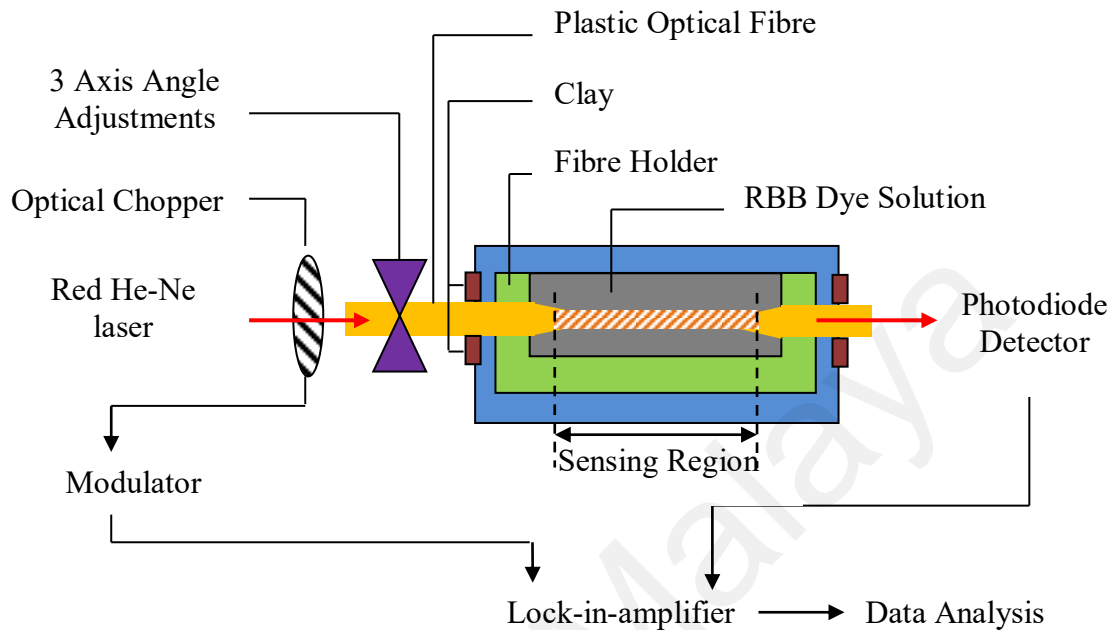


Figure 3.2: The tapered POF based sensor system for RBB concentration measurement

3.3 Silica-based Fibre Optic Sensors

The index of refraction of an optical fibre will change when it is subjected to an environmental perturbation. The versatility of silica-based fibre optic sensors in measuring chemical parameters for continuous monitoring makes them an attractive tool for industrial applications and wastewater treatment quality control. Interferometric techniques can be used to perform the detection (Udd & Jr, 2011) and provided a sophisticated of sensitivity to the measurement parameters that matches those achieved with conventional sensor technology (Nolan, Blaszyk, & Udd, 1991). Thus, there are two tapered optical fibre sensors based on interferometric approach were chosen and developed in this research, i.e. core mismatch fibre optic sensor and non-adiabatic tapered fibre optic sensor.

3.4 Core Mismatch Fibre Optic Sensor

3.4.1 Preparation for Core Mismatch Optical Fibre Sensor

The core mismatch fibre optic sensor (CMFOS) was prepared by using two single-mode fibres (SMF28) and a short section (approximately 20 mm) multimode fibre (MMF FSC 105/125). Firstly, both ends of the multimode fibre (MMF) were spliced with an single mode fibre (SMF) to form an SMF_1 -MMF- SMF_2 configuration. The MMF was then tapered using flame brushing technique to obtain the desired diameter through real time monitoring so that the core section can be exposed to different concentrations of RBB dye solution. The sensitivity of the probe is enhanced by adopting thinner tapered MMF that allows larger portion of evanescent field (Lim et al., 2012) to interact with the sensing medium (Soldano & Pennings, 1995; Wang, Farrell, & Yan, 2008) which can induce variation in the interference signal (Lee et al., 2012).

3.4.2 Working Principle of Core Mismatch Optical Fibre Sensor

Suppose light travels from the SMF_1 to the SMF_2 after passing through the middle MMF, as illustrated in Figure 3.3 (b). As the input light from the SMF_1 reaches the tapered MMF, it will be split into two modes due to the core diameter mismatch between the SMF and the MMF. The first is called the core mode as it continues to travel in the core of the MMF. The second is the cladding mode and it travels in the cladding of the MMF. Both modes will recombine and interfere when they enter the SMF_2 to form an interference pattern which becomes more prominent as the diameter of the MMF decreases with tapering (Luna-Moreno, Monzon-Hernandez, Villatoro, & Badenes, 2007; Villatoro & Monzon-Hernandez, 2006). More specifically, the evanescent field that is a part of the cladding mode penetrates into the analyte medium that surrounds the MMF before recombining with the core mode in the SMF_2 , as

illustrated in Figure 3.3 (b). The transmission spectrum of the fabricated sensors can be expressed as Equation (3.1).

$$I = I_{\text{core}} + I_{\text{clad}} + 2\sqrt{I_{\text{core}} I_{\text{clad}}} \cos(\Delta\varphi_{MF}) \quad (3.1)$$

where I_{core} and I_{clad} are the light intensity in the core mode and the dominant low-order cladding mode respectively, $\Delta\varphi_{MF}$ is the phase shift of the microfibre. When the ambient refractive index (RI) varies, the phase shift of the microfibre can be described as Equation (3.2).

$$\Delta\varphi_{MF} = (\beta_1 - \beta_2) \cdot L \quad (3.2)$$

where β_1 and β_2 are the propagation constant of the light initial and after altering the RI, respectively; L is the length of the tapered region, λ is the wavelength of the input light, and n_{eff} is the effective refractive index change between tapered fibre and analyte. The n_{eff} of the core modes with ambient analyte which function as passive cladding of sensor will induce the output power, I and phase differences, $\Delta\varphi$ change eventually resulting in the variation of propagation constant, β . It can be inferred that linear relationship between the β with the RI changes, as stated in Equation (3.3).

$$\Delta\beta = 2\pi/\lambda \cdot \Delta n_{\text{eff}} = Kn_2 \quad (3.3)$$

where β and n_2 refer to the propagation constant and ambient RI variation, respectively. K is linear coefficients of slope when graph β versus n_2 is plotted.

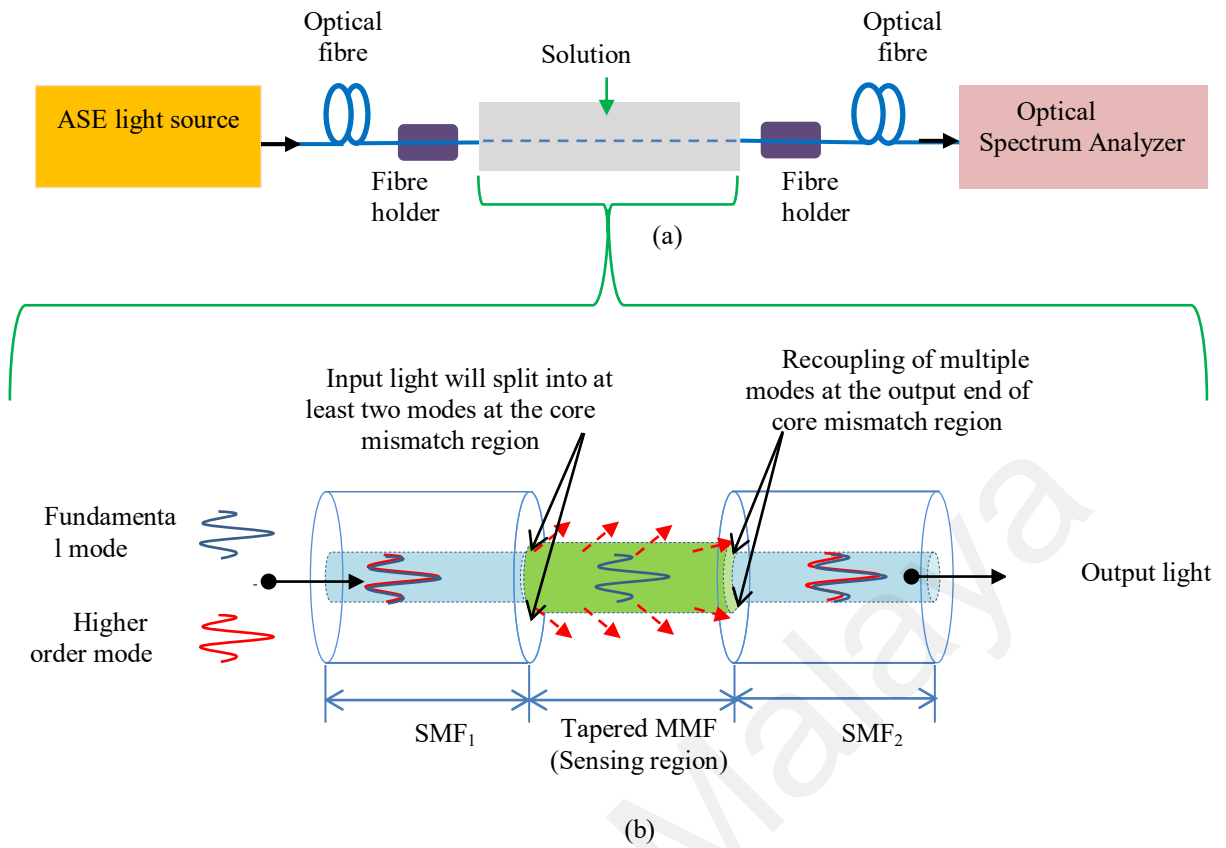


Figure 3.3: The propagation of modes of the proposed MZI with (a) experimental setup and (b) tapered MMF structure

3.4.3 Experimental Setup for CMFOS Sensing System

The experimental set-up for CMFOS sensing system is illustrated in Figure 3.3 (a). The end of the SMF_1 was connected to an Erbium amplified spontaneous emission (ASE) source while the end of the SMF_2 was connected to an optical spectrum analyzer (OSA model Anritsu MS9710B). Tapered MMF with three different diameters of $d = 27.7 \mu\text{m}$, $23.3 \mu\text{m}$ and $19.5 \mu\text{m}$ are immersed in Remazol Black B (RBB) dye solution with different concentrations. When the sensor is immersed into analyte, light transmission can be easily detected by monitoring the peak wavelength shifts. In order to reduce the error caused by mechanical vibrations, the experimental set-up was arranged horizontally on a vibration free table. Before each experimental run, the sensor was dipped into a RBB solution-filled container and the spectra were recorded later.

3.5 Non-adiabatic Tapered Optical Fibre Sensor

3.5.1 Preparation for NATFOS

First, a NATFOS probe was fabricated by stretching a silica single mode fibre (SMF28) using flame brushing technique. In this process, a short section of the SMF (~30 mm) was heated by moving a butane oxygen flame along the section while getting stretched slowly by a pair of stages controlled by a computer. During the tapering process, an input light signal from an Erbium amplified spontaneous emission (ASE) source with operated wavelength range from 1520 nm to 1560 nm was launched into the fibre and its spectral response was continuously monitored via an optical spectrum analyzer (OSA model Anritsu MS9710B). This was done to ensure that the tapered section was not overextended beyond its intended diameter. The resulting microfibre had a final diameter of approximately 13.2 μm over a length of about 30 mm with conical transitions at both ends.

3.5.2 Working Principle of Non-adiabatic Tapered Optical Fibre Sensor

The non-adiabatic tapered fibre optic sensor (NATFOS) is designed to have a non-adiabatic transition region as shown in Figure 3.4 (b), the input light will split into at least two modes at the input conical region. The two light modes are the fundamental mode (LP_{01}^{core} and LP_{01}^{clad}) and higher order mode (e.g. LP_{02}). The fundamental mode keeps propagating in the core while the higher order mode travels through the passive cladding (sensing medium) along the tapered region. The interaction between the higher order mode and the sensing medium occurs at tapered waist region. As the two modes propagate in media with different effective refractive indices, phase shift occurs when they recombine at the output end of the conical region of the microfibre. Back-and-forth coupling occurs between the multiple modes of the microfibre's waist region and results in a comb spectrum (H. Latifi, M. I. Zibaii, S. M. Hosseini, & P. Jorge, 2012) which

performs as a modal interferometer with transmission spectra given by Equation (3.4) (Wen Bin, Huan Huan, Swee Chuan, Kin Kee, & Lim, 2012).

$$I = I_{\text{core}} + I_{\text{clad}} + 2\sqrt{I_{\text{core}} I_{\text{clad}}} \cos(2\pi \cdot n_{\text{eff}} \cdot L/\lambda) \quad (3.4)$$

where I_{core} and I_{clad} are the light intensity in the core mode and the cladding mode, n_{eff} is defined as effective index of the core and the cladding modes, L is the length of the tapered region and λ is the input wavelength.

3.5.3 Experimental Set Up for NATFOS Sensing System

The experimental setup is depicted in Figure 3.4 (a) where ASE light source is injected into the NATFOS and the output is analyzed by OSA and power meter. The experiment starts by immersing the tapered section of the NATFOS into the sample with 0 ppm of RBB (pure distilled water) to obtain the initial sensing value as a reference point to investigate the change in output intensity and spectra shift of the interference peaks when the NATFOS is subjected to different concentrations of RBB later (Hu, Zhao, & Hu, 2014).

3.6 Precaution Steps

In order to reduce possible measurement error caused by mechanical vibrations, the experimental set-up was arranged horizontally on a vibration free table. Furthermore, to avoid strain or mechanical tension cross sensitivity, the fabricated sensor was properly fixed horizontally when placed inside a customized chamber. Before each experimental run, the sensor as well as the chamber were cleansed and subsequently dried to ensure there is no residue left behind. The sensor is fragile, thus caution should be exercised when cleaning it. With the help of a micro pipette, a

consistent amount of solution, approximately 10 mL, was dripped onto the sensor before taking measurement data. This amount was sufficient to fully immerse the sensor.

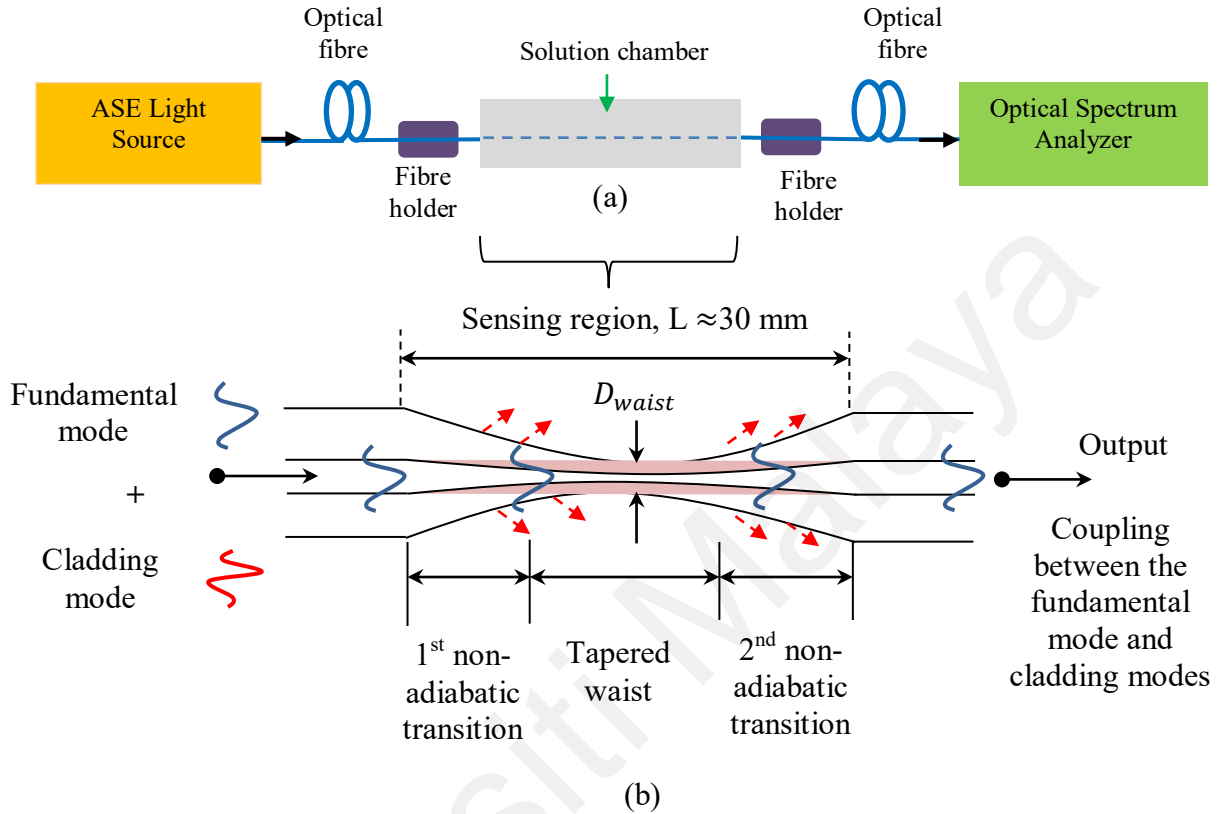


Figure 3.4: (a) Experiment setup for dye concentrations sensing. (b) Non-adiabatic tapers for fundamental order core modes transfers' power to higher-order cladding modes

3.7 Sensing Medium Preparation

Remazol Black B (RBB) was chosen as a model pollutant due to its recalcitrant nature, wide application in textile industry, and is commonly used as a model contaminant in research studies. Stock solution in 1000 ppm was prepared by dissolving 1.0 gram of RBB dye powder which supplied by Sigma-Aldrich in one liter of distilled water and ppm is the concentration unit of the related sensing medium. Then RBB solutions of different concentrations were prepared by diluting the stock solution to the desired concentrations. The RBB dye solution was chosen as a test medium as it has a distinctive absorption spectrum, which depends on the concentration. The absorption

spectrum of the RBB sample was investigated using a UV-Vis spectrophotometer (Model SQ Pharo 300, Merck, Germany). Figure 3.5 shows the measured absorption spectrum of the RBB samples at various concentrations in ppm. As shown in the figure, RBB has a distinctive absorption spectrum ranging from 550 nm to 650 nm and greater light absorption is achieved with increasing concentration of RBB.

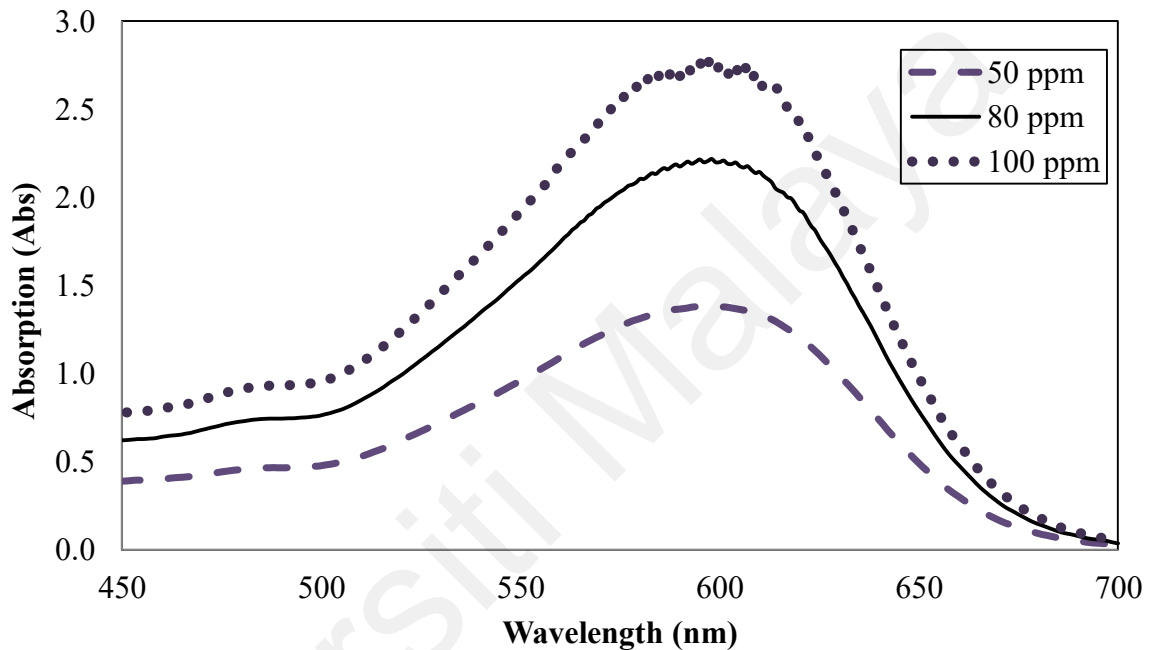


Figure 3.5: Absorption spectra of the RBB aqueous solution for concentrations range from 50 ppm, 80 ppm to 100 ppm.

The output transmission spectrum is monitored as the tapered fibre probe is immersed into the RBB solution of different concentrations. The wavelength shift will be investigated when the concentration of the analyte medium is varied. The amount of wavelength shifted corresponds to a changes of analyte concentration of which strongly dependent on the refractive index (RI) of the sensing medium. Therefore, the corresponding refractive indices of RBB analytes from 0 ppm (pure distill water) to 300 ppm had been measured via refractometer (model Mettler Toledo RE400). The refractive index of distill water was measured in order to obtain the initial sensing value

as a reference point to investigate the change in refractive index at different concentrations of RBB. There exist a linear relationship between the RI and different concentrations of RBB analyte, see Figure 3.6.

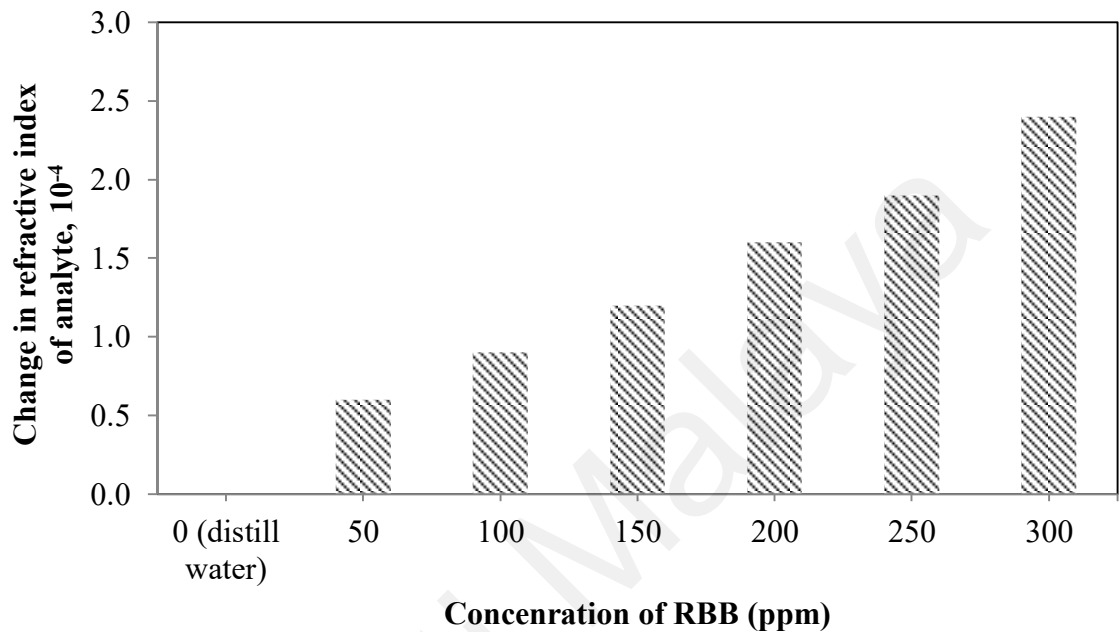


Figure 3.6: The change in RBB dye concentration from 50 to 300 ppm corresponds to a change in refractive index where refractive index of distill water as a reference point.

3.8 Summary

In this chapter, the construction and working principle of both tapered plastic optical fibre and silica fibre based sensors were described. At first, we discussed on tapered POF, which the working principle was based on an intensity modulation approach. Then, two Mach-Zehner interferometer fibre optics sensors, namely core mismatch fibre optic sensor and non-adiabatic tapered fibre optic sensor were developed for dye concentration measurements. Working principle and sensors preparation also been discussed. Experimental design and sample preparation for each sensor along with data analysis for achieving the research objectives will be discuss in Chapters 4, 5 and 6 respectively.

CHAPTER 4: TAPERED PLASTIC OPTICAL FIBRE SENSOR

4.1 Introduction

Plastic optical fibre based technology has gained a tremendous attractive in recent years due to the low cost combined with high data-rates at short to medium distances, compared to traditional alternatives such as copper wire. POFs are also being heralded as fibres of choice for various sensing applications (Bilro et al., 2012; Peters, 2011b). This is attributed to the particular physical properties of polymer materials can convey unique characteristics to POF sensors, which would not be achievable with silica fibres. A number of applications of tapered POF sensors have been reported, such as for salinity detection (Lu et al., 2012; Rahman et al., 2011), refractive index measurement (De-Jun et al., 2014), liquid level monitoring, humidity level assessment (Ribeiro et al., 2002), and remote flood monitoring (Kuang et al., 2008). Designing an effective evanescent field based sensor requires knowledge of certain parameters and how they influence the sensitivity and dynamic range of the sensor. The surrounding environment affects the amount of power loss from the signal that passes through the tapered region. In this chapter, the feasibility of using a tapered plastic optical fibre sensor (TPOF) to detect the concentration of Remazol Black B (RBB) in aqueous medium is investigated and demonstrated with the help of numerical methods to improve the practicability. The operation of the proposed sensor is based on intensity modulation principle where the change in output intensity is investigated at various RBB concentrations. The effect of the tapered section diameter on the sensitivity of the proposed sensor is also investigated. In order to obtain a more accurate model, the effect of the pH and temperature of the medium on the output intensity is also investigated. Then multiple linear regression (MLR), central composite design (CCD) and adaptive neuro-fuzzy inference system (ANFIS) models are developed to identify the

relationship between the output intensity ratio of RBB to distilled water and the different RBB concentrations using TPOF sensor of different diameters. The models relate the intensity ratio as a dependent variable to the sensor's diameter and RBB concentration as independent variables. Moreover, a performance comparison of models developed using MLR, CCD and ANFIS is carried out to evaluate their prediction capability. The accuracy of prediction models is assessed based on the statistical indicators: root mean squares error (RMSE), value accounted for (VAF), mean absolute percentage error (MAPE) and square correlation coefficient (R^2) of the empirical and predicted data of the dependent variable.

4.2 Experimental Set-up

At first the sensor probe is prepared by etching the POF chemically as demonstrated in the section of 3.2 in the previous chapter. In the etching process, acetone is applied to the surface of POF to form milky white foam which is then removed by the sand paper. This procedure is repeated until the tapered fibre sample has a desired waist diameter, $d=0.65$ mm, 0.45 mm and 0.35 mm before it is neutralized and cleansed using de-ionized water so that it can be used as a sensor probe. Remazol Black B (RBB) dye, a sulfonated diazo dye, with chemical formula of $C_{26}H_{21}N_5Na_4O_{19}S_6$ was used as a sensing medium in this study without further purification. The test solutions with concentrations ranging from 10 to 70 ppm were prepared by diluting the stock solution as described in the previous chapter.

Figure 4.1 shows the real image of the experimental setup used in this experiment. It consists of a He-Ne laser light source, an optical chopper, a tapered POF probe and a silicon photo-detector, which is connected to lock-in amplifier. The modulated light source was launched into POF with 10 mm taper which immersed in a customized container that filled with the RBB solution during the experiment running.

An optical chopper is rotating stably in front of the light source, so as to filter the harmonics which generated from the power line and also modulating intensity of the light beam. The photo-detector is highly sensitive which detects the light signal and produces a photocurrent which is amplified by a lock-in amplifier. This is applied to enhance the signal-to-noise ratio. The output signal that is resulted by the operational amplifier is send to a computer via an RS232 port interface and analyzes using Delphi software. All the measured data were normalized against the output for distilled water. The experiment was conducted under ambient temperature and the temperature deviation not more than 2°C which does not affect the output intensity. To further increase the accuracy of the measurement, the light source, the POF on the fibre holder and the detector are positioned in a straight line to minimize bending loss that may occur in the POF.

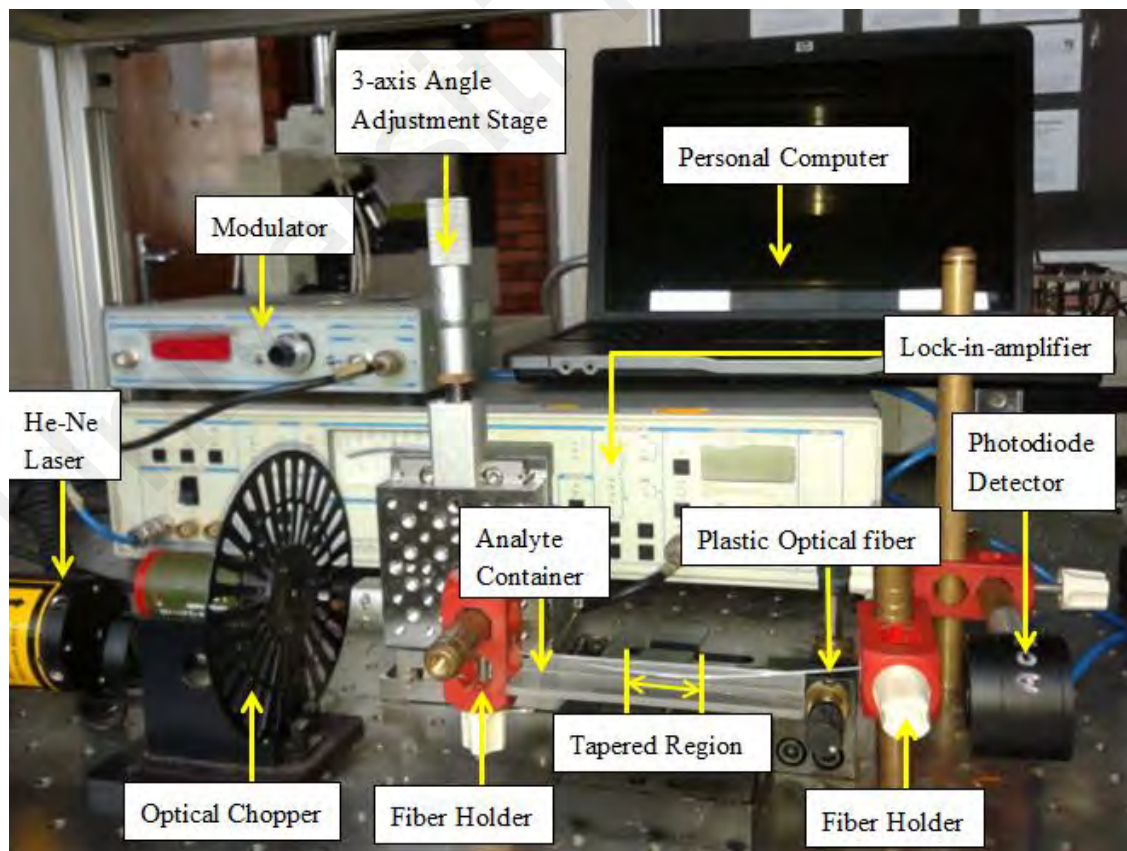


Figure 4.1: The tapered POF based sensor system for RBB concentration measurement

4.3 Performance of the TPOF Sensor

Charge interaction between the surface of the POF sensor and the molecules in the medium plays an important role that dictates the output intensity (rise linearly or decrease linearly) as a function of the analyte concentration (Batumalay, Rahman, et al., 2014). Increasing the analyte concentration increases chromophore content of the solution. As a result, these positively polar charged chromophores will accumulate around the negatively polar charged surface of the fibre (Ogita, Nagai, Mehta, & Fujinami, 2000). When the concentration of the analyte increases, the chromophores form a layer of electrostatic sheath around the surface of the fibre (Armin, Soltanolkotabi, & Feizollah, 2011; P G Lye, M Boerkamp, A Ernest, & D W Lamb, 2005). This might enlarge the pathway for the signal to pass through. Consequently, the output power also begins to rise linearly for this study, with increasingly concentrated sample solutions since the propagating light is more confined in the core of the tapered POF (Ogita et al., 2000), as shown in Figure 4.2. The sensitivity of these sensors can be enhanced by increasing the amount of the evanescent field generated (Lim et al., 2012). For sensors that employ tapered fibre probe, the amount of evanescent field produced can be influenced by the diameter of the tapered section. By adopting thinner fibre, a stronger evanescent field is made available which in turn increases the probe's sensitivity (Batumalay, Rahman, et al., 2014). Figure 4.2 shows the output intensity ratio, I_{RBB}/I_{dw} of various concentrations of RBB solution, measured using TPOF with tapered diameter 0.65 mm, 0.45 mm and 0.35 mm.

The tapered section for these sensor probes was approximately 10 mm. As seen in Figure 4.2, as the diameter of the tapered POF decreases, sensitivity increases. The relative sensitivities of the sensor are obtained at $7.0 \times 10^{-4}/ppm$, $61.0 \times 10^{-4}/ppm$ and $77.0 \times 10^{-4}/ppm$ for tapered fibre diameters of $d = 0.65$ mm, $d = 0.45$ mm, $d = 0.35$ mm respectively. It is found that the one with waist

diameter of 0.65 mm does not demonstrate substantial sensitivity to the concentration of the analyte. The sensitivity increases as the diameter reduces due to the fraction of the evanescent wave energy, which gets larger with the reduction of the cladding diameter (Bilro et al., 2012). The lack of sensitivity demonstrated by the sensors with thicker cladding is most probably due to lesser interaction between the evanescent field and the external medium (Guo & Albin, 2003). In addition, a few relevant statistical criteria are performed to estimate the accuracy of the models. They are regression coefficient values, standard deviation, limit of detection and linearity as outlined in Table 4.1. It is observed that the sensor with $d = 0.45$ mm shows the highest square of R, (R^2 equal to 0.9864) and linearity ($R > 99\%$) values. The results obtained verify that the sensor in this diameter is adequately stable with small value in limit of detection.

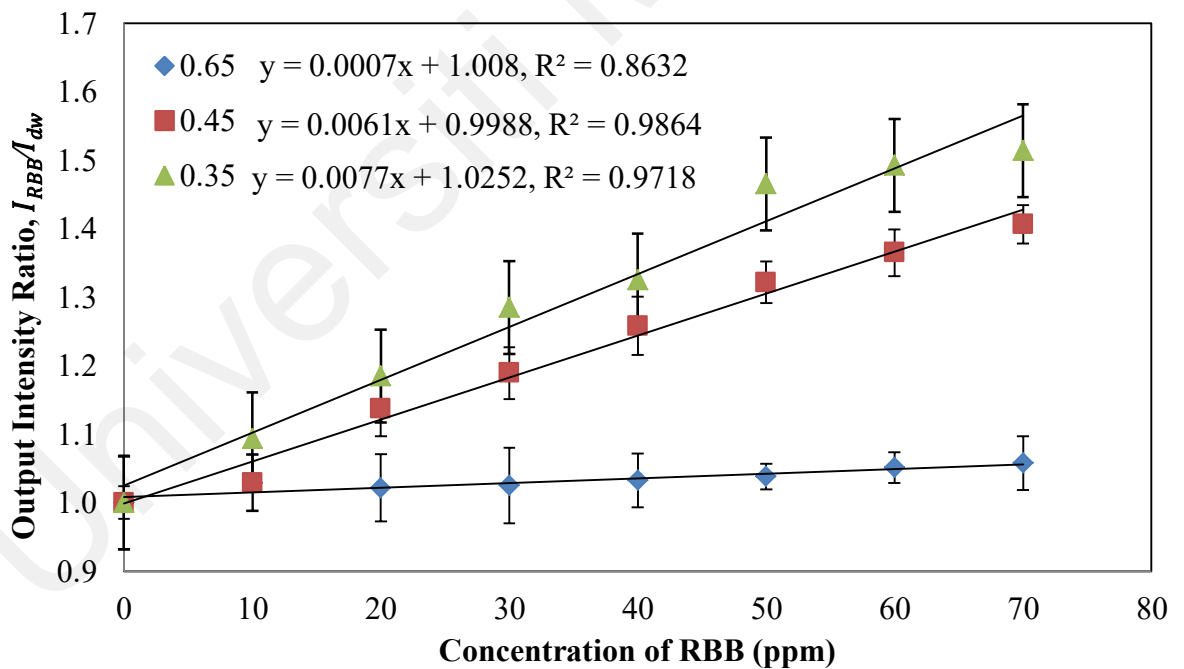


Figure 4.2: The variation of the output intensity ratio with tapered fibre diameters $d = 0.65$ mm, 0.45 mm and 0.35 mm for RBB at various concentrations

Table 4.1: Performance of tapered POF with three different diameter, $d = 0.65$ mm, 0.45 mm and 0.35 mm, respectively.

Parameters	Diameter of POF (mm)		
	0.65	0.45	0.35
Sensitivity (/ppm)	7.0×10^{-4}	61.0×10^{-4}	77.0×10^{-4}
Regression coefficient value	0.8632	0.9864	0.9718
Standard deviation (ppm)	0.0132	0.0476	0.0991
Limit of detection (ppm)	18.8571	7.8033	12.8701
Linearity (%)	92.9086	99.3177	98.5799

In study (Beres, de Nazaré, de Souza, Miguel, & Werneck, 2011), tapers with waist diameters 0.40 to 0.50 mm showed good sensitivity to refractive index variations whereas those with waist diameters above 0.55 mm and below 0.30 mm did not demonstrate substantial sensitivity and were discarded. Therefore, sensitivity demonstrated by the sensors with diameter 0.65 mm is increasing significantly when tapering change to optimum diameter, 0.45 mm. However, the increment sensitivity sensor with diameter 0.45 mm to 0.35 mm is lesser almost 5 times than 0.65 mm to 0.45 mm. The difference in sensitivity increment between 0.65-0.45 mm and 0.45-0.35 mm, most probably the sensor with diameter 0.35 mm is close to the optimum diameter range (0.40 mm to 0.50 mm). Thus, changes between 0.45mm to 0.35 mm is less noticeable if compare to 0.65 mm to 0.45mm.

4.4 Cross Sensitivity

The experiment was conducted under room temperature wherein a variation of ± 2 °C did not appear to affect the output intensity. There were no other contaminants besides RBB dye in the solution. However, cross sensitivity from the temperature variation and the presence of other contaminants in the water apart from RBB could

affect the accuracy of the sensor. For further study, effects of temperature and pH are investigated. By utilizing Equation (4.1), the relative error (RE) between the reference values and experimental values can be calculated.

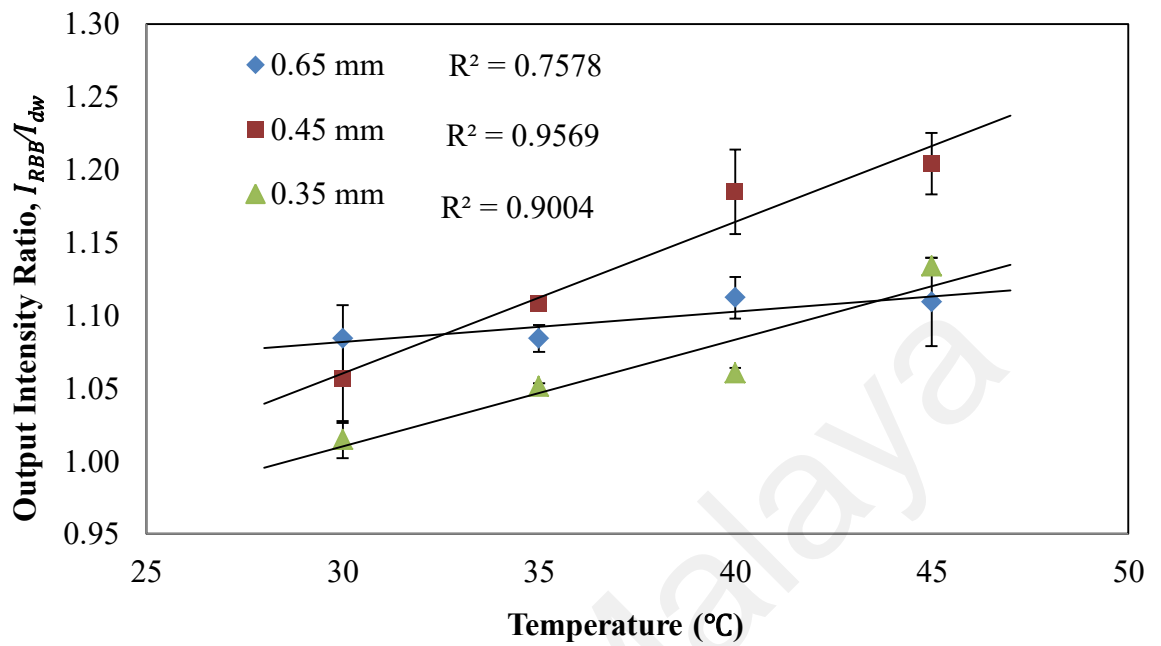
$$\text{Relative error, } \Delta = \frac{I_{\text{experimental}} - I_{\text{calculated}}}{I_{\text{calculated}}} \times 100\% \quad (4.1)$$

4.4.1 Effects of Temperature

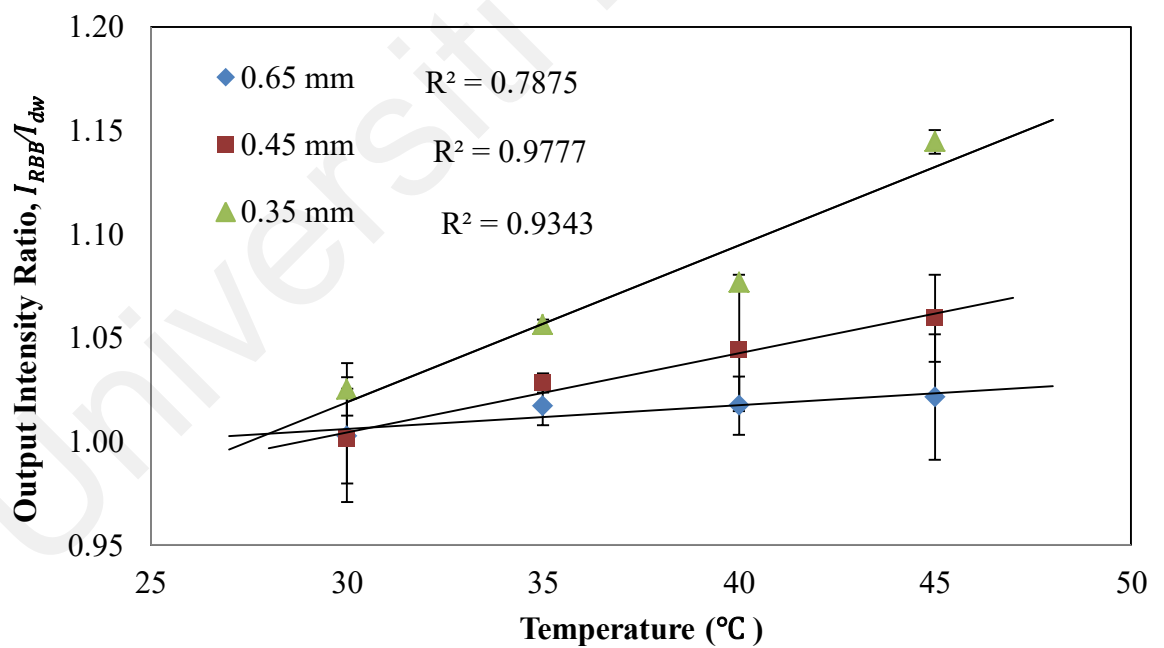
One of the factors that affect the performance of the sensor and the behavior of the sensing medium is temperature. If the temperature of the analyte is known to vary considerably, corrective measure against temperature bias must be considered. Temperature change may affect the equilibrium of surrounding compound and thermal expansion coefficient of the tapered fibre (Kamikawachi et al., 2008). To investigate the effect of temperature on RBB concentration sensing, an experiment was carried out where the RBB concentration was fixed at 50 ppm and 100 ppm, while the temperature was increased from 30 °C to 45 °C in 5 °C steps. The experimental results are shown in Figure 4.3 where the output intensity ratio is shown to linearly increase with temperature. From the results, the sensor with $d=0.45$ mm demonstrates the highest linearity compared to the others.

Since the transmitted intensity is linearly dependent on both the concentration and temperature of the RBB solution, an multiple linear regression (MLR) analysis was performed to combine them in a single equation. MLR analysis involves exploring the linear relationship between a dependent variable and two or more independent variables. A general MLR model is usually written as Equation (2.3). In this section, the MLR analysis was performed using MATLAB (R2010b) software where the dependent variable is the normalized output intensity and the independent variables are the dye

concentration and temperature. In matrix form, the equation can be written as Equation (4.2).



(a)



(b)

Figure 4.3: Responses of sensors toward temperature increment at (a) 50 ppm and (b) 100 ppm analyte.

$$\begin{bmatrix} y_1 \\ \vdots \\ y_i \\ \vdots \\ y_k \end{bmatrix} = \begin{bmatrix} \alpha_1 \\ \vdots \\ \alpha_n \end{bmatrix} \begin{bmatrix} 1 & C_{11} & T_{12} \\ \vdots & \vdots & \vdots \\ 1 & C_{i1} & T_{i2} \end{bmatrix} + \begin{bmatrix} \epsilon_1 \\ \vdots \\ \epsilon_i \\ \vdots \\ \epsilon_k \end{bmatrix} \quad i = 1, 2, \dots, k \quad (4.2)$$

where y , α , C , T , and ϵ are dependent variable, coefficient of independent variables, RBB concentration variation, operational temperature variation and random errors of model, respectively. The resulting equation (Equation (4.2)) contains a number of parameters that must be calculated from the experimental data. By writing the MATLAB script using matrix commands as in Appendix A, the α coefficients of the independent variables can be found and the model for sensors with $d=0.65\text{mm}$, 0.45mm and 0.35 mm are given by Equations (4.3), (4.4) and (4.5) respectively. One additional step is to compute the maximum error, ϵ which indicates the accuracy of the model. The corresponding ϵ of Equations (4.3) to (4.5), are 0.04, 0.20 and 0.24 respectively. The resulting equation was then validated experimentally.

$$y_{0.65\text{ mm}} = 0.9989 - (0.0004 * \text{Temperature}) + (0.0011 * \text{Concentration}) \quad (4.3)$$

$$y_{0.45\text{ mm}} = 1.3929 - (0.0102 * \text{Temperature}) + (0.0017 * \text{Concentration}) \quad (4.4)$$

$$y_{0.35\text{ mm}} = 1.6211 - (0.0135 * \text{Temperature}) + (0.00036 * \text{Concentration}) \quad (4.5)$$

The validation experiment was conducted at 27°C with RBB concentrations of 80 ppm, 90 ppm and 100 ppm to verify the accuracy of the developed model. By utilizing Equation (4.1), the relative error between the calculated and experimental responses is calculated and shown in Table 4.2. From the results, the sensors with diameter of 0.65mm , 0.45 mm and 0.35 mm register discrepancies of less than 7%, 5% and 6% respectively. The best agreement between the calculated and experimental

results was achieved by the sensor with $d=0.45$ mm where the minimum discrepancy is less than 5%. It is observed that the sensor with $d=0.45$ mm shows the highest square of R, (R^2 equal to 0.9864) and least square ($R>99\%$) values. Besides, the results obtained while operating in certain temperature range verify that the sensor in this diameter is adequately stable (R^2 more than 0.95 for both concentrations of RBB) with a high repeatability. Furthermore, the relative error between the calculated and experimental values in validation dataset is the least compared to that of the other two diameters (RE less than 5%).

Universiti Malaya

Table 4.2: Model validation of the developed TPOF sensors.

Concentration (ppm)	Temperature (°C)	Output Intensity Ratio, I_{RBB}/I_{dw}								
		$d=0.65$ mm			$d=0.45$ mm			$d=0.35$ mm		
		Cal. ⁽¹⁾	Experimental	Δ (%) ⁽⁴⁾	Cal. ⁽²⁾	Experimental	Δ (%) ⁽⁴⁾	Cal. ⁽³⁾	Experimental	Δ (%) ⁽⁴⁾
80	27	1.1125	1.0735	-3.51	1.4537	1.4158	-2.61	1.5257	1.4382	-5.73
90	27	1.1235	1.0568	-5.94	1.4707	1.4396	-2.11	1.5293	1.4734	-3.66
100	27	1.1345	1.0645	-6.18	1.4877	1.4585	-1.96	1.5329	1.6001	4.41

⁽¹⁾ Calculated according Equation (4.3)

⁽²⁾ Calculated according Equation (4.4)

⁽³⁾ Calculated according Equation (4.5)

⁽⁴⁾ Relative error were calculated according Equation (4.1)

4.4.2 Effects of pH

One of the concerns is possible reduction or increase in sensitivity of the sensor in acidic and alkaline RBB solution. Its measuring stability was studied using tapered POF with $d=0.45\text{mm}$ immersed into RBB solutions with concentration of 50 ppm. In the experiments, the pH of the dye solutions was adjusted over the range of pH 4.03 to pH 9.97 using 0.5M hydrochloric acid or 0.5M sodium hydroxide solutions. The sensor response was found affected for acidic and alkaline RBB solution. By utilizing Equation (4.1), the relative error (RE) between the reference values, RBB with 50 ppm without pH adjustment and experimental responses is calculated and these results are illustrated in Figure 4.3. The relative error of sensor response is below 5% within the pH range of 6.50 to 8.03. It suggests that the spectral transmission is not affected within that range. But when the pH range is extended to pH 4.03 and pH 9.97 respectively, relative error becomes considerably. Regarding the experimental results show that the sensor could still provide accurate measurement if the pH value falls between 6.50 and 8.03.

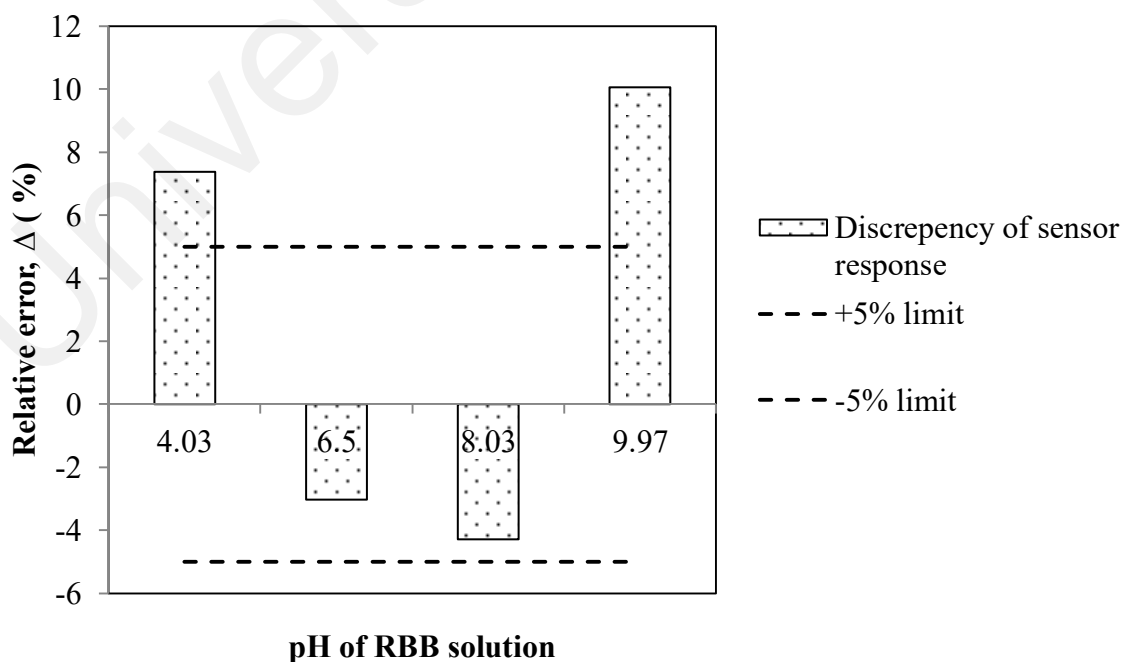


Figure 4.4: Responses of sensor toward pH variation at 50 ppm

4.5 Predicting Using Soft Computing Techniques

Multiple linear regression (MLR) is one of the classical statistical tools used to describe quantitative relationships between a dependent and independent variable. Here, MLR analysis is used to correlate the empirical output to diameter of fibre and concentration of the analyte. Central composite design (CCD) is a useful statistical-based experimental design tool which has been widely used to identify and optimize the performance of complex systems (Ghafari, Aziz, et al., 2009; Nosrati et al., 2011). CCD models allow researchers to visualize interaction among independent factors under different experimental conditions. Compared to the conventional approach which considers an individual parameter separately, CCD is able to evaluate the interaction of a few parameters simultaneously. Besides that, it can also yield good estimations of output variable with the help of the established model. Another common modeling tool is neural network type called ANFIS. ANFIS is a hybrid intelligent system that possesses good learning and prediction capabilities to deal with uncertainties in many different systems (Ghose et al., 2013; Rezaeianzadeh et al., 2014). This tool has been used by researchers for identification and real-time prediction of various engineering systems due to its adaptability to a wide range of uncertainties. It has the capability of mapping input and output variables in mathematical form.

In Section 4.5, data analysis and prediction are executed with the help of CCD and ANFIS and compared to that of the traditional MLR model. The intensity ratio of the transmitted light over the base intensity obtained when the sensor was immersed in distilled water was calculated. MLR, CCD and ANFIS models were developed using the data accumulated. The relationships between the output intensity ratios of the different RBB concentrations using tapered POF sensors of different diameters were established. The models treat the intensity ratio as a dependent variable while the sensor's diameter and RBB concentration are regarded as independent variables.

Moreover, a performance comparison of MLR, CCD and ANFIS models is carried out to evaluate their prediction accuracy based on root mean square error (RMSE), value accounted for (VAF), mean absolute percentage error (MAPE) and square correlation coefficient (R^2). To establish predictive models among the parameters, data of the output intensity ratios of various RBB concentrations from the sensors of different diameters are required. The diameters of the sensors and concentrations of the analyte can be regarded the inputs or independent variables while the intensity ratio of the transmitted light is the output or dependent variable.

4.5.1 Multiple Linear Regression Model

In this sub-section, MLR analysis was performed using IBM SPSS Statistics 22 software to correlate the empirical output, I_{RBB}/I_{dw} to diameter of fibre and concentration of the analyte. The relation between the output and the two inputs are approximated using a linear function as shown in Figure 4.2. The results are summarized in Table 4.3. Since the correlations are found to be linear, an MLR analysis was performed to associate them in a single equation to predict the I_{RBB}/I_{DW} . The resulting equation can be defined by the Equation (4.6).

$$I_{RBB}/I_{dw} = 0.005 \times \text{Concentration} - 1.008 \times \text{Diameter of fiber} + 1.505 \quad (4.6)$$

All the obtained variables were evaluated via the student's t-test at confidence level of 95% of which found to be statistically significant, as shown in Table 4.4. The results indicated that the mentioned parameters provide significant effect during sensing process and must be included from the experimental and predicted values as well. Besides, correlation coefficient of the experimental and predicted values is a good statistic indicator to evaluate the prediction performance of the model. The relationships

between the experimental data and predicted values attained from the MLR model, was illustrated in Figure 4.5 with square correlation coefficient, R^2 equal to 0.8713.

Table 4.3: The variation of the output intensity ratio for tapered fibre with diameters of 0.65 mm, 0.45 mm and 0.35 mm for RBB at various concentrations

Diameter of Fibre (mm)	Equation	R^2
0.65	$y = 0.0008x + 1.0070$	0.9447
0.45	$y = 0.0061x + 0.9988$	0.9864
0.35	$y = 0.0078x + 1.0252$	0.9642

Table 4.4: Statistical results obtained from the MLR analysis

Independent Variables	Coefficient	Std. Error	t-Value	Sig. Level
Constant	1.505	0.066	22.851	<0.0001
Concentration (ppm)	0.005	0.001	6.374	<0.0001
Diameter of Fibre (mm)	-1.008	0.118	-8.537	<0.0001

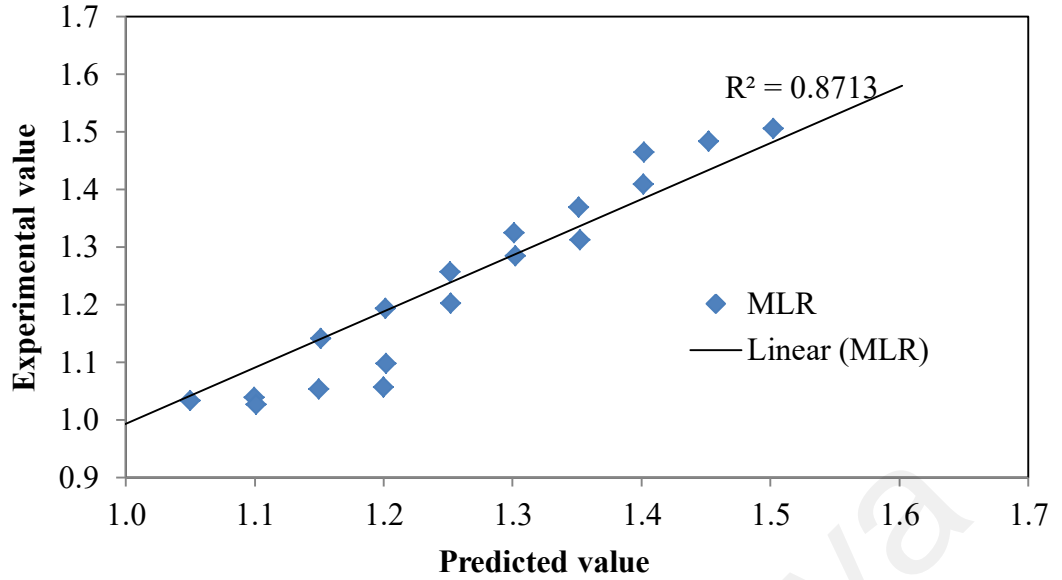


Figure 4.5: Cross-correlation of empirical and predicted values of I_{RBB}/I_{dw} for multiple linear regression model

4.5.2 Central Composite Design Model

It is widely known that the regression technique can only ascertain relationship of individual parameter but does not consider the effect of the interaction amongst the independent variables (Yilmaz & Kaynar, 2011). CCD is a form a regression that is especially introduced to overcome this shortcoming. The CCD used to analyze the data was developed by Design of Experiment software, version 6.0 (Stat-Ease, USA). After running the data analysis, the software is used determined the relationship between the dependent variable and the independent variables based on the Equation (4.7):

$$Y = \alpha_0 + \sum_{i=1}^k \alpha_i X_i + \sum_{i=1}^k \sum_{j=1}^k \alpha_{ij} X_i X_j + \sum_{j=1}^k \alpha_j X_j^2 \quad (4.7)$$

where Y is the dependent variable, X_i and X_j are the independent variables. α_0 is the constant, α_i , α_{ij} , and α_j , are the regression coefficients. In the analysis, the output intensity ratio, I_{RBB}/I_{dw} is assigned as Y while the diameter of the fibre and

concentration of the analyte are designated as X_i and X_j , respectively. A three levels design for low, medium and high are chosen to ensure that the axis can cater the values of the squared variable (Baroutian, Aroua, Raman, & Sulaiman, 2011). In order to ensure accurate of the model, the experiments were repeated by replicating the central point measurement for five times. The design parameters of experiment as well as the output result were presented in Table 4.5.

Table 4.5: Operating conditions and results for the sensing process

Run	Diameter (mm)	Concentration RBB (ppm)	Output intensity ratio, I_{RBB}/I_{dw}	
			Experimental	Predicted
1	0.35	10	1.0930	1.0804
2	0.35	40	1.3255	1.3109
3	0.35	70	1.5140	1.5413
4	0.45	10	1.0290	1.0881
5	0.45	30	1.1893	1.1968
6	0.45	40	1.2590	1.2511
7	0.45	40	1.2404	1.2511
8	0.45	40	1.2670	1.2511
9	0.45	40	1.2690	1.2511
10	0.45	40	1.2780	1.2511
11	0.45	50	1.3215	1.3054
12	0.45	70	1.4069	1.4141
13	0.65	10	1.0216	1.0092
14	0.65	40	1.0325	1.0373
15	0.65	70	1.0578	1.0654

The significance of the operating parameters for estimating of the CCD model was evaluated. The regression coefficient values, standard error, and Prob.>F value (probability) are given in Table 4.6. It was found that diameter of fibre (X_i), concentration of analyte (X_j), the interaction coefficients (X_{ij}), the quadratic coefficients, diameter power of two (X_{ii}) were significant at 95%-confidence level since Prob>F of the model was less than 0.0001. In fact, value of Prob.>F less than 0.05 indicate the model term is significant (Ghafari, Hasan, & Aroua, 2009). Therefore, the second-order polynomial effect of all variables is influential parameters. Based on the parameter estimation in Table 4.6, the cross-relationship between the dependent variable (Y) and studied independent variables is shown in Equation (4.8).

$$Y = 1.209 - 0.137 X_i + 0.129 X_j + 0.101 X_{ij} + 0.035 X_{ii} \quad (4.8)$$

Table 4.6: Estimated regression coefficients and significance level

Parameter	Code	Coefficient Value	Standard Error	F-value	Prob.>F (%)	Remarks
Model	-	-	-	112.2	<0.0001	Significant
Constant	α_0	1.209	0.011	-	-	-
Diameter	X_i	-0.137	0.011	167.70	<0.0001	Significant
Concentration	X_j	0.129	0.010	152.11	<0.0001	Significant
Diameter power of two	X_{ii}	0.035	0.016	4.99	0.0495	Significant
Diameter and concentration	X_{ij}	0.101	0.013	63.57	<0.0001	Significant

A three-dimensional response surfaces and contour graph were plotted based on the model equation, Equation (4.8) to estimate the responses surface over independent variables, as shown in Figure 4.6. The plots given in this figure reveal the relative effects of two variables on the sensing efficiency. The goodness-of-fit of regression model would be evaluated regarding coefficient of determination, R^2 . It was observed from Figure 4.7, that the regression model had a high value of $R^2=0.9751$. This value indicates that 97.8% of the variations for the sensing process can be explained by the regression equation (Mook et al., 2013). The results indicate that there is good agreement between the experimental and predicted values.

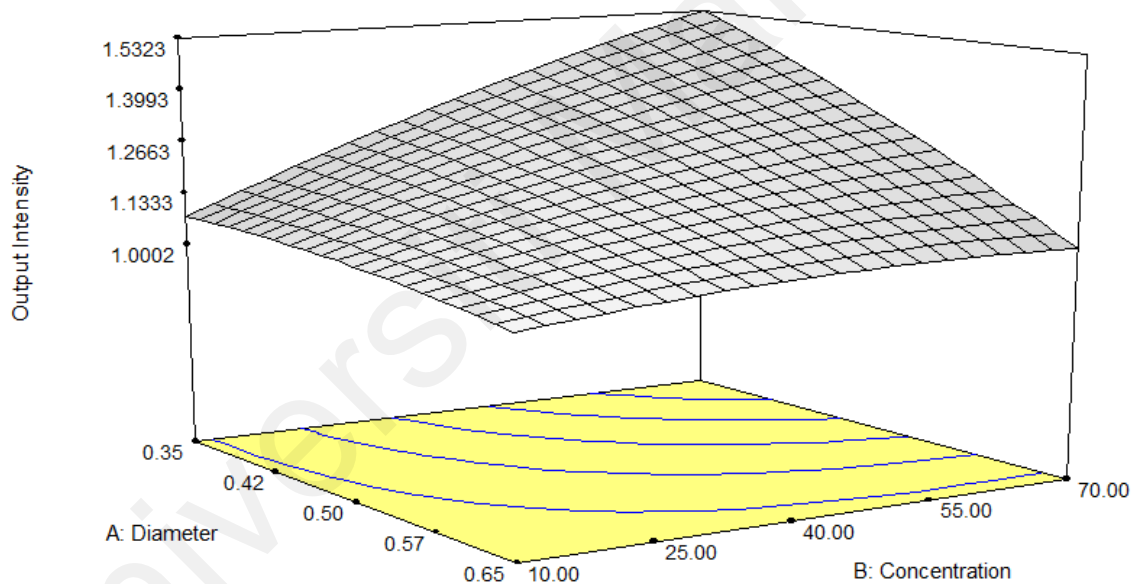


Figure 4.6: Plots for Response surface and contour of the effects of diameter of POF and concentration of RBB on the output intensity ratio sensing

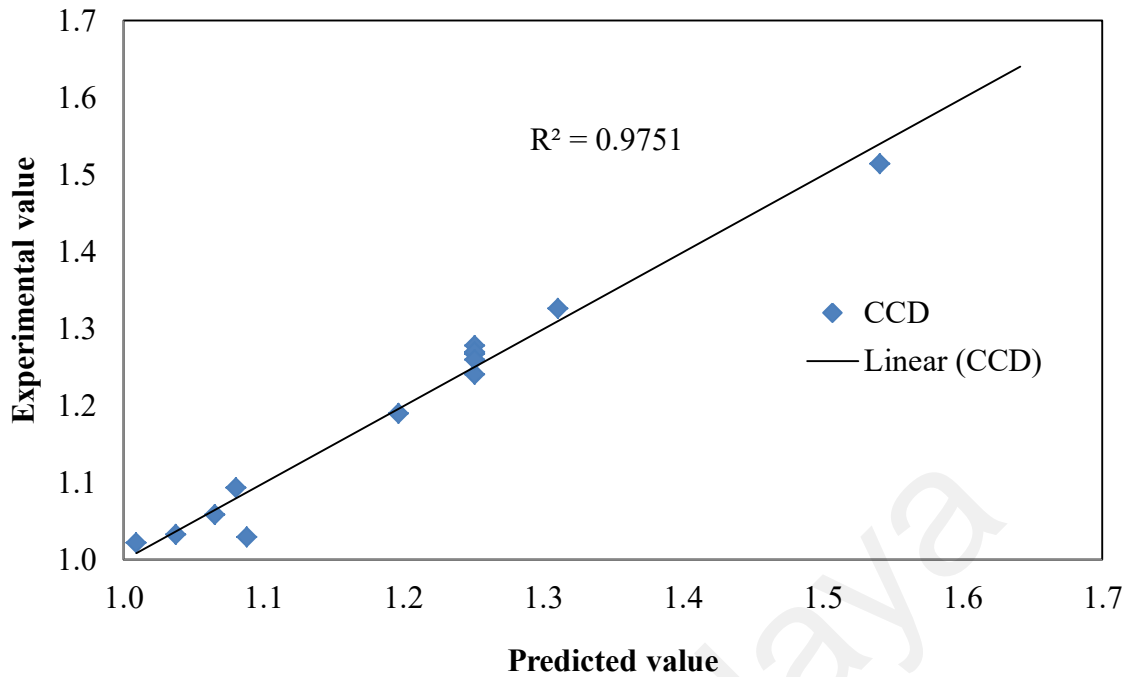


Figure 4.7: Cross-correlation of the empirical and predicted output of central composite design model

4.5.3 Adaptive Neuro-Fuzzy Interference System Model

A hybrid intelligent system called adaptive neuro-fuzzy inference system (ANFIS) was developed to assess the sensor responses, I_{RBB}/I_{dw} for sensors with various diameters (0.65mm, 0.45mm and 0.35mm) to dye solution of different concentrations (10ppm to 70ppm). Then 50% of the data were used for training while the other 50% were used for evaluating the prediction capability of the model. The ANFIS editor offers eight different types of membership functions to choose from: triangular (trimf), trapezoidal (trapmf), bell (gbellmf), Gaussian (gaussmf), two-sided Gaussian (gauss2mf), pi-shaped (pimf), difference between two sigmoidal (dsigmf), and product of two sigmoid (psigmf). Similar to the study by Güneri et al. (Güneri, Ertay, & Yücel, 2011), the ANFIS networks were trained individually by the empirical data using eight different membership functions with the help of MATLAB software version 7.1 (R2012b). A hybrid learning algorithm is utilized to optimize and train the model for

200 epochs. The hybrid approach is pragmatic since it shrinks the search space of the back propagation method, eventually it can converge much faster in ANFIS networks (Yilmaz & Kaynar, 2011). The summation output can be defined as a linear combination among the consequent parameters. After training, error measure criteria for each type of membership function were computed and summarized in Table 4.7. This error measure was determined over the training and testing data set to evaluate the performance of the ANFIS model of various membership functions. The error measure used to train the aforementioned ANFIS is expressed as Equation (4.9) (Loukas, 2001).

$$E = \sum_{k=1}^n (y - y')^2 \quad (4.9)$$

where y and y' are the k_{th} empirical and predicted output, respectively, and n is the total number of experiment data in the training set.

Table 4.7: Computed error measure criterion for ANFIS functions

ANFIS Function	Error measure, E	
	Training Scheme	Testing Scheme
trimf	0.00517	0.00764
trapmf	0.00794	0.01120
gbellmf	0.00676	0.00914
gaussmf	0.00804	0.01076
gauss2mf	0.00786	0.01103
pimf	0.00854	0.01212
dsigmf	0.00505	0.00773
psigmf	0.00497	0.00714

The product of two sigmoid MF (psigmf) had the lowest errors of 0.00497 and 0.00714 for the training and testing data. Therefore, psigmf membership function was chosen for subsequent study because it minimized the error measure. Afterwards, the ANFIS networks were trained using the optimum membership function. The decision surface of the estimated response is shown in Figure 4.8. As three level membership functions are allocated for two inputs, nine different rules are necessary to produce the output value. ‘Low’, ‘Medium’ and ‘High’ linguistic values are assigned for the IF rule of each input. The rule structure is analyzed and formed as shown in Table 4.7. Then, a cross-correlation between the empirical values and predicted responses is illustrated by the ANFIS model, as shown in Figure 4.9. A good agreement between the experimental and predicted results was achieved. This could be justified from $R^2 = 0.9959$.

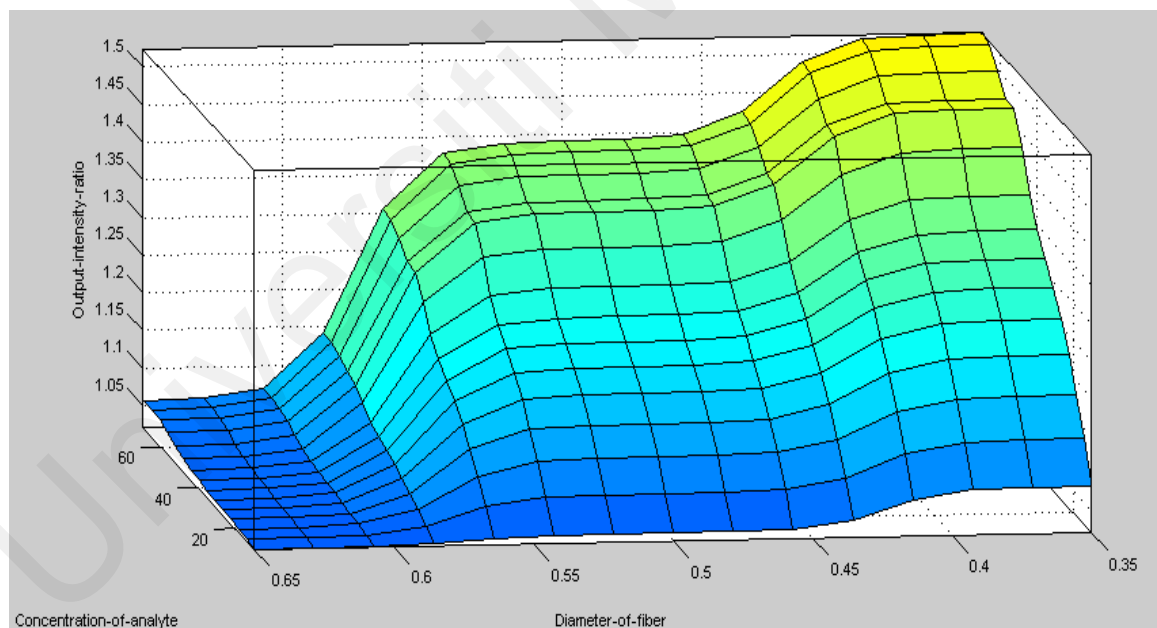


Figure 4.8: Response surface contour plots to estimate the responses surface of fibres with different diameters for various RBB concentrations

Table 4.8: ANFIS rule structure

No	Rule structure
1	If Concentration of RBB is 'Low' and Diameter of fibre is 'Low' then output is out1mf1
2	If Concentration of RBB is 'Low' and Diameter of fibre is 'Medium' then output is out1mf2.
3	If Concentration of RBB is 'Low' and Diameter of fibre is 'High' then output is out1mf3
4	If Concentration of RBB is 'Medium' and Diameter of fibre is 'Low' then output is out1mf4
5	If Concentration of RBB is 'Medium' and Diameter of fibre is 'Medium' then output is out1mf5.
6	If Concentration of RBB is 'Medium' and Diameter of fibre is 'High' then output is out1mf6
7	If Concentration of RBB is 'High' and Diameter of fibre is 'Low' then output is out1mf7.
8	If Concentration of RBB is 'High' and Diameter of fibre is 'Medium' then output is out1mf8
9	If Concentration of RBB is 'High' and Diameter of fibre is 'High' then output is out1mf9.

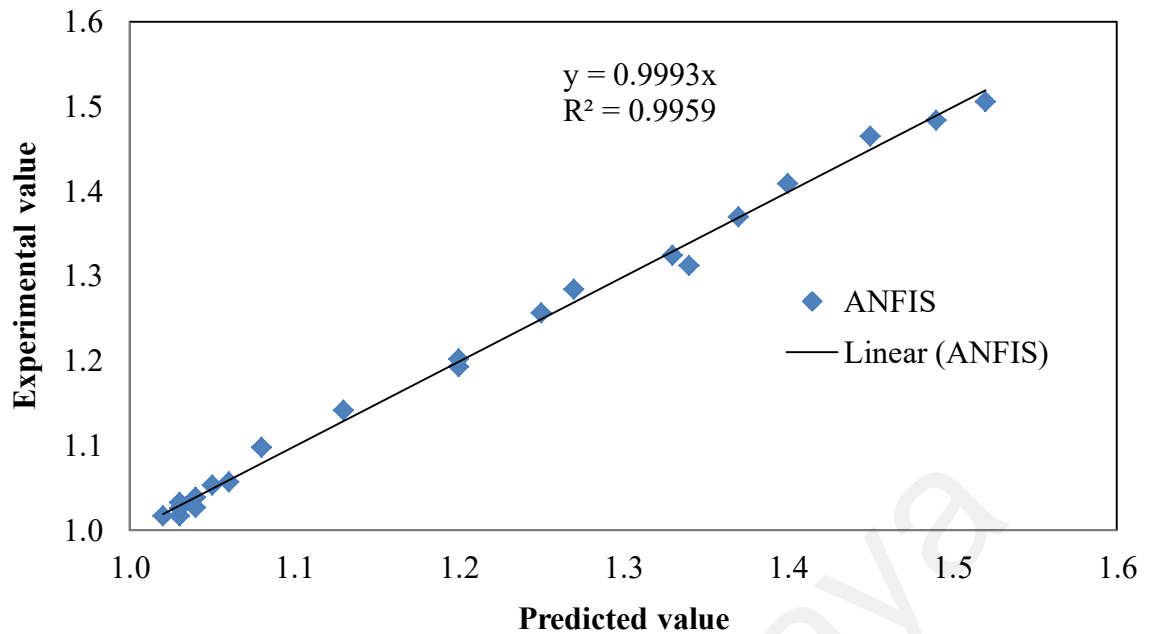


Figure 4.9: Scatter plots of the predicted value compared to experimental value using the ANFIS model.

4.5.4 Evaluation of Model Performances

In order to estimate the prediction accuracy of the models, the difference between the predicted and measured output intensity ratio values were evaluated according to the statistical criteria of correlation coefficient (R^2) and root mean square error (RMSE), as in Equation (2.12) and (2.13) respectively (Prakash Maran, Sivakumar, Thirugnanasambandham, & Sridhar, 2013; Rajendra, Jena, & Raheman, 2009). A prediction model is considered good if R^2 is close to 1 and RMSE is low (close to 0). For good measure, mean absolute percentage error (MAPE), as in Equation (2.14) also applied for assessment of the prediction performances of the established models. Table 4.8 summarized the performance indices.

Table 4.9: Performance indices (RMSE, MAPE and R^2) for models

Model	Performance indices		
	RMSE	MAPE	R^2
MLR	0.06163	3.7041	0.8713
RSM	0.02216	1.3908	0.9751
ANFIS	0.01083	0.7006	0.9959

From the results of simple regression analyses, the sensor output appears to increase significantly when its diameter decreases which demonstrated in Figure 4.2. For example, for RBB concentration of 60 ppm, sensor output intensity ratios for sensors with diameters of 0.65 mm, 0.45 mm and 0.35 mm are 1.05, 1.37, and 1.50 respectively. The model predicts that the percentage of the output would increase until 42.8% if the diameter of the sensor reduces from 0.65mm to 0.35mm. The MLR, CCD, and ANFIS models were then constructed using two inputs and one output. According to Tamunaidu and Bhatia (Tamunaidu & Bhatia, 2007), value R^2 greater than 80% must be achieved to obtain a good agreement between the predicted and experimental results. With high R^2 value, appreciable results (more than 0.80) were seen for all models. It shows that each model performs successfully. Furthermore, a comparison of RMSE, VAF, and MAPE indices was carried out to investigate which prediction model offers the highest reliability. The calculated values of these statistical criteria is summarized in Table 4.8. The following observations can be made:

- a. MLR model shows a good performance in predicting I_{RBB}/I_{DW} with R^2 of more than 0.800.
- b. CCD model is more reliable compared than the MLR model since its RMSE and MAPE are lower and its VAF is higher.

- c. ANFIS model has the lowest RMSE and MAPE. Small value in RMSE and MAPE (minimum equal to 0) and high value in VAF (maximum equal to 100) of the model implied that the prediction error was relative low. Thus, ANFIS model is the best.

4.6 Summary

The performance of tapered plastic optical fibre (TPOF) sensor of different diameters in measuring the concentration of RBB aqueous solution was investigated. The sensors are simple to fabricate and easy to handle with a good sensitivity, linearity and reproducibility. Although the sensitivity of the sensor is enhanced when the thickness of its cladding decreases, knowledge of the optimum diameter of the tapered sensor for the operating pH, temperature and RBB concentration range is necessary for the development of an efficient sensor for the target application. The TPOF with $d = 0.45$ mm displays good sensitivity with small value in limit of detection and adequate stability was achieved within the tested temperature range 30°C to 40°C and pH range 6.50 to 8.03 with an deviation of less than 5%. The measurement and prediction of dye concentration is important in the design, planning and management of wastewater treatment. In this study, Central Composite Design (CCD) and adaptive neuro-fuzzy inference system (ANFIS) are employed to identify and predict the output intensity ratio of light that passes through a TPOF sensor in Remazol Black B (RBB) dye solution of different concentrations. The predictive performances of these models are compared to that of the traditional Multiple Linear Regression (MLR). The accuracies of MLR, CCD and ANFIS models are evaluated in terms of square correlation coefficient (R^2), root mean square error (RMSE), value accounted for (VAF), and mean absolute percentage error (MAPE) against the empirical data. It is found that the ANFIS model exhibits higher prediction accuracy than the MLR and CCD models. However, the drawback of

the intensity-based modulation measurement is that, once the concentration of the analyte reaches a certain level, there will not be enough transmission data available due to the opacity of the analyte. This limitation impede their widespread use in high level of dye concentration measurement. For the next chapter, author will utilize a silica-based fibre optics sensor by analyzing the spectral shift response to infer the dye concentration in wider range.

Universiti Malaya

CHAPTER 5: TAPERED FIBRE OPTIC SENSOR BASED ON CORE- MISMATCH STRUCTURE

5.1 Introduction

One of the popular structures used to construct the sensor probe is Mach-Zehnder interferometer (MZI) that is based on core mismatch (Dong, Su, Shum, Chung, & Chan, 2006). Attempts to develop core mismatch optical sensors for environmental sensing applications, specifically for measuring the concentrations of water-based solutions where the refractive index value is around 1.3325 have never been reported to the best of our knowledge. For this purpose, authors will develop an MZI based sensor by bridging two single mode fibres (SMF₁ and SMF₂) with approximately 20 mm, tapered multimode fibre (MMF), namely core-mismatch fibre optics sensor (CMFOS).

5.2 Dye Concentrations Measurement Using CMFOS

Since the sensitivity of the sensor is heavily influenced by the MMF diameter, sensors with three different diameters of $d = 27.7 \mu\text{m}$, $23.3 \mu\text{m}$ and $19.5 \mu\text{m}$ are constructed and immersed in different Remazol Black B (RBB) dye concentrations from 40 to 240 ppm. Two outputs are recorded and they are the intensity ratio of RBB solution to distilled water, I_{RBB}/I_{dw} and wavelength shift, $\Delta\lambda$. In this study, Response Surface Methodology (RSM) is applied to visualize the interactions between dependent and independent factors, which interpret the obtained results in a statistic form. Unlike the conventional approach that considers individual parameters separately, this analysis technique is able to evaluate the interaction of operating parameters simultaneously hence, yields good estimations of engineering processes. On the other hand, a reliable predictive model that correlates the sensor output with the relevant input parameters in a quick, low-cost and nondestructive manner is essential in predicting the dye

concentration of analytes containing RBB. A modeling approach, adaptive neuro-fuzzy inference system (ANFIS) has been selected and used in this study due to its adaptability to a wide range of uncertainties. ANFIS is deployed as a predictive model using given responses of the sensor: intensity ratio and wavelength shift to determine dye concentration based on the effects of the diameter of the sensors. The performances of the models are evaluated according to coefficient of correlation (R^2), root mean square error (RMSE) and mean absolute percentage error (MAPE).

5.2.1 Experimental Set-up

The CMFOS structure is assembled by concatenating a section, approximately 20 mm of tapered MMF with two standard SMFs (SMF_1 and SMF_2). The details of the sensor probe preparation were discussed in Section 3.3.1 of Chapter 3. It was reported that the sensitivity of the sensor probe could be enhanced by adopting thinner tapered MMF that allows larger portion of evanescent field (Lim et al., 2012) to interact with the sensing medium (Soldano & Pennings, 1995; Wang et al., 2008). The change in the tapering diameter is expected to induce variation in the interference signal of the CMFOS structure (Lee et al., 2012). Therefore, at first, the effect on tapered MMF diameter on the transmission spectrum of the sensor probe is investigated. In this investigation, the end of the SMF_1 was connected to an Erbium amplified spontaneous emission (ASE) source while the end of the SMF_2 was connected to an optical spectrum analyzer (OSA model Anritsu MS9710B). The MMF is then tapered using a flame brushing technique to obtain various diameters through real time monitoring. The tapering process was halted the moment the desired diameter was obtained. The test solutions were obtained by diluting the stock solution of RBB in 1000 ppm to the desired concentrations. In the experiment, the concentration of dye solutions is varied

from 0 to 240 ppm with 40 ppm increment. Figure 5.1 shows the transmission spectra at various tapered MMF diameters.

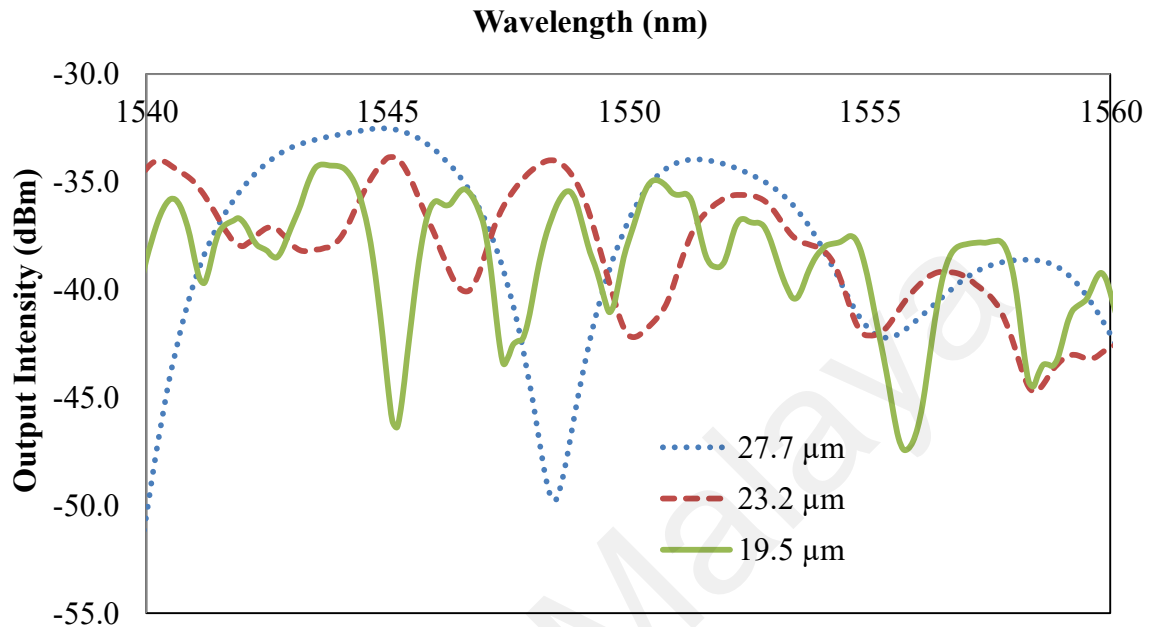


Figure 5.1: Transmission spectrum of the SMF₁-MMF-SMF₂ sensor with MMF diameter, $d=27.7 \mu\text{m}$, $23.2 \mu\text{m}$ and $19.5 \mu\text{m}$.

5.2.2 Response Surface Methodology

The RSM analysis was implemented using the Design of Experiment (DOE) software Version 6.0. The process parameters are the diameter of MMF between $19.5 \mu\text{m}$ to $27.7 \mu\text{m}$ and the concentration of the RBB solution ranging from 40 ppm to 240 ppm. In this design, intensity ratio of the transmitted light, I_{RBB}/I_{dw} and wavelength shift, $\Delta\lambda$ were chosen as the responses of sensor. After running the data analysis, the software determined the relationship between the dependent variable and the independent variables. The analysis of variance (ANOVA) was applied to test the significance and adequacy of the model. The main indicators that show the significance of the model are the Fisher variation ratio (F-value), probability value (Prob > F) with 95% confidence level and adequate precision (AP). Furthermore, the fitness of the

polynomial models is expressed by the coefficients of determination, R^2 , adjusted R^2 (R_{adj}^2) and predicted R^2 (R_{pred}^2).

5.2.3 Effects of the Variables on Sensing Efficiency

The analysis of variance (ANOVA) was carried out regarding the response surface models and the results are given in Table 5.1. The statistical significance was evaluated by the F-test based on a probability value with 95% confidence level. The F-value of intensity ratio model was 35.34 and the wavelength shift model was 25.39 respectively. It was found that the value probability error of F-value, Prob.> F for both models was less than 0.0001, which implied that the models were significant and represented a low probability of being affected by noise (Ghafari, Hasan, et al., 2009). Additionally, the adequacy of all the models generated were also evaluated through lack-of-fit (LOF) (Atadashi, Aroua, Abdul Aziz, & Sulaiman, 2012). The lack-of-fit values for both models were 0.1983 and 0.8906 respectively, implying that the models were not relatively significant to the pure error since the probability values were more than 0.05. The F-value and lack-of-fit both implied that the models were in accordance with the range of the predicted variables. The quality of the model was also assessed based on the correlation coefficient value, R^2 . An appreciable R^2 results (>0.90) were seen for all models in this study. In addition, predicted R^2 and adjusted R^2 were both above 80% for the responses in the experiments conducted, indicating again that the experimental results fit well into the models. The difference between the predicted and adjusted R^2 should be lower than 0.20 (20%) to show that they are in good agreement (Nosrati et al., 2011). Furthermore, adequate precision (AP) of the models measures the signal to noise ratio. A well-performed model, AP should be greater than 4 to reveal that the noise is not significantly contributing to any error in the response surface (Ghafari, Aziz, et al., 2009). Consequently, AP equal to 18.924 and 17.414 were

achieved for model intensity ratio and wavelength shift respectively during the dye solution sensing. These values were much higher than 4, indicating adequate signal was obtained from the models. These statistical analyses showing the adequacy of the models can be used to navigate the outputs of sensors.

In order to assess the effects of the variables against the sensing responses, two graphs were developed as shown in Figure 5.2 and Figure 5.3 respectively. From Figure 5.2, it was found that the sensor reacted to the sensing medium by decreasing output intensity ratio. This might be due to the increasing chromophore content in the solution, which absorbs the propagating light. This relation follows Beer-Lambert's law where greater light absorption is achieved with increasing concentration of RBB. In addition, as the analyte concentration increased, the intensity ratio decreased at a different rate. It can be observed that the slope of the curve dropped more significantly when adopting a thinner diameter of MMF, thus indicating that the efficiency of RBB solution sensing increased. This is owing to the diameter of the tapered region, which in turn dictates the sensitivity of the sensor. By adopting a thinner MMF, a stronger evanescent field would be generated, which will result in higher sensitivity of the sensor towards ambient RI. Based on the result, the fibre with a diameter of 19.5 μm obtained the highest sensitivity among the others.

Table 5.1: ANOVA for the response surface models.

Response	Prob>F ^{a)}				R ²	Adj. R ²	Pred. R ²	AP ^(c)	SD ^(d)
	Model	Remark	LOF ^{b)}	Remark					
I_{RBB}/I_o	<0.0001	Significant	0.1983	Non-significant	0.9315	0.9051	0.7997	18.924	0.0057
$\Delta\lambda$	<0.0001	Significant	0.1216	Non-significant	0.9558	0.9388	0.8332	26.542	0.0260

a) Prob>F: probability error of F-value;

b) LOF: lack of fit;

c) AP: adequate precision;

d) SD: standard deviation

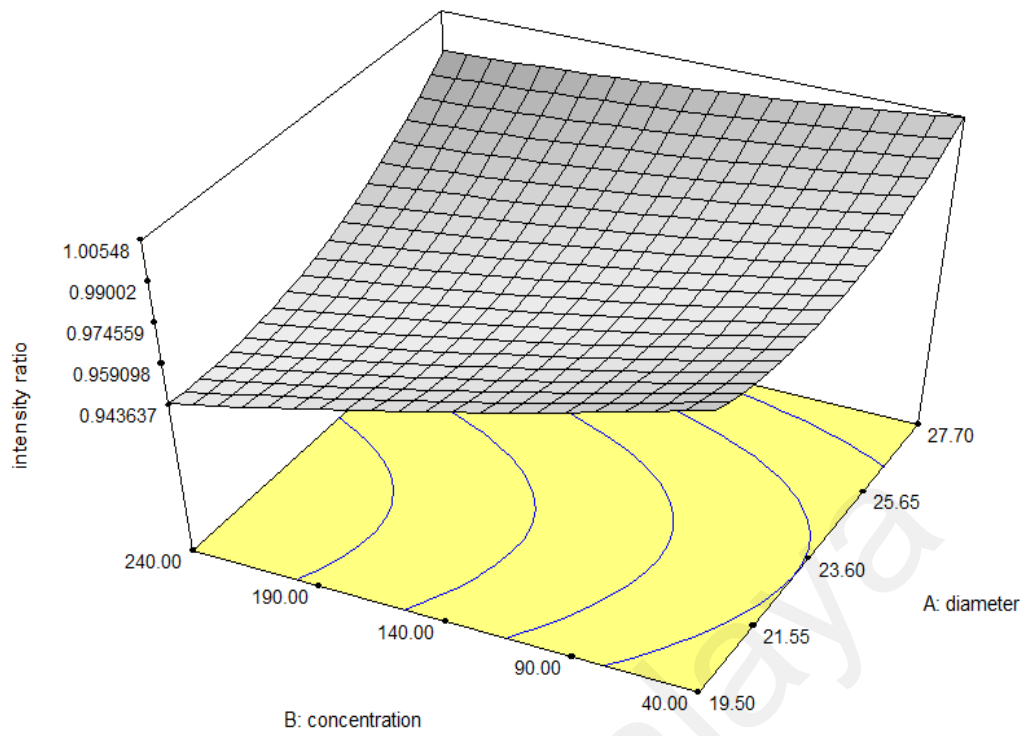


Figure 5.2: Response surface plot for intensity ratio interact with independent variables.

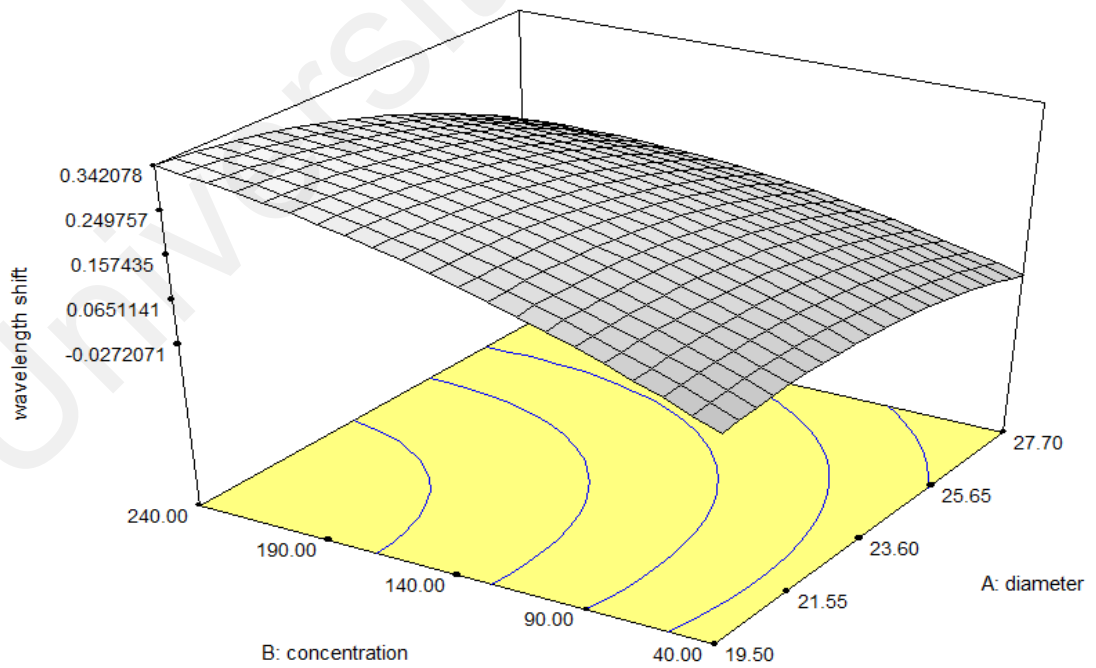


Figure 5.3: Response surface plot for wavelength shift interact with independent variables.

It was found that the wavelength shifted to longer wavelength when increasing the concentration of the RBB, as in Figure 5.3. According to (3.3), the β change caused by RI variation results in a phase shift since wavelength shift in spectrum transmissions relies on the effective refractive index within the fibre and sensing medium. Figure 5.4 demonstrates a linear relationship between β and ambient refractive index (RI) variation. The RI of the RBB solution is measured using a refractometer with model METTLER Toledo RE40D. The K value, linear coefficients of slope could be obtained from gradient of Figure 5.4. As thinner MMF support stronger evanescent field, K value increase from 594.64, 599.86, to 603.62 for MMFs with diameters of 27.7, 23.2, and 19.5 μm , respectively. This indicates that the sensor in $\text{SMF}_1\text{-MMF-SMF}_2$ configuration with a smaller MMF diameter is more sensitive towards the ambient RI variation and provides a higher sensitivity in responses.

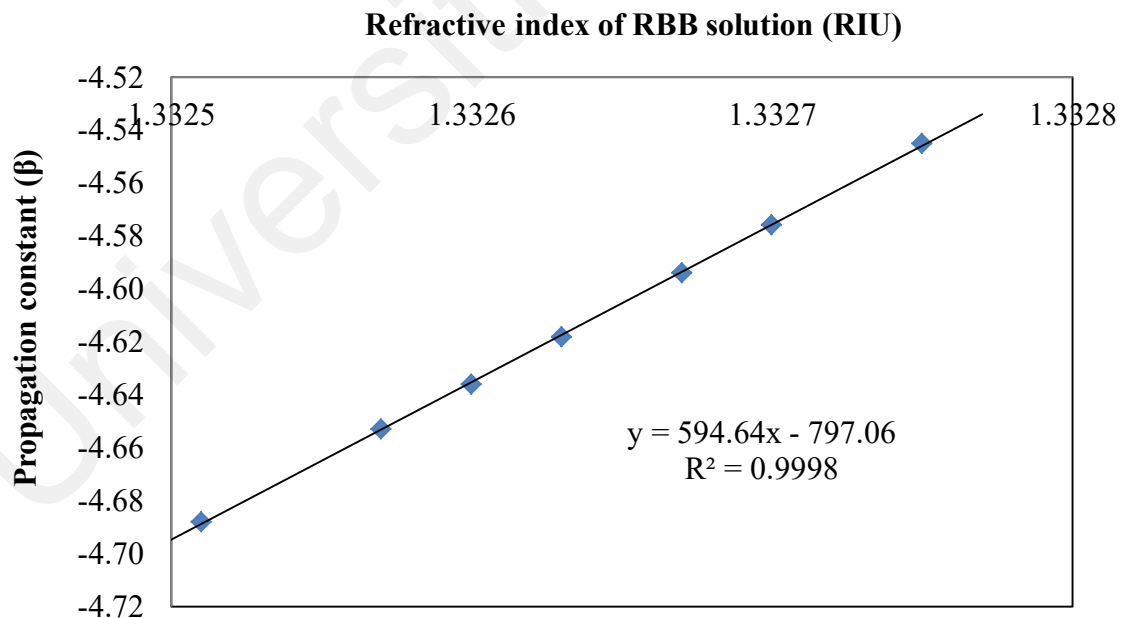


Figure 5.4: Propagation constant at various ambient RI using tapered MMF with $d=27.7 \mu\text{m}$.

5.2.4 Estimate the Prediction Accuracy of the Model

The fundamental construction of an ANFIS model comprises of three mechanisms: a preference of fuzzy rules; definition of the membership functions (MFs) applied in the fuzzy rules; and performing the inference practice upon the rules to acquire a rational output. The rule is set in terms of 'IF-THEN' of Sugeno fuzzy system, as in Equation (2.4). The ANFIS model was designed where it was used to estimate the responses of sensors with two inputs: diameter of MMF and concentration of RBB solution. The architecture consisted of five layers. **Layer 1** supplies the input values to the next layer. Parameters in this layer are defined as premise parameters. **Layer 2** is a membership layer that receives the inputs from the first layer and multiplies the incoming signal before exporting the output. **Layer 3**: The third layer is called the rule layer. Every node calculates the ratio of the rule's firing strength to the sum of all rules' firing. **Layer 4**: The fourth layer is named as defuzzification layer. It offers the output values of which generating from the inference of rules. **Layer 5**: The fifth layer is called the output layer which sums up all the inputs coming from the fourth layer. This node computes the overall output as the summation of all incoming signals.

Modeling the sensing process with ANFIS network comprises of two stages: training and testing with the experimental data. In addition, the number of rules and types of MF are playing an essential role especially in solving actual problems. It may be noted that finding suitable fuzzy rules and membership functions of an ANFIS model requires a trial-and-error procedure to develop the optimal ANFIS model. In order to obtain the optimum membership function that provides superior results in comparison with other network topologies, all ANFIS structures were trained using the ANFIS editor of the MATLAB (version R2012a) software based on Hybrid learning method (Singh & Deo, 2007). The rules have constant output, which is performed by grid partitioning of the data space with 200 epochs. Their training efficiencies of network

topologies are compared and the optimized model is chosen regarding the minimized mean relative absolute error (MRAE) (Gulbag & Temurtas, 2006; Salmasnia, Baradaran kazemzadeh, & Mohajer Tabrizi, 2012). The gbell membership function gave the smallest errors in both output variables compared to the other membership functions and was therefore selected for the development of the subsequent model (Tsourveloudis, 2010).

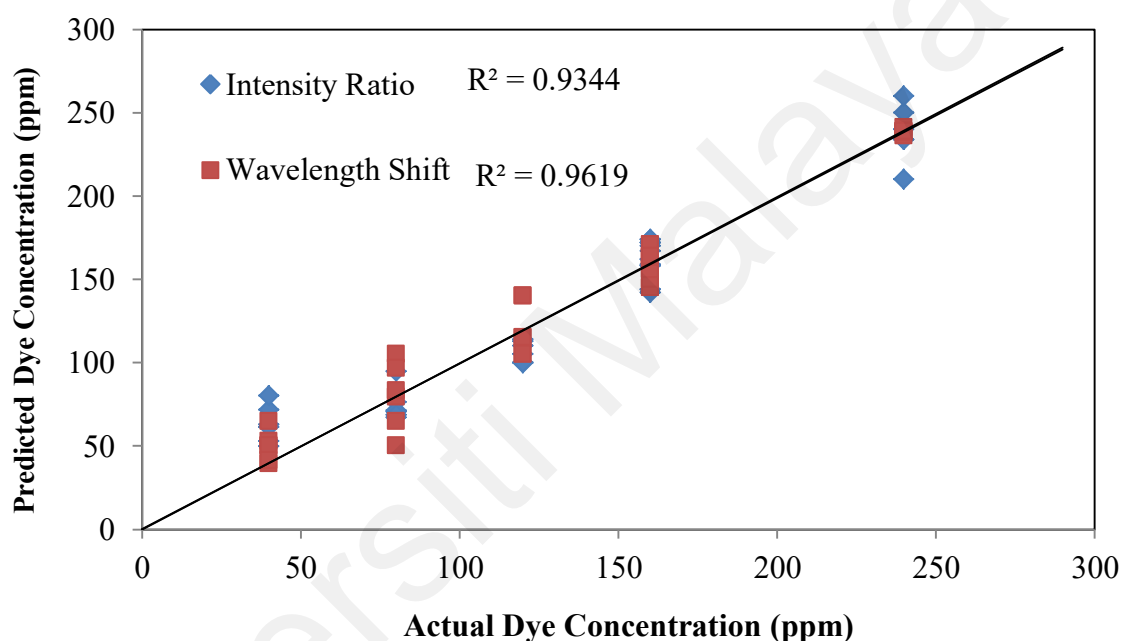


Figure 5.5: Cross-correlation the actual and predicted RBB dye concentration using given responses of the sensor: intensity ratio only, wavelength shift only and combination of the two outputs.

Two output variables in the form of intensity ratio and wavelength shift were used to infer the dye concentration of an analyte containing Remazol Black B. Therefore, use intensity ratio, and wavelength shift on dye concentration predictions were compared and delineated in Figure 5.5. The differences between the actual and predicted dye concentration values were justified in terms of the correlation coefficient (R^2) which might indicate correlation of the developed models to the studied responses. In order to evaluate the accuracy of the predictive models developed in this study: the

root mean square error (RMSE) and mean absolute percentage error (MAPE) were determined. These errors reflect the difference between the observed and expected outputs for the given corresponding inputs (Kermani, 2007). Higher prediction accuracy for the constructed model was found when the value of R^2 is closer to 1.0 and exhibited relatively low RMSE and MAPE. The values of these statistical criteria are given in Table 5.2. The model that employs wavelength shift in predicting dye concentrations has provided better prediction capabilities i.e. having the highest R^2 and the lowest RMSE and MAPE. In current study, it can be deduced that using wavelength shift forecast is superior to those using intensity ratio.

Table 5.2: Performance Indices for Predictive Models

Output variable	R^2	RMSE	MAPE (%)
Intensity Ratio	0.9344	15.3226	12.5731
Wavelength shift	0.9619	11.8712	9.7981

Two models demonstrated high performance in forecasting dye concentration, given the output intensity ratio or wavelength shift. The model derived using the wavelength shift variables showed better performance than the other model. The measurements in the optical system presented here was only tested on Remazol Black B in a limited range of concentrations (0 to 240 ppm). It is noteworthy to point out that the author is mainly interested in investigating performance of core mismatch fibre optic sensor with different MMF diameters in measuring the concentrations of RBB aqueous solution in this section.

5.3 Measurement of Dye Concentrations and Temperature

Core mismatch fibre optic sensor (CMFOS) was developed as a sensing device in this chapter by bridging two SMFs with a short section of tapered MMF. The transmission peaks of the interference spectrum were found to exhibit different responses toward the changes of the surrounding parameters since different cladding modes responded differently towards varied ambient environment. By selecting a specific transmission peak of the interference spectrum, dye concentration can be measured (Xiong et al., 2014) if the wavelength shift sensitivity of parameter can be determined. As shown in previous section, CMFOS has a great potential for dye concentration measurement at a designated location, which makes them an attractive monitoring tool for wastewater quality control. Nevertheless, optical fibre sensors is inherent cross-sensitivity between the analyte and temperature (Farahi, Webb, Jones, & Jackson, 1990). This persistent drawback has limited their sensing capability and practicability. As such, many researchers have put forward methods to improve FOSs and overcoming these issues by compensating the cross-sensitivity effect or minimizing the cross-sensitivity itself (Kim et al., 2012). However, most of the existing sensing models dealing with cross-sensitivity require cost consuming fabrication equipment and complex compensation processes to solve the inherent cross-sensitivity problem. One of the interesting practices of CMFOS is capable to spatially differentiate the analyte along an identical fibre length. In Section 5.3, the author proposed and demonstrated a fibre optics sensor based on core mismatch structure for realizing multi parameters measurement by utilizing cross sensitivity effect. The discrepancy between the actual and predicted dye concentrations and temperature, respectively are also evaluated.

5.3.1 Experimental Set-up

Based on the study by (Sun et al., 2014), the free spectral range (FSR) between the two adjacent interference minima or maxima can be expressed as Equation (5.1).

$$\lambda_k - \lambda_{k-1} = \frac{16n_{core}d^2}{(m-n)[2(m+n)-1]L} \quad (5.1)$$

where d , L and n_{core} are respectively the diameter, length and refractive index of the MMF core, k is integer, $m > n$. It can be seen from Equation (5.1) that FSR decreases as the interferometer length, L increases. Longer tapered region will induce interference in the larger spectral measurement range since FSR is inversely proportional to the length of the tapered MMF. The main drawback of longer tapered MMF is it is difficult to demodulate it due to large intensity loss. On the other hand, the interference pattern becomes more prominent as the diameter of MMF decreases (Luna-Moreno et al., 2007; Villatoro & Monzon-Hernandez, 2006). However, lower mechanical strength and more complex fabricating difficulty are the main limitations of its pragmatic use for monitoring purpose. In this section, the suitable diameter and length of the MMF used in order to guarantee high sensitivity, obvious interference pattern and appropriate mechanical strength were determined to be 25.4 μm and 20mm, respectively. The injected ASE spectrum is also shown in Figure 5.6 as a solid line as a comparison purpose. By comparing both spectra, it is estimated that the insertion loss of the CMFOS is about 18 dB. The test solutions were obtained by diluting the stock solution to the desired concentrations: 0, 50, 100, 150, 200, 250, 300, 400, 500, 800 and 1000ppm. A digital hotplate (WiseStir, model MSH-30D) was used to control ambient temperature and maintain the test environment with the desired temperature.

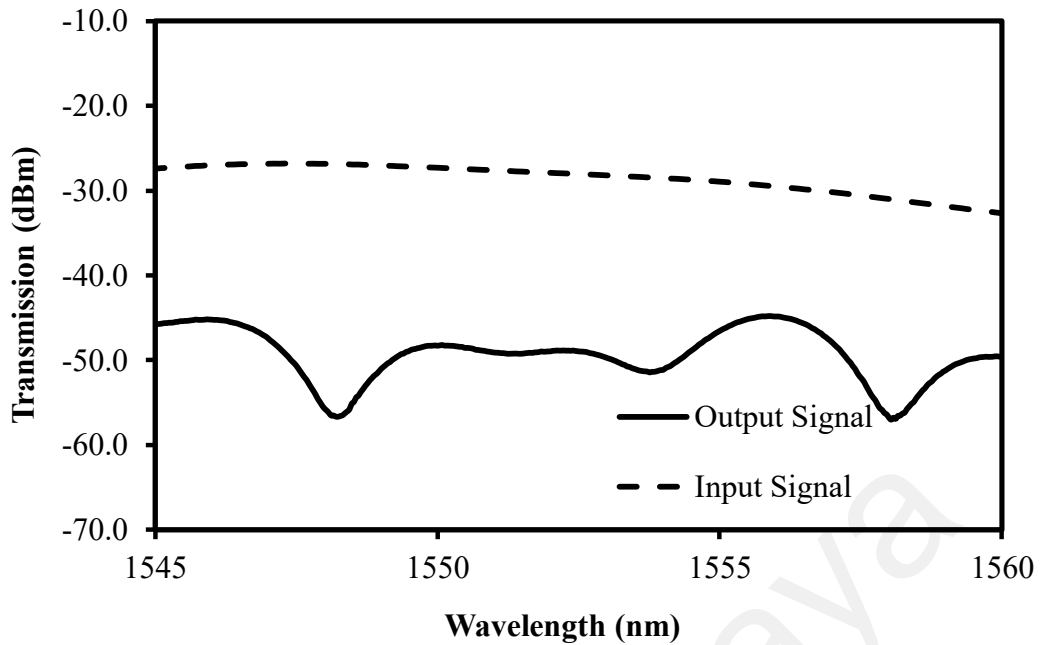


Figure 5.6: Input and output ASE spectra to/from the tapered CMFOS measured at wavelength range from 1545 nm to 1560 nm

5.3.2 Dye Concentrations Measurement

In the experiment, the hotplate temperature is fixed at 27°C and the transmission spectrum is monitored at various concentration of RBB solution. As shown in Figure 5.7, the inhomogeneous interference pattern is clearly seen in the transmission spectrum, which indicates that there must be more than two high-order eigenmodes that were excited to contribute to the interference. It is observed that the resonance wavelength range of 1553 nm to 1557 nm has the largest extinction ratio and thus it was chosen as a reference peak to investigate the spectral change with the variation of the surrounding dye concentrations and temperature. Figure 5.7 shows the output spectra of the propose CMFOS at three different dye concentrations. It was observed that the wavelength of transmitted spectrum shifted to the direction of longer wavelength as the ambient dye concentration increased. The change in dye concentration from 0 to 1000 ppm corresponded to a change in the refractive index (RI) in the order of 7.4×10^{-3} RIU when measured using a refractometer (model Mettler Toledo RE400). This indicates

that the wavelength of transmitted spectrum shifts to long wave direction with the ambient RI increase. Even though the resulting change in the RI was small, the change had considerable effects on the higher-order modes that propagate in the cladding of CMFOS. It changes the phase of the propagating light and thus red shifts the resonance wavelength. The relationship between the wavelength shift and RBB concentrations is then investigated during both increasing and decreasing processes and the results are shown in Figure 5.8. The performance of the sensor towards dye concentration is summarized in Table 5.3.

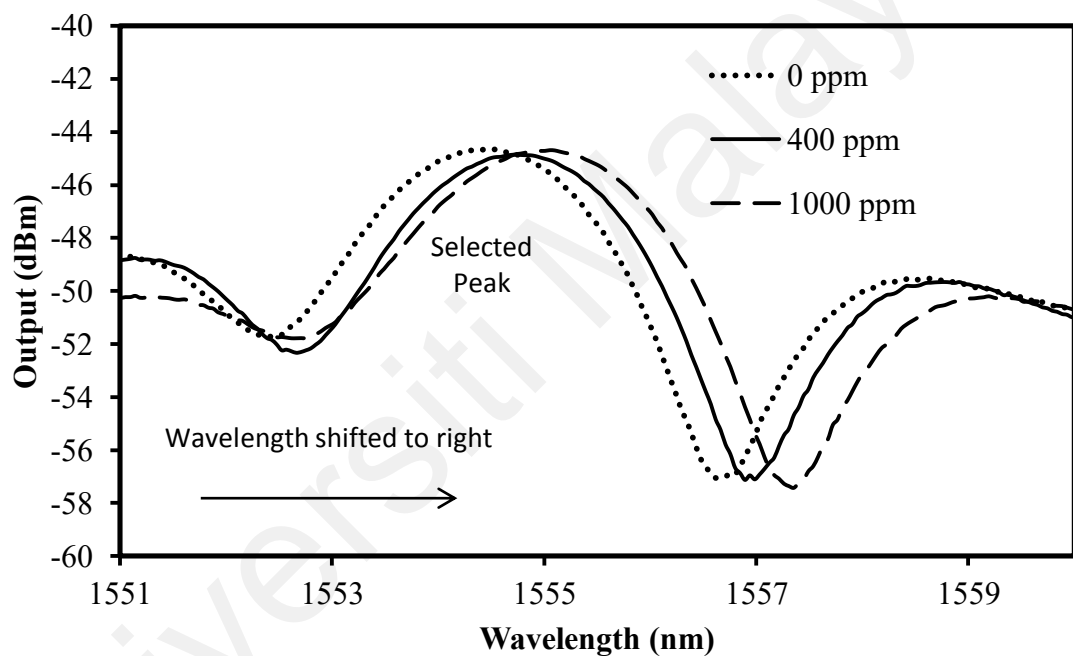


Figure 5.7: Transmitted spectra of CMFOS device in different concentrations of RBB solution

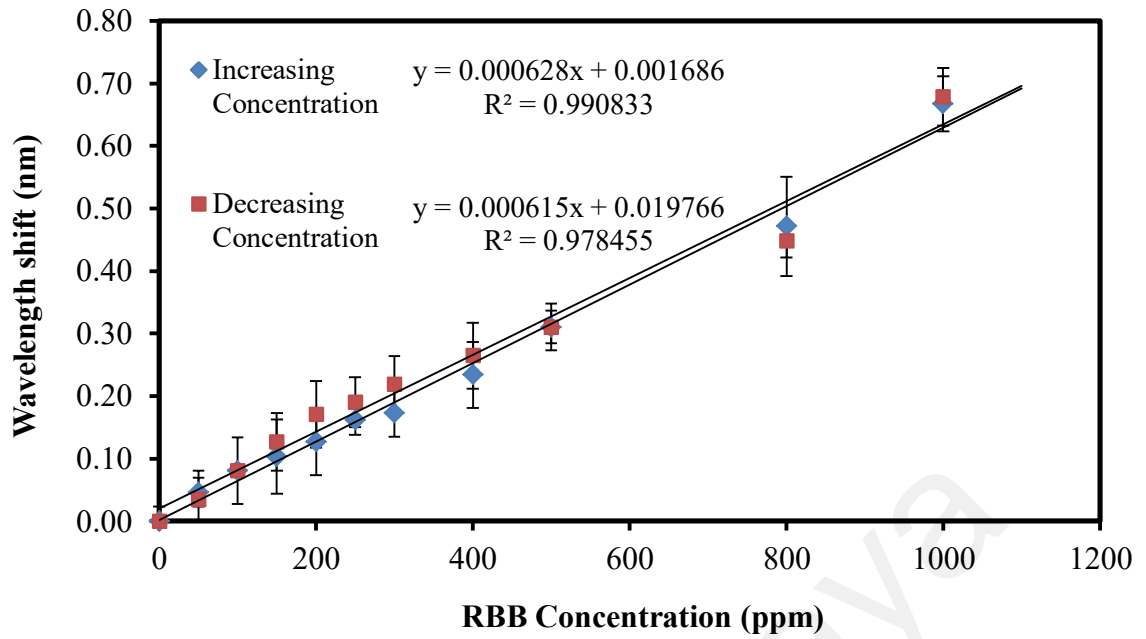


Figure 5.8: Delineating curves of the measured wavelength shift as a function of concentration of RBB

5.3.3 Temperature of Dye Solution Measurement

Cladding modes have different mode field areas and the phases differ with the change of ambient conditions such as temperature. In this subsection, effect of the temperature of dye solution on spectral response of the proposed sensor was investigated by heating the solution temperature with a hot plate from the room temperature and recorded the transmitted spectrum for every five degrees interval. In the experiment, the RBB concentration is fixed at 100 ppm and the sensor was remained stable for 30 seconds before every record to get stable and credible test data. Considering the boiling point of water, temperature test was implemented in the range of 25–80 °C. Figure 5.9 shows the transmitted spectra of this proposed sensor under different ambient temperatures. It is obvious from this figure that the transmitted spectrum is shifted to left wavelength direction as the temperature of solution increases. The relationship of the resonance wavelength with respect to ambient temperature in heating and cooling processes is shown in Figure 5.10. As can be seen from this figure,

resonance wavelength and temperature are close to a linear relationship. The slope of fitted line represented temperature sensitivity is approximately $-0.10 \text{ nm}/^\circ\text{C}$.

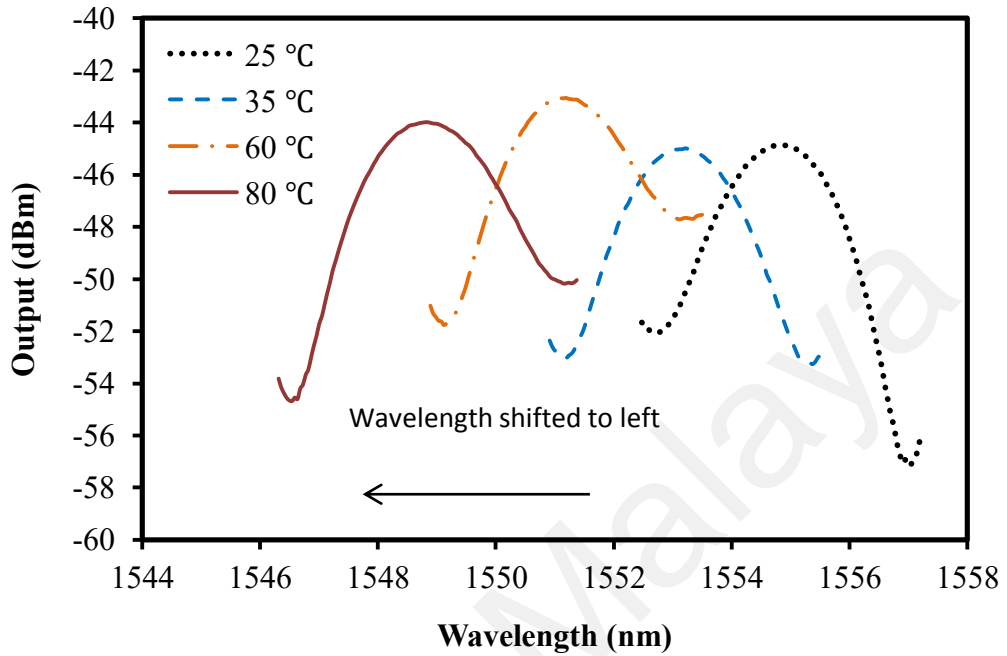


Figure 5.9: Transmitted spectra of CMFOS device in various temperatures with constant concentration 100 ppm of RBB solution.

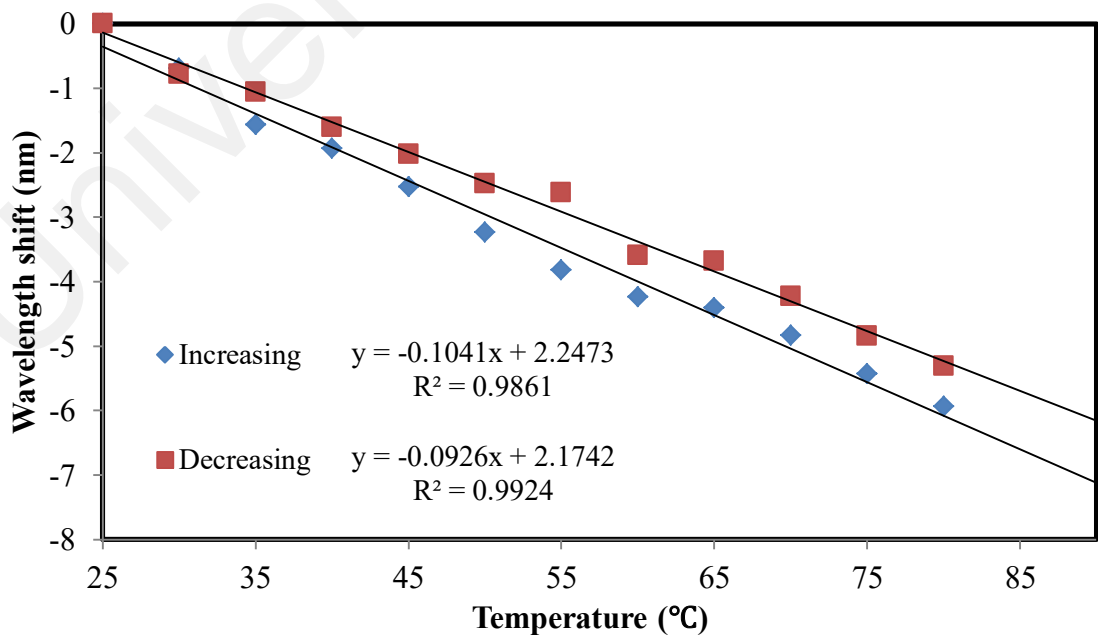


Figure 5.10: The measured wavelength shift for temperature of analyte sensing with fixed concentration of RBB.

The inherent temperature effects were distinguished based on the induced changes in the refractive index. The changing rate of refractive index with respect to temperature variation ($\partial n/\partial T$) at the operating wavelength can be defined as thermo-optic coefficient and expressed as Equation (5.2).

$$\begin{aligned}\Delta\lambda/\lambda &= ([\partial n_{core}/\partial T \times n_{core}] + [2\partial d/\partial T \times d] - [\partial L/\partial T \times L])\Delta T \quad (5.2) \\ &= (\gamma + \delta)\Delta T\end{aligned}$$

where $\Delta\lambda$ denotes the changes of wavelength shift, γ is the thermal expansion coefficient of the fibre and δ is the thermo-optic coefficient of the modal index difference, respectively. Since the reported value of γ and δ is about 5.0×10^{-7} (Villatoro, Finazzi, Minkovich, Pruneri, & Badenes, 2007) and approximately 7.0×10^{-6} (Sun et al., 2014) respectively for pure silica, the calculated corresponding sensitivity of the sensor towards temperature variation, $\Delta\lambda/\Delta T$ was $11.63 \text{ pm}/^\circ\text{C}$ at the operation wavelength of 1550 nm based on Equation (5.3). The experimental results demonstrated that the $\Delta\lambda/\Delta T$ of the fabricated sensor was $-104.1 \text{ pm}/^\circ\text{C}$ which was almost nine times the calculated sensitivity. This proves that the high sensitivity of the temperature response can be achieved. The performance of the sensor with temperature is summarized in Table 5.3. The aqueous medium plays the role of CMFOS cladding, it will be more easily affected by ambient temperature because the thermo-optic coefficient of water is two orders of magnitude larger than that of air. Thus, this effect will make the sensor with higher temperature sensitivity compared with the theoretical value which calculated according air medium.

Reversibility of the results is an important factor in the operation of any sensors. Therefore, in this work, the measurements were also repeated under similar conditions using RBB solutions when the concentration decreases from 1000 ppm to 50 ppm and

temperature decreases from 80 °C to 25 °C. The results were presented in Figure 5.8 and Figure 5.10 for the RBB concentration and temperature variations, respectively. As shown in both figures, there was a slight difference in the sensitivity when the measurement was taking in increasing and decreasing processes. However, this difference was statistically insignificant ($p < 0.05$) based on the paired t-test by SPSS (version 22). No noticeable difference was observed in reversible measurements, indicating that there were no significant changes in the measurement efficiency of the sensor.

Table 5.3: Performance of sensor.

Parameter	Concentration of RBB (ppm)		Temperature of solution (°C)	
	Increasing	Decreasing	Increasing	Decreasing
Sensitivity	6.28×10^{-4} <i>nm/ppm</i>	6.20×10^{-4} <i>nm/ppm</i>	-0.1041 <i>nm/°C</i>	-0.0926 <i>nm/°C</i>
Linearity	99.54 %	98.92 %	99.30 %	99.62 %
Standard Deviation	0.0201	0.0230	0.2335	0.1533
Limit of detection	32.01 ppm	37.47 ppm	2.24 °C	1.66 °C

5.3.4 Validation of RBB Concentration Measurement Results

The same sensing probe was repeatedly exposed to RBB solutions with various concentrations ranging of 50 ppm to 1000 ppm under controlled temperature in order to investigate the discrepancy between the actual and predicted dye concentrations and temperature so that the accuracy of the sensor can be validated. Figure 5.11 shows the cross correlation of actual and predicted values of RBB dye concentrations when operating under controlled temperature. As shown in the Figure 5.11, the relationship

between the actual and predicted values indicates a satisfactory goodness of fit (R^2 more than 0.9) with RMSE=21.7355 and MAPE=5.2702. The forecasted temperature results were also obtained. In the experiment, the temperature measurement was carried out within a range from 25 °C to 80 °C using 200 ppm and 300 ppm of RBB concentrations in order to demonstrate that the sensor was exclusively sensitive to ambient temperature variation, as shown in Figure 5.12. The relationship between actual and predicted results were in good agreement with high R^2 , low RMSE and MDPE which indicated that the developed sensing device retained its capability for measuring RBB concentrations and temperature accurately after repeated use. They showed a good agreement between the actual and predicted values with high R^2 (0.9468) and relatively low RMSE (4.7846) and MAPE (5.8970).

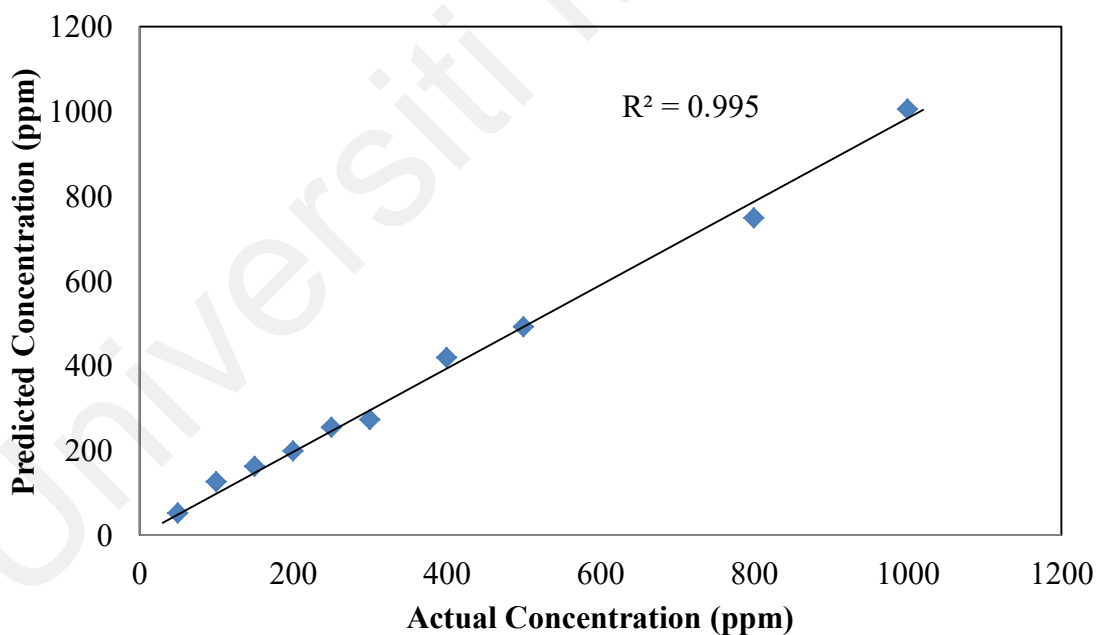


Figure 5.11: Cross correlation of actual and predicted values of RBB dye concentrations ranged 50 ppm to 1000 ppm of which operated under controlled room temperature.

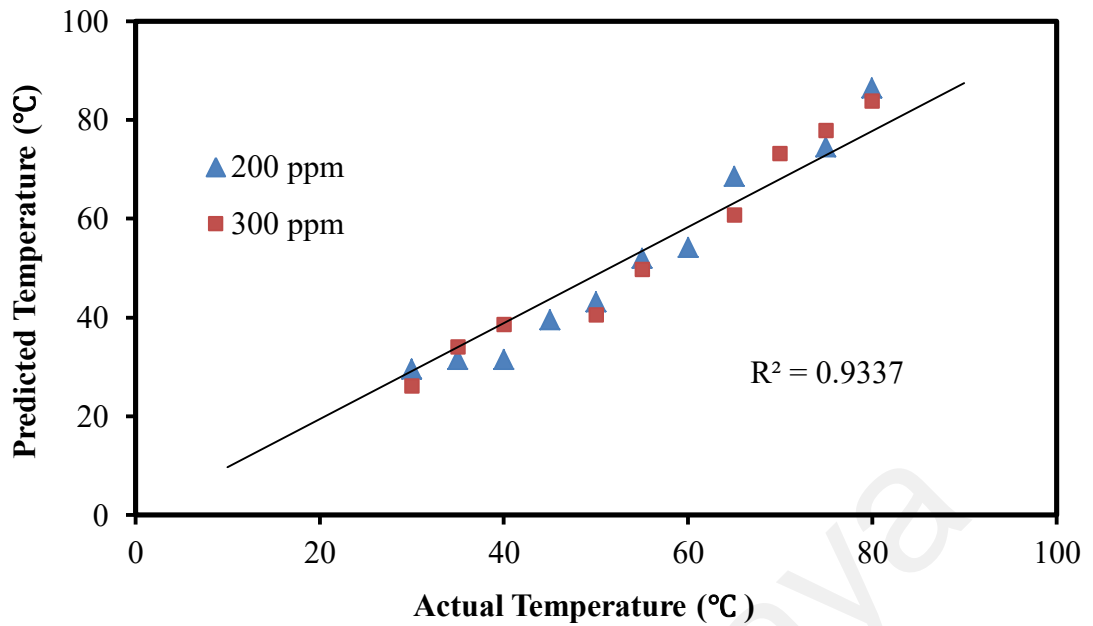


Figure 5.12: Cross correlation of actual and predicted values of RBB solutions temperature when the RBB concentrations are fixed at 200 ppm and 300 ppm.

5.4 Summary

A reliable core mismatch fibre optic sensor (CMFOS) was constructed by bridging two single mode fibres with short section of multimode fibre, which was tapered to expose the evanescent field of the propagating light with the surrounding Remazol black B (RBB) solution. The sensitivity of the (CMFOS) was investigated for three different tapered fibre diameters of 27.7, 23.2 and 19.5 μm . The sensor was immersed in a RBB solution of various concentrations where the output intensity ratio and wavelength shift were observed to mainly dependent on the tapering diameter of the MMF and the concentration of the RBB dye solution. Response surface methodology was then utilized to evaluate the interactions of few parameters simultaneously as well as to interpret the obtained results in statistical form. Furthermore, a modeling approach, adaptive neuro fuzzy interference system (ANFIS) is deployed to construct two empirical models with the given responses from the sensor; hence, predicting the concentration of the RBB solution. The sensor was also demonstrated for realizing dye

concentration and temperature measurement by utilizing cross sensitivity effect. The sensor allows interference between the core and the cladding modes that induces resonance wavelength shift with the change of the surrounding refractive index. It is observed that the wavelength is shifted to right in the order of $6.18 \times 10^{-4} \text{ nm/ppm}$ when dye concentrations increased. On the other hand, the wavelength is shifted to left with the temperature increment with sensitivity of $-0.1041 \text{ nm/}^\circ\text{C}$. Reversibility and validation experiments were also performed to validate the accuracy of the sensor. The proposed CMFOS offers a few advantages over the previous tapered POF sensor where it is easily reproducible and has demonstrated a higher linearity (more than 90%), wider range of dye concentrations measurement (0 ppm to 1000 ppm) and better stability even when it is operated in high temperature range (25°C to 80°C). In addition, the results indicated that the fabricated sensor could reduce system complexity as only one optical fibre sensor was needed for both dye concentrations and temperature sensing. This would otherwise be sophisticated to do using tapered POF sensor. However, higher cost of sensor probe fabrication is still involved since two types of silica fibre are required to develop the proposed configuration (SMF-tapered MMF-SMF). In order to minimize the cost of sensor probe fabrication, another type of Mach-Zehnder sensor with higher sensitivity, more obvious interference pattern and using only a single fibre, will be investigated in the next chapter.

CHAPTER 6: NON-ADIABATIC TAPERED FIBRE BASED SENSOR

6.1 Introduction

Non-adiabatic tapered fibre optics sensors (NATFOS) are widely used in research. They are commonly used for monitoring physical quantities like acoustic vibration (Xu et al., 2012), strain and temperature (Muhammad et al., 2013). They can be used to monitor biological processes and chemical compounds such as antimicrobial activity (Mohammad Ismail Zibaii et al., 2014), α -amino acids in aqueous (M I Zibaii et al., 2010) and can even operate in magnetic fluid (Layeghi et al., 2014). With some modifications, optical sensors can also be deployed for water quality monitoring to replace expensive and bulky instruments. For instance, a tapered fibre can be used to measure the concentration of a specific analyte quickly and accurately.

6.2 Dye Concentration Determination with Cross Sensitivity Compensation

Continuous development in sensing technologies has improved the efficiency and precision of the latest sensors. Detecting the concentration of chemicals in industrial effluents, using optical fibre based sensors is convenient since they are small and non-destructive (Ronot-Trioli, Trouillet, Veillas, El-Shaikh, & Gagnaire, 1996). In general, fibre optic sensors have been shown to have a promising potential for many applications including concentration measurement. A number of researchers have used fibre optic sensors to determine the concentration of analytes based on changes in their refractive index (RI) (Hang-Zhou et al., 2014; Su & Huang, 2007). However, there is still an inherent cross-sensitivity issue caused by changes in other variables that degrades the accuracy of the measurement. As such, many researchers have put forward methods to improve fibre optic sensors and overcoming these issues by compensating the cross sensitivity effect or realizing the multi parameters sensing capability through

overcoming the cross-sensitivity (Kim et al., 2012). A number of notable works that investigate cross sensitivity between refractive index and temperature in liquid using fibre optic sensors are listed in Table 6.1. For instance, two fibres Bragg grating (FBG) are used simultaneously where one of them is designed to detect the refractive index change of the surrounding environment while the other measures the temperature (Pereira, Frazaõ, & Santos, 2004). Cascaded long period gratings (LPG) with refractive index (RI) matched material coating were used by Jinhua et. al (Jinhua, Zhang, Li-Yang, Jin-Fei, & Sailing, 2007) for measuring the refractive index and temperature simultaneously. Another approach employs a coreless multimode fibre segment which inserted into a high birefringence fibre loop mirror to realize multi parameters sensing (Gouveia, Chesini, Cordeiro, Baptista, & Jorge, 2013). A hybrid configuration using a pair of FBG and one LPG was introduced by Trono et. al to detect RI while compensating strain and temperature cross-sensitivity effects (Trono, Baldini, Brenici, Chiavaioli, & Mugnaini, 2011). Sometimes, coating the fibre structure with suitable materials seems to enhance the evanescent interaction and thus increase the sensitivity of the sensor (J. Grochowski, M. Myśliwiec, P. Mikulic, W.J. Bock, & Śmietana, 2013; Smetana, Bock, & Mikulic, 2011).

However, developing interferometer sensors using FBGs or LPGs often requires special fibres, a grating writing equipment and a complex system (Muhammad et al., 2013). Besides, cumbersome procedures are required due to the immobilizing the indicator on the surface of a fibre. Hence, the use of high sensitivity of interferometric sensor to resolve cross-sensitivity with less cumbersome preparation and fabrication is required. Non-adiabatic tapered fibre optic sensor (NATFOS) is susceptible to refractive index variation (H. Latifi, M. Zibaii, S. Hosseini, & P. Jorge, 2012) and thus are suitable for biological or chemical sensing applications that involve minute changes in the RI of the surrounding. In Section 6.2, an investigation on the use of a NATFOS

to monitor dye concentration based on the wavelength shift of a transmission interference spectrum is presented. Dye concentration measurement errors due to cross-sensitivity are somewhat complex in nature and vary from sensor to sensor. The influence of cross sensitivity from other parameters in the form of changes in suspended solids, temperature, and pH on the dye concentration measurement is also investigated. The compensation method was chosen to establish a model to compensate the error may result due to cross sensitivity. The proposed sensor does not require a separate wavelength source for any particular wavelength. It can operate in any spectral region as long as the optical fibre can transmit light. Therefore, the cost of this sensor should be considerably less than that of a conventional sensor.

Table 6.1: Selected previous studies resolved cross-sensitivity issue.

Fibre optic sensor	Categories	Solution used in study	Parameters measurement	Measurement range	Sensitivity of sensor	Reference
Fibre Bragg Grating	Multi-parameter sensing	Salt water	Refractive index and temperature	Refractive index =1.333 to 1.341 Temperature =27 °C to 45 °C	Refractive index =1.28 pm/% Temperature =9.69 pm/%	(Pereira et al., 2004)
Long-period grating	Multi-parameter sensing	Water	Refractive index and temperature	Refractive index =1.3334 to 1.4016 Temperature =30 °C to 64 °C	Dip A Refractive index =-72.003 nm/RIU Temperature =-0.3921 nm/°C Dip B Refractive index =-262.38 nm/RIU Temperature =-0.3760 nm/°C	(Jinhua et al., 2007)
High-Birefringence fibre loop mirrors	Multi-parameter sensing	Water and salinity water	Refractive index and temperature	Refractive index =1.3360 to 1.3440 Temperature =25 °C to 30 °C	Dip MMI Refractive index =90 nm/RIU Temperature =0.01 nm/°C Dip HiBi Refractive index ≈ no response Temperature =2.36 nm/°C	(Gouveia et al., 2013)

Table 6.1: Continued

Fibre optics sensor	Categories	Solution used in study	Parameters measurement	Measurement range	Sensitivity of sensor	Reference
Long period grating	Multi-parameter sensing	Water and glycerine	Refractive index and temperature	Refractive index =1.3300 to 1.3993 Temperature =30.2 °C to 70.1 °C	Refractive index =-618 nm/RIU - Temperature =0.22 nm/°C	(J. Grochowski et al., 2013)
Hybrid LPG–FBG sensing element	Compensation approach	Water and glycerol	Refractive index and temperature	Refractive index =1.334 to 1.457	Refractive index = 3120 nm/RIU	(Trono et al., 2011)

6.2.1 Experimental Set-up

A non-adiabatic tapered fibre which is immersed into the solution chamber is used as a probe and its preparation process was explained in detail in Chapter 3. In the tapering process, a small section of an optical fibre is stretched by flame brushing technique. The tapered region allows cladding modes to leak out from the core of the fibre and interact with the surrounding through the first non-adiabatic transition region. They re-enter the core through the second non-adiabatic transition region and couple with the fundamental mode that has always been propagating inside the core to create an interference pattern as shown in Figure 3.4 (b). An abrupt change in the taper angle of the transition regions causes the mode couplings to occur primarily among the cladding modes, such as LP_{01} , LP_{02} , and LP_{03} (mainly between LP_{01} and LP_{02}) (Xu et al., 2012). The result of back and forth coupling between the fundamental mode and the cladding modes of the taper produces an oscillatory spectral response. Therefore, a NATFOS behaves like a Mach–Zehnder modal interferometer (Salceda-Delgado, Monzon-Hernandez, Martinez-Rios, Cardenas-Sevilla, & Villatoro, 2012).

6.2.2 Preparation

The efficiency of this coupling is dependent on the relative phase of the participating modes. The cladding modes that interact with the surrounding medium in the tapered zone are highly sensitive to changes in the refractive index (RI) of the medium and thus can be used as a sensor with a high resolution. Mode coupling between cladding modes with different propagation constant and the fundamental mode generates a transmission spectrum with irregular fringes (Harun, Lim, Tio, Dimiyati, & Ahmad, 2013) as shown in Figure 6.1 (straight line). Because of the tapering, the overall intensity of the output spectrum reduces and it is estimated that the insertion loss of the NATFOS is approximately 19 dB. When the sensor is immersed in distill water, the noise in the spectrum almost disappears and a smoother fringe pattern can be

observed as shown in Figure 6.1 (dotted line). This is attributed to the reduction in the index contrast between water and silica compared to that of air and silica media. Subsequently, cladding modes with low eigen numbers are eliminated while the sensor is immersed in water (Harun, Jasim, Rahman, Muhammad, & Ahmad, 2013). Therefore the simplified model for the two wave interferometer transfer function is given by Equation (3.4).

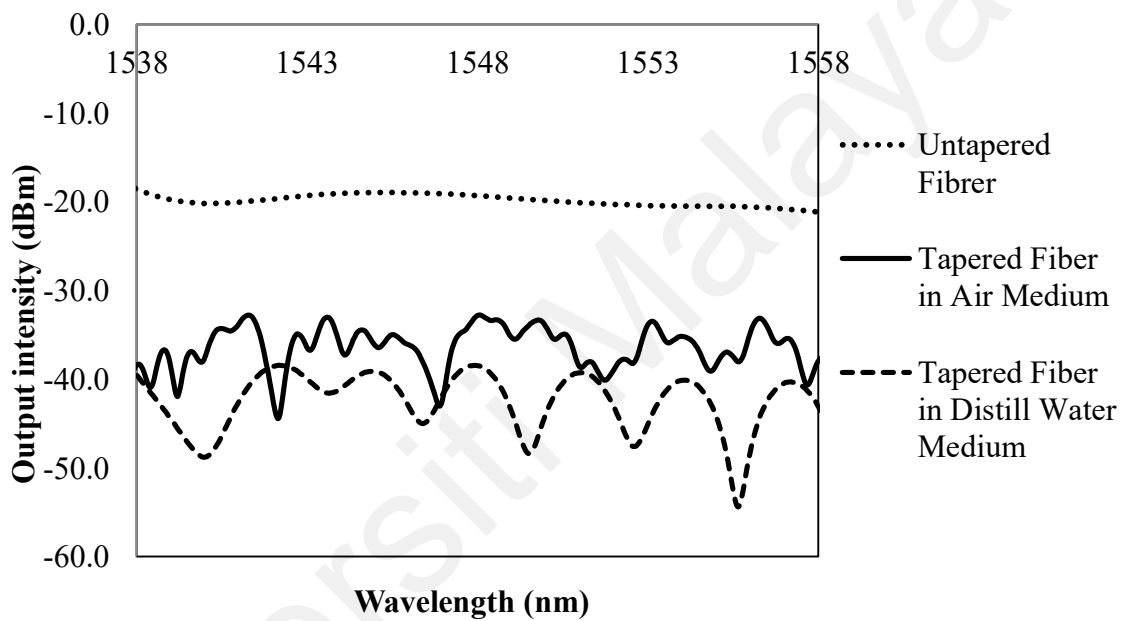


Figure 6.1: Output spectra responses for untapered fibre (dotted line), non-adiabatic tapered fibre in air medium (solid line) and non-adiabatic tapered fibre immersed into distilled water (dashed line), respectively.

The fibre sensor used in this study was fabricated by stretching a small section of a single-mode optical fibre (SMF28) by heating and drawing. The diameter of the tapered waist region, D_{waist} steadily decreased from 125 μm to about 13.2 μm under the drawing speed of 0.03mm/s. The length of the tapered section, L is approximately 30 mm. During the tapering process, light signal from an Erbium amplified spontaneous emission (ASE) source was launched into the input end of the fibre and its spectral response was monitored by an optical spectrum analyzer (OSA model Anritsu

MS9710B). Authors will focus on one particular of spectral interval, from 1549 nm to 1553 nm for the analysis as it could provide sufficient wavelength shift features to indicate RBB concentration. Increment in the analyte concentration increases the refractive index of the surrounding medium, thus decreasing the difference between the refractive indices of the core and that of the analyte. The changes in the RI difference induce the wavelength shift.

6.2.3 Remazol Black B Concentration Measurement

The sensor was immersed in Remazol Black B (RBB) solutions of different concentrations (0, 50, 100, 150, 200, 250, 300, 400, 500 and 800 mg/L). The RBB solutions were prepared by dissolving an appropriate amount of RBB powder purchased from Sigma Aldrich in distilled water. Shift of the interference peaks subject to different concentrations of RBB was measured from the baseline value of 0 ppm (distilled water). The baseline value measurement was repeated before each new RBB concentration measurement in order to maintain accurate response. This sensing baseline is only applicable for polar group dyes. As solvent is used to dissolve non-polar dyes instead of distilled water, their baseline measurement should be established using solvent rather than distill water.

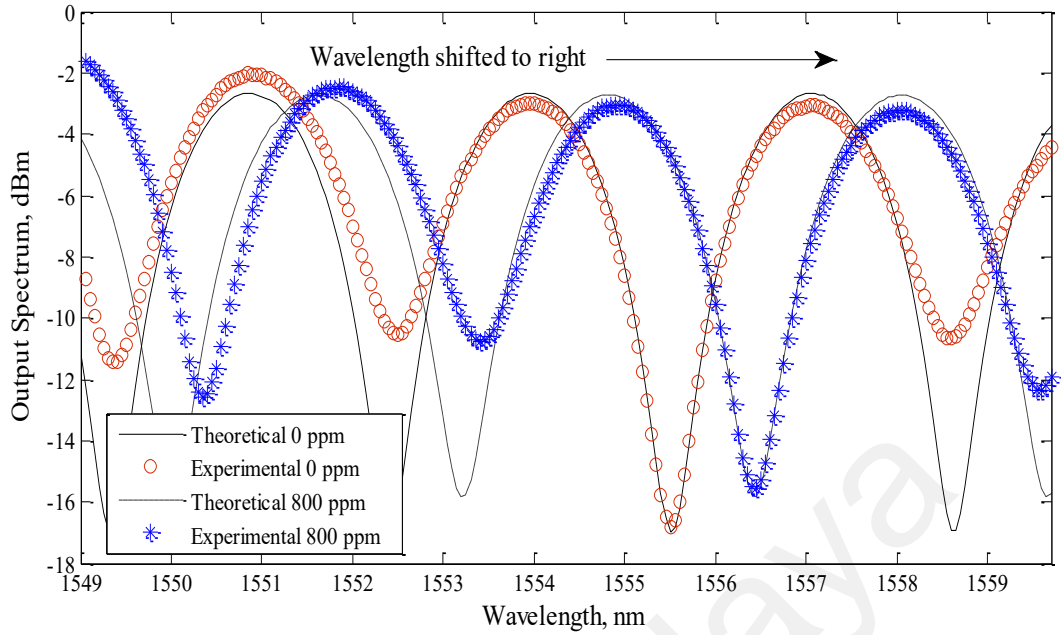


Figure 6.2: The experimental data and its best-fit curve for RBB concentration 0 ppm and 800 ppm based on the value of $I_{\text{core}}=0.28$ and $I_{\text{clad}}=0.26$ where $n_{\text{eff}}=1.3337$ and 1.2866 respectively.

The transmission spectrum of the sensor was obtained at the moment it was fully immersed in the analyte. Wavelength shift of transmission spectrum caused by the change in analyte concentration from 0 ppm to 800 ppm for experimental data fitted with the theoretical model given by Equation (3.4) is demonstrated in Figure 6.2. The transmission spectrum is shifted to right as the dye concentration in the solution increases. The refractive index of the solution increased in the order 7.0×10^{-3} RIU to a change in dye concentration from 0 to 800 ppm when characterized using a refractometer with sodium D line 589.3 nm (model Mettler Toledo RE400). Since the wavelength of the selected peak is 1550.8 nm, the value of RI measured at 589.3 nm might be different from its value at 1550.8 nm, due to the different optical dispersion characteristics of the analyte at the two wavelengths. Note also that according to studied in references (El-Kashef, 2000; Fogg, Hixson, & Thompson, 1955), the optical dispersion characteristics of the solutions are a relevant factor for the RI measurements.

The necessary adjustments had better be made using the Cauchy equation in order to obtain accurate RI value at different wavelength. Since our argument is on the change of RI value (ΔRI) relative to the baseline value at 0 ppm but not the exact RI value for each concentration. It is noteworthy to point out that the trend and rate of increase for the RI against the concentration of solutions is wavelength independent (Pereira et al., 2004). Hence, in the current study, the difference in RI that causes the wavelength to shift should be the same for both wavelengths. The plot of the wavelength shift feature against the difference in RI is shown in Figure 6.3. The sensitivity and resolution of the sensor are $1317.31 \text{ nm}/RIU$ and $2.67 \times 10^{-5} RIU$, respectively.

The wavelength shift can be utilized to infer the dye concentration of the medium with a good accuracy. The relationship between the wavelength shift and dye concentration is depicted in Figure 6.4. Its sensitivity is 0.0013 nm/ppm with a good linearity of more than 99%. Reversibility is an important feature of any sensor as it represents its sensing reliability. As shown in Figure 6.4, the output measurements were recorded as a function of concentration for two different runs with increasing and decreasing concentrations at room temperature. The results indicate that the data from the two consecutive measurements agree well with one another. Even though there appear to be differences in analyte concentration measurements between the two runs, the difference is statistically insignificant ($p < 0.05$) based on the paired t-test by SPSS (version 22). It suggests that the sensor offers a high reliability in dye concentration sensing and the overall performance evaluation of the sensor is summarized in Table 6.2.

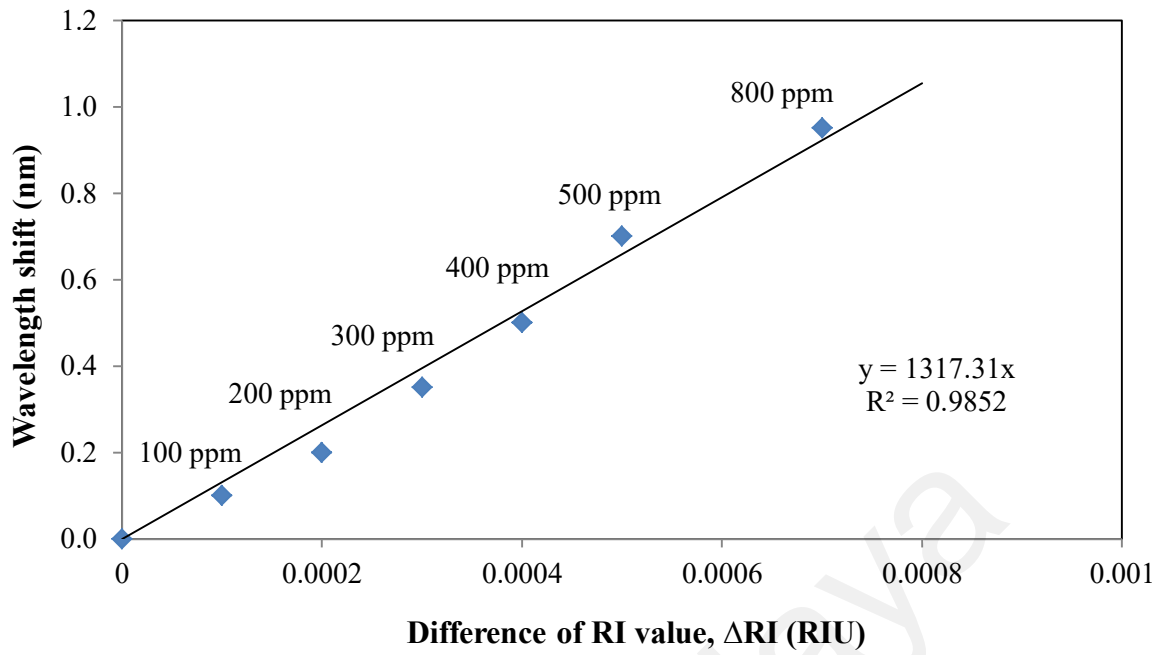


Figure 6.3: Measured wavelength shifted to right as a function of difference refractive indices of RBB solution.

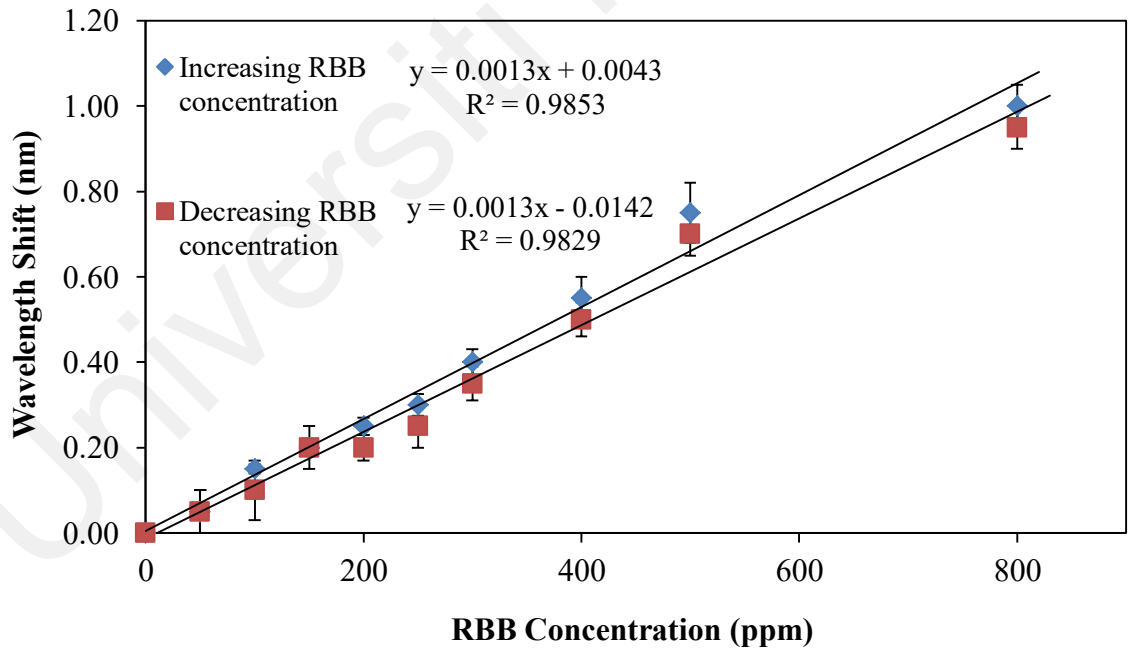


Figure 6.4: Measured wavelength shifted to right as a function of concentration for two different runs with increasing and decreasing RBB concentrations.

Table 6.2: Overall performance of the developed sensor.

Parameters	Concentration (ppm)		Refractive index (RIU)
	Increasing	Decreasing	
Sensitivity	0.0013 nm/ppm	0.0013 nm/ppm	1317.31 nm/ppm
Linearity	99.26%	99.14%	99.25%
Standard deviation	0.0408 ppm	0.0421 ppm	0.0352 RIU
Resolution	31.41 ppm	34.46 ppm	$2.67 \times 10^{-5} RIU$

6.2.4 Effect of pH

Alteration in pH to optimize the performance of water treatment sometimes is necessary. As a sensor which might operate in wastewater treatment plant, accurate measurement in diverse and challenging fields is required. One of the concerns is possible reduction or increase in sensitivity of the sensor in acidic and alkaline RBB solution. Its measuring stability was studied using RBB solutions in concentration of 100, 200 and 300 ppm. In the experiments, the pH of the dye solutions was adjusted over the range of pH 2.41 to pH 11.10 using 0.5M hydrochloric acid or 0.5M sodium hydroxide solutions. The wavelength response was found shifted to the left for highly acidic RBB solution while the opposite was observed for alkaline RBB solution. These results are illustrated in Figure 6.5. In this study, bias less than or equal to 10 % against actual value of measurement can be considered less susceptible towards the cross-sensitivity. It seems the wavelength of the spectrum peak, is only affected at the extreme ends of pH range. Further investigation using t-test result from SPSS (version 22) shows that the shift is statistically insignificant ($p < 0.05$) within the pH range of 3.07 to 10.09. It suggests that the spectral transmission is not affected within that range. But

when the pH range is extended to pH 2.41 and pH 11.35 respectively, it becomes statistically significant ($p > 0.05$).

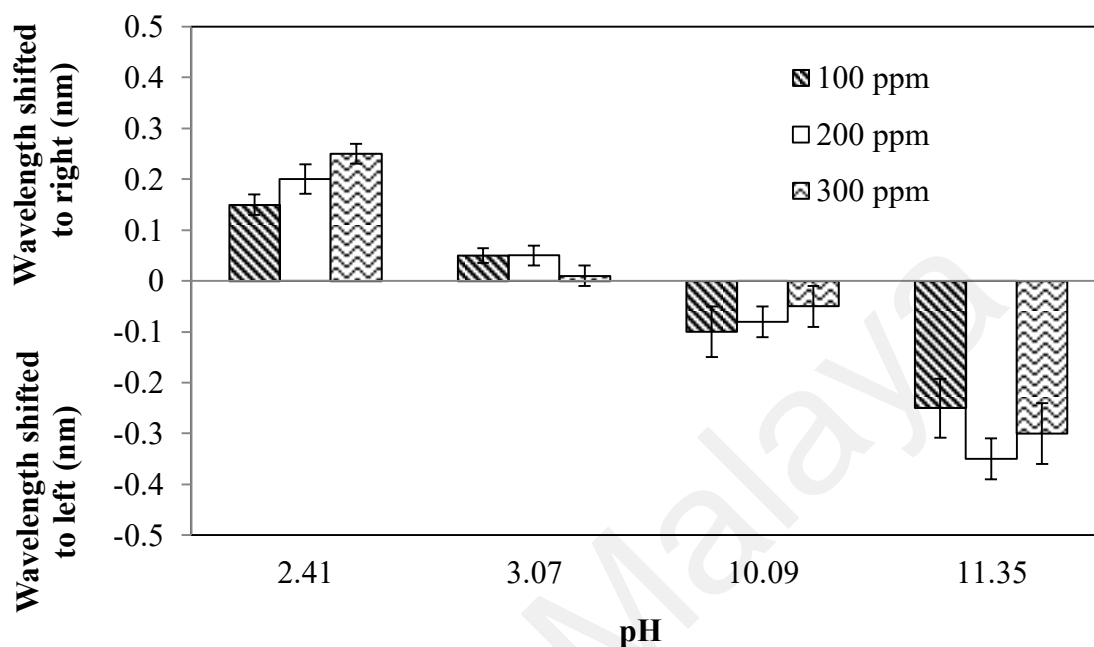


Figure 6.5: Plot showing the stability of the sensor during repeats measurement of analyte in 100, 200 and 300 ppm respectively over pH ranged 2.51 to 11.35.

It was found that the refractive index of the RBB solutions is independent of the pH within the range of 2.41 to 11.35. Therefore, the shift of wavelength was not due to changes in the optical properties of RBB but the interaction between the dye and the silica of the fibre core (Deboux, Lewis, Scully, & Edwards, 1995). In neutral condition, the surface of silica was without net surface charge or potential. When the silica was immersed in aqueous solution, H^+ and OH^- ions reacted with the surface to form an amphoteric hydroxylated layer. At low pH, there was a high concentration of H^+ ions which induced positive surface charge on the silica. As the pH of the solution increased, the concentration of H^+ ions reduced and the solution contained an excess of OH^- ions which caused a net negative surface charge on the silica. At a lower or higher pH value, more positive or negative charges accumulate on the fibre surface and thus attract a

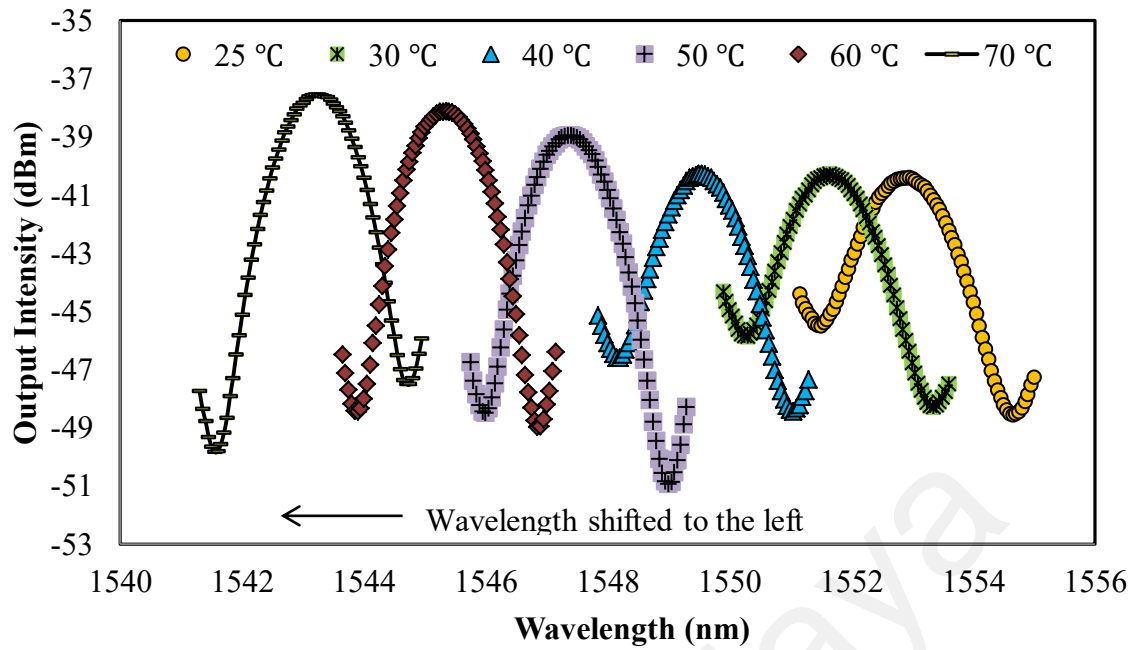
larger number of polar chromophores within the evanescent field region (P. G. Lye, M. Boerkamp, A. Ernest, & D. W. Lamb, 2005). This accumulation leads to changes in optical throughput which increases the wavelength shift in the spectra. In pH adjustment experiment, strong acid (acid hydrochloric) and strong base (sodium hydroxide) were used since they completely dissociate and ionized in dilute aqueous solutions. If buffer solution is used to adjust the pH of the analyte, a greater amount of buffer is required since it is a weak acid or base of which decreasing the effective mass ratio of RBB and aqueous.

6.2.5 Effect of Suspended Solid On Sensing Efficiency

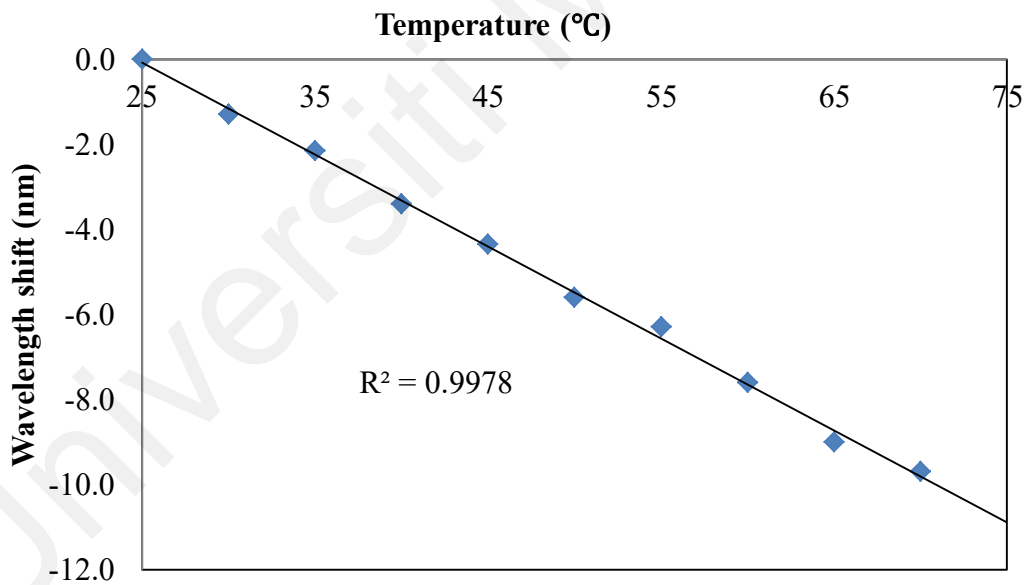
In this subsection, the effect of turbidity on the sensor performance is investigated. Turbidity is defined as the cloudiness of water or the extent to which light is scattered in water (Campbell, Laycak, Hoppes, Tran, & Shi, 2005). During sensing, light beam could be scattered or absorbed by suspended solids (SS) in a water sample, affecting the accuracy of measurement. In this work, the system performance was evaluated using clay suspensions (1mg/L, 3 mg/L, 5mg/L and 10 mg/L) by suspending clay particles with a size ranging from 0.001–0.002 mm in water (refractive index approximately equal to 1.33 in room temperature). It is obtained that the experimental results were fluctuated except for the sample with the lowest SS, 1mg/L. It was suggested that great variability could be caused by high content of suspended particles, which could be detected by visual inspection. In fact, SS in the sample can affect the light transmission between the emitter and receiver fibres, causing signal variability. The results suggest that the sensor could be used for sensing but mainly for water with a low concentration of suspended sediments (approximately 1mg/L). Pre-filtration of sample is necessary to minimize the interference of suspended solids during sensing.

6.2.6 Effect of Temperature on Sensing Efficiency

Changes in the temperature of the analyte can shift the peak of the spectrum. This is because cladding modes may have different mode field areas and sensitivities under different ambient conditions. The effect to the higher order modes that propagate in the cladding of the sensor is considerable as it is highly sensitive to the refractive index of the sensing medium. The effect of temperature variation was studied at a constant RBB concentration of 400 ppm within the temperature range of 25°C to 70°C with a temperature interval of 5 °C. The wavelength shift against temperature change is outlined in Figure 6.6 (a). The Figure 6.6 (b) shows the wavelength is shifted to left in a linear function as the solution temperature increases from 25 °C to 70 °C due to the thermo-optic effect that changes in the effective RI of the medium (Villatoro et al., 2007). In turn, the change in the effective RI of the medium alters the optical path of the different modes, thus changing the optical path difference (OPD) of the fundamental and cladding modes that prompts the wavelength shift (Gong et al., 2014). Therefore, different amount of wavelength shift was used to infer the temperature and dye concentration of an analyte containing Remazol Black B.



(a) Output spectrum against temperature



(b) The peak wavelength shift against temperature

Figure 6.6: The performance of the proposed sensor at various ambient temperatures when the RBB dye concentration is fixed at 400 ppm (a) output wavelength and (b) wavelength shift.

6.2.7 Development of a Temperature Compensation Model

If the temperature of the analyte is not kept constant during the dye concentration measurement, error may result due to cross sensitivity. Therefore, there is a need to compensate for this temperature effect and modify the model obtained at room temperature to account for temperature variation using the so-called temperature compensation model (Gardner, Young, Sloan, Robinson, & Miner, 2006).

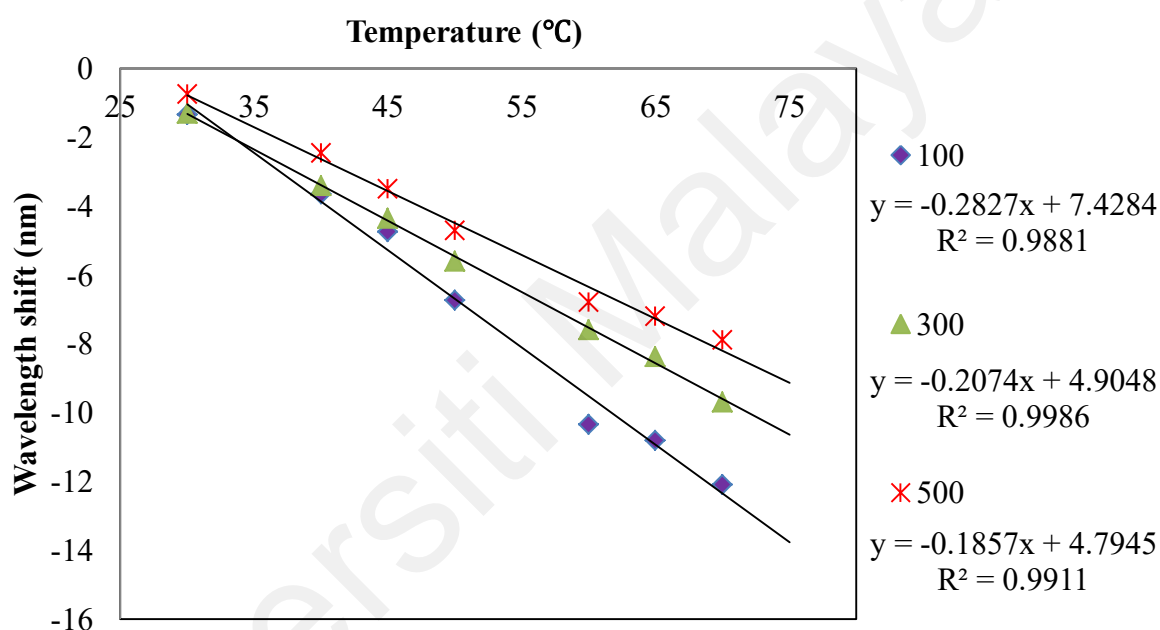


Figure 6.7: Responses of wavelength shift for the RBB with different concentrations which operate in temperature ranged from room temperature up to 70°C.

The temperature effect was experimentally measured by using RBB solution with concentrations of 100 200, 300 400 and 500 ppm respectively where the temperature of the analyte was increased from room temperature up to 70 °C. This temperature range is sufficient for dye concentration measurement in most industries and experimental conditions. The experimental results are shown in Figure 6.7 and it is observed that the wavelength shift to left linearly with the increase in temperature from 26° and 70° C. It can be observed that as the temperature increases, the measured

wavelength shift is more noticeable. The sensitivity of the sensor towards temperature in each concentration is represented by the slopes of the lines. The negative sign in the slopes shows that the spectrum shifts to a shorter wavelength as the temperature increases. The slopes attained at various dye concentrations are plotted in Figure 6.8. Then a curve is fitted to the slope values to obtain a relation as expressed in Equation (6.1).

$$\text{Slope, } \Delta\lambda/\Delta T = 0.0416 * \ln(\text{Concentration of analyte}) - 0.4491 \quad (6.1)$$

where $\Delta\lambda$ and ΔT can be calculated based on the values of the current λ and T with the reference values of RBB in 0 ppm at room temperature. Then the concentration of the analyte can be predicted from Equation (6.1). Using this equation, the effect of temperature variation can be compensated and dye concentration can be determined.

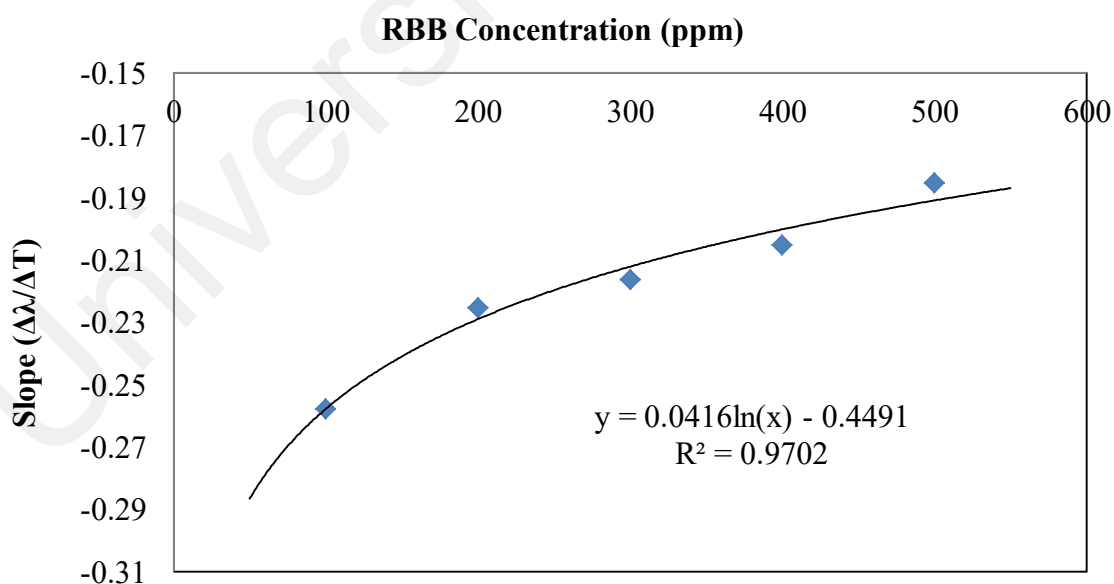


Figure 6.8: A temperature correction factor model developed from various sensitivity of sensor towards temperature in different concentrations of solution.

In order to verify the accuracy of the sensor, the established models are utilized to predict dye concentration with the effect of cross sensitivity by temperature. The model validation experiments were conducted to predict various concentrations of RBB solutions at temperatures of 35, 45, 55, and 65 °C. The experimental and predicted results are shown in Figure 6.9. The reliability of the developed sensor with presence of temperature cross sensitivity were evaluated in terms of correlation coefficient (R^2), root mean square error (RMSE) and mean absolute percentage error (MAPE), respectively. The following interpretations can be made regarding the sensor performance evaluation. There was good agreement between the predicted and actual value if the high R^2 value (maximum equal to one) and low RMSE and MAPE value (minimum equal to zero) could be achieved and accordingly indicates that the model performs successfully as expected. The calculated values of these statistical criterias are $R^2 = 0.9782$, $RMSE = 18.9040$, $MAPE = 6.9677$. Temperature compensation model eliminates most of the temperature dependent measurement error from the sensor. Thus, it minimizes the error induced by temperature variations and the expected measurement value of dye concentration could be achieved with low RMSE and MAPE.

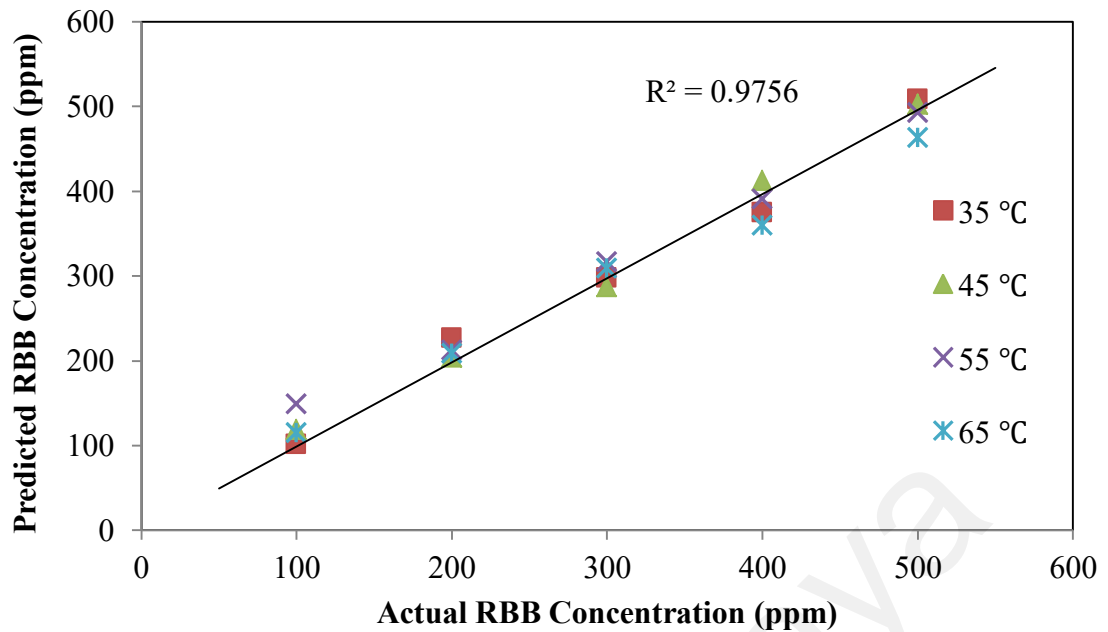


Figure 6.9: Cross-correlation of the actual and predicted dye concentration by taking the temperature effects of cross sensitivity into account.

Refractive index spike may occur if other contaminants are present in the solution. Thus, the temperature compensation provided by the Equation (6.1) may not be totally effective. Another validation experiments conducted under similar conditions were performed using RBB dye solution with 100, 200, 300, 400, and 500 ppm mixed with potassium hydrogen phthalate (KHP) solution (200 mg/l CRM traceable to SRM from NIST solution to distilled water). KHP was chosen as it is a common standard for chemical oxygen demand testing which quantify the amount of oxygen required to oxidize organic compounds to carbon dioxide and water. The same sensor was subjected to the validation experiments and the results are shown in Figure 6.10. It can be observed that there exists a good agreement between the predicted and actual data with a goodness of fit (R^2) of more than 0.9. However, the RMSE and MAPE increase to 35.9441 and 17.8434 respectively. This might be attributed to the presence of other contaminants which might affect the refractive index of solution and induce a different behavior of the mix towards temperature (Tan & Huang, 2015). The temperature

compensation model presented here was developed according to Remazol Black B as sensing medium and examined in a limited range of concentrations. In order to improve the applicability of temperature compensation model, the model can be established and tested holistically by including a series of representative organics and inorganics solutions with many concentration levels.

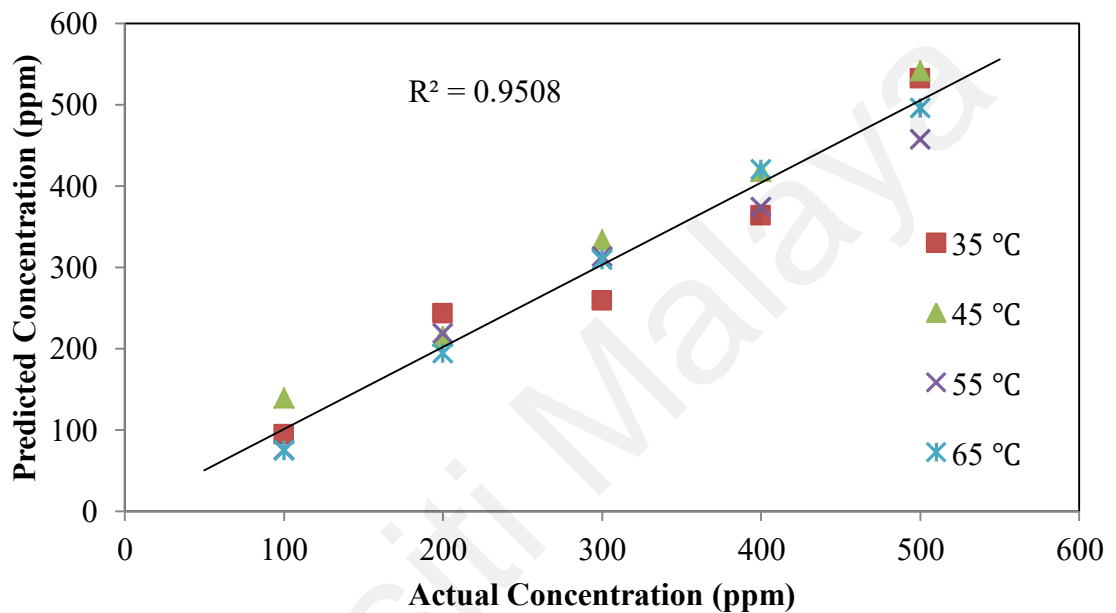


Figure 6.10: Cross-correlation of the actual and predicted dye concentration from mixture solution (RBB and KHP) by taking the temperature effects of cross sensitivity into account.

6.3 Dual Output Approach in Dye Concentrations Determination

Measuring the refractive index or concentration of a solution by analyzing the spectral shift response of a fibre optics sensor is a powerful method. However, in reality, absorbance measurement technique is normally used to characterize its dye concentration. The drawback of the absorbance measurement is that, once the concentration of the analyte reaches a certain level, there will not be enough transmission data available due to the opacity of the analyte. Usually, the absorption spectrum (intensity ratio) and the refractive index of a medium are measured separately

using different experimental setups. However, a more accurate dye concentration measurement may be achieved if the absorption spectrum and the refractive index of the medium are analyzed together. In section 6.3, the concentration of Remazol Black B (RBB) dye solution is firstly determined by characterizing the absorption spectrum of the transmitted light. Then the dye concentration is predicted from the refractive index of the analyte inferred from the peak wavelength shift. Finally, both parameters are used simultaneously to estimate the dye concentration. The novelty of this work lies in combining the absorption spectrum and wavelength shift from a single experimental setup to provide an accurate dye concentration estimate. Then the concentration estimates from absorption spectrum only, wavelength shift only and their combination are compared in terms of accuracy, sensitivity and validity.

6.3.1 Preparation

The experimental setup is depicted in Figure 3.4 (a) where ASE light source is injected into the NATFOS and the output is analyzed by OSA and power meter. The resulting microfibre had a final diameter of approximately 10 μm over a length of about 30 mm with conical transitions at both ends. Then Remazol Black B (RBB) solutions of different concentrations (50 until 250 ppm with 50 ppm increment) were prepared by diluting the stock solution to the desired concentrations. The experiment starts by immersing the tapered section of the NATFOS into the sample with 0 ppm of RBB (pure distilled water) to obtain the initial sensing value as a reference point to investigate the change in output intensity and spectra shift of the interference peaks when the NATFOS is subjected to different concentrations of RBB later (Hu, Zhao, & Hu, 2014).

6.3.2 Absorption Characteristics

The performance of the sensor is evaluated by measuring the output intensity of the transmitted light, absorption characteristics and extinction ratio of the output comb spectrum at different concentrations of RBB solution. 1546 nm to 1553 nm region was chosen for the analysis as it could provide enough absorption features for dye solution that is sufficiently higher and more dominant than the other light intensity attenuation effects occurring in the analyte (Harun, Jasim, et al., 2013). By increasing the dye concentration, the difference in the effective refractive index between the NATFOS and analyte (sensing medium) also increases which results in wavelength shift. This wavelength shift can also be used to infer the dye concentration. In order to improve the accuracy of the system, dye concentration estimation was also carried out by coupling the output intensity and wavelength shift. The RBB dye concentration, C is first determined by measuring the change in output intensity, I_{dye} arising from the evanescent field of light in the sensing region, L . The relation between the output intensity and the RBB dye concentration follows the Beer-Lambert's law, as in Equation (2.3). This is due to the increase of chromophore content in the solution which absorbs the propagating light. The relation between the light absorbance, concentration of solution and the length of the tapered fibre region, l , can be expressed as in Equation (6.2) (Garcia-Rubio, 1992):

$$\ln (I_{dye}/I_0) = -\varepsilon Cl + E_1 \quad (6.2)$$

where I_{dye} , I_0 , ε , C , l , E_1 are interpreted as output intensity of analyte sensing, output intensity of distilled water (baseline) sensing, absorption coefficient, concentration of analyte, length of tapered fibre (absorbing path) and experiment constant value, respectively. The peak absorption data plotted in the logarithmic scale against the

concentration of RBB displays a linear relationship where the value of the absorption coefficient, ϵ could be derived from slope of the straight line, as illustrated in Figure 6.11. Evanescent field generated around the tapered area of the optical fibre causes light to scatter from the tapered region into the RBB solution (sensing medium). The analyte absorption directly affects the penetration depth and energy of the evanescent wave. It is observed that more light is absorbed at the given wavelength when the chromophore content of the aqueous solution increases. This decreases the output intensity of light transmission, resulting in reduction of the in-fibre light energy. This finding can be used to estimate the dye concentration of an RBB analyte based on its absorption spectrum.

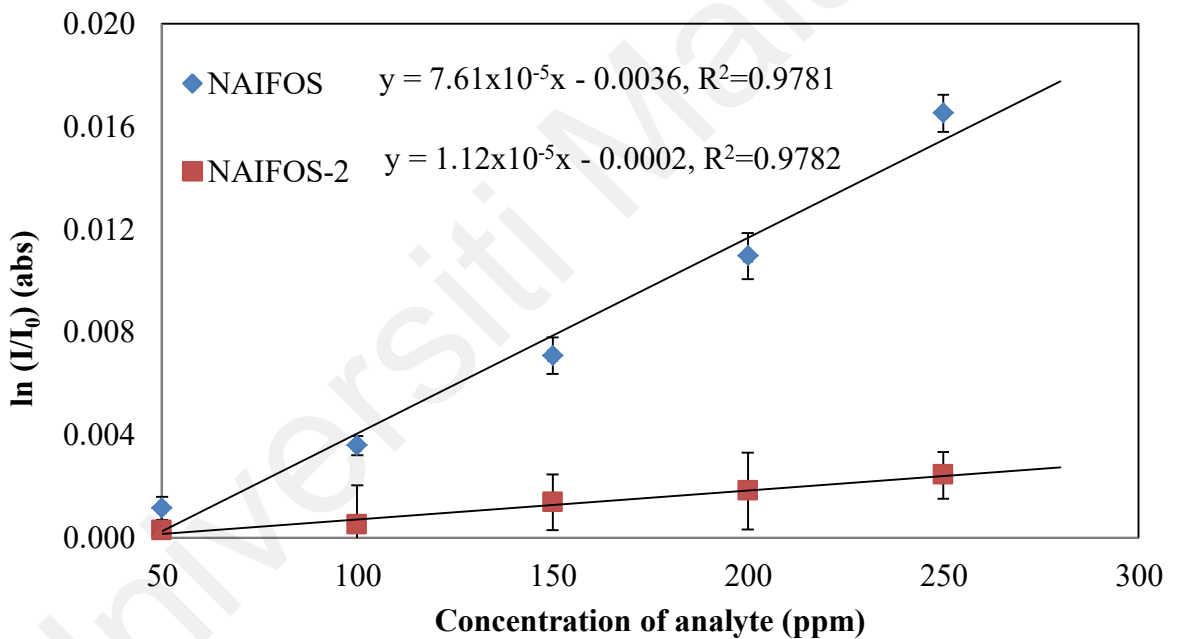


Figure 6.11: Delineating curves of the absorbance for analyte sensing with different concentrations of RBB.

6.3.3 Wavelength shift Characteristics

The wavelength shift can also be used to infer the dye concentration of the RBB solution. The two light modes that propagate in the core and passive cladding (sensing medium) interact along the NAFOS and recombine at the output end of the conical transition region. As the two modes propagate in media with different effective

refractive indices, phase shift occurs when they recombine causing interference pattern in the transmission spectrum. Changes in the concentration of the analyte can be inferred from the interference pattern of the transmitted light, in particular the wavelength shift. A considerable right-shift in the wavelength of the output spectrum is observed with increasing dye concentration in the analyte. Changes in dye concentration in aqueous solution cause different polarities of the ground and excited states in the solution. The difference in energy (increment or reduction) between these level states is called dipolar coupling which can cause interference spectral shifts (Helseth, 2012). This affected the evanescent field, leading to changes in optical throughput. Characteristic shift-to-right (red shift) occurs while the dye concentration in the solution was increased in the studied system. It can be observed that it shifts to the right as the dye concentration increases. The amount of wavelength shift against the increment of concentration is shown in Figure 6.12, which indicates a linear relationship with sensitivity of 0.0045nm/ppm. Therefore, working backward, the attenuation wavelength shift can also be used to infer the dye concentration of the medium. Regression coefficient values, R^2 alone is not sufficient to estimate the accuracy of the models. Therefore, a few relevant statistical criteria are added and they are regression coefficient values, standard deviation, limit of detection and linearity as outlined in Table 6.2. The sensor is observed to be sufficiently stable for absorption and wavelength shift changes with standard deviations of 0.0015 and 0.0647 nm respectively. In summary, both the absorption $\ln(I_{\text{dye}}/I_0)$ and wavelength shift $\Delta\lambda$ of the output can be used to predict the concentration of the medium.

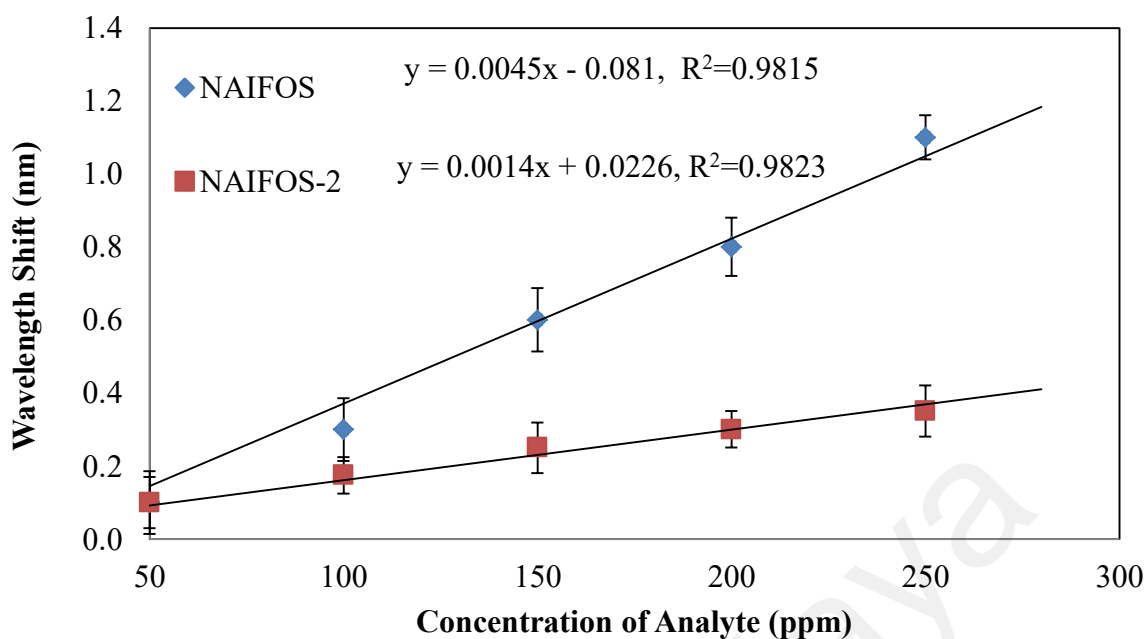


Figure 6.12: Measured attenuation wavelength shifted to right as a function of concentration of RBB

Table 6.3: Performance of NAFOS with two different predictive models

Parameter	Output	
	Absorption (abs)	Wavelength shift (nm)
Sensitivity (slope of graph)	0.000076	0.0045
Regression coefficient value	0.9781	0.9815
Standard deviation	0.0015	0.0647
Limit of detection	20.04 ppm	14.39 ppm
Linearity	98.89%	99.07%

6.3.4 Coupling the Two Responses and Validation

Perhaps, coupling these two responses would result in a more accurate determination of dye concentration. A simple dye concentration prediction that

combines both the absorption and spectral shift is obtained by averaging the results of the ones determined using absorption, and attenuation wavelength shift, $\Delta\lambda$ separately. The accuracy and performance of the three models using i) absorption only ii) wavelength shift only and iii) the average of the two, are tested in measuring RBB analytes with concentrations ranging from 50 to 250 ppm. The difference between the actual and predicted dye concentrations were evaluated according to correlation coefficient (R^2), root mean square error (RMSE) and mean absolute percentage error (MAPE), as stated in Equation (2.12), (2.13) and (2.14), respectively.

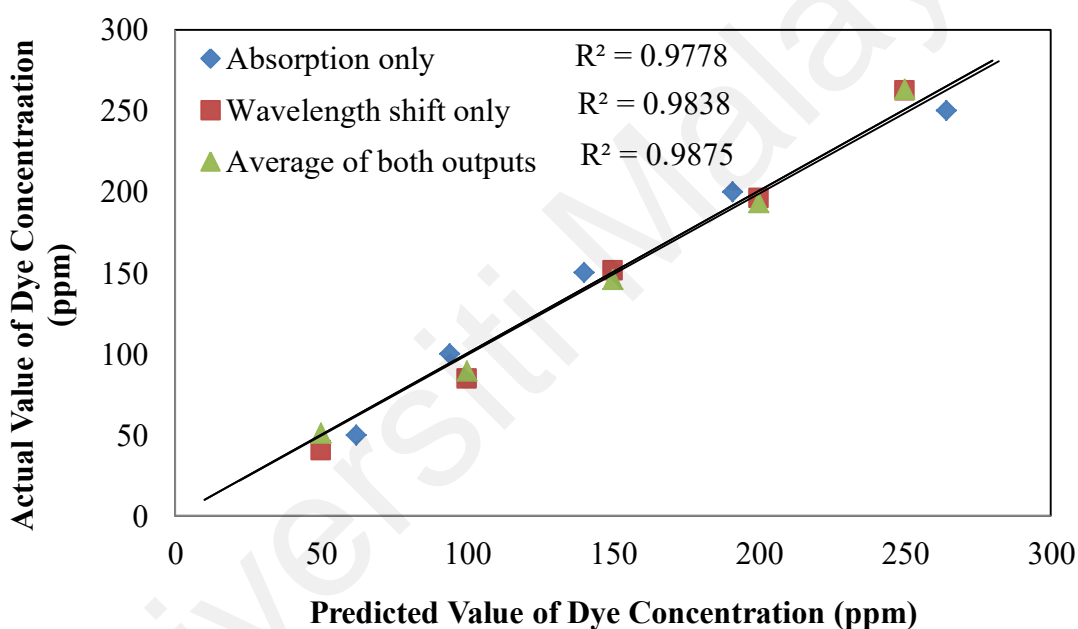


Figure 6.13: Cross-correlation of actual and predicted values of RBB dye concentrations in three approaches

The results obtained using absorption and wavelength shift are compared with the one acquired using the average of the two, as illustrated in Figure 6.13. The R^2 for the models using absorption only, wavelength shift only and their average are 0.9778, 0.9838 and 0.9875 respectively. The model that employs the average of the two responses achieves the best prediction with the highest R^2 and the lowest RMSE and MAPE. This finding shows that the accuracy of dye concentration obtained from

averaging the two responses is more accurate than the ones obtained from using absorption or wavelength shift alone. The values of these statistical criteria are given in Table 6.4.

The experiments were repeated under similar conditions using another NATFOS, namely NATFOS-2 to show repeatability of the proposed method in predicting the dye concentrations from 50 to 250 ppm. NATFOS-2 had a diameter of approximately 21.4 μm over a length of about 30 mm with conical transitions at both ends. The results are analyzed as before and demonstrated in Figure 6.11 and Figure 6.12. In addition, the cross-correlation of the actual and predicted values of RBB dye concentration by the three approaches were evaluated and shown in Figure 6.14. It can be observed that there are a considerable agreement with a satisfactory goodness of fit (R^2 more than 0.9) between the actual and predicted data for the three models. The model that uses both absorption and attenuation wavelength shift together records the highest R^2 and the lowest RMSE and MAPE. Therefore, it can be inferred that the accuracy of the dye concentration predicted by the combined model is higher than the ones obtained using absorption or wavelength shift only. Table 6.4 summarizes the results of the three approaches.

In short, a better prediction is obtained by averaging the outputs of the two models using intensity absorption and spectral shift. It is worth noting that there exist a possibility where both models over or under estimating the actual concentration. Under these circumstances, the average will be worse than the better of the two. So far, in an extended experiment involving many concentration levels using both NATFOS and NATFOS-2 sensors, the results are positive. From the data gathered, the possibility of both models over- or under-estimating the actual concentration is less than 0.3. This suggests that in the majority of the cases, averaging them increases the accuracy of the

prediction. Since in most practical applications users do not know the actual value, averaging the two measurements is the best option.

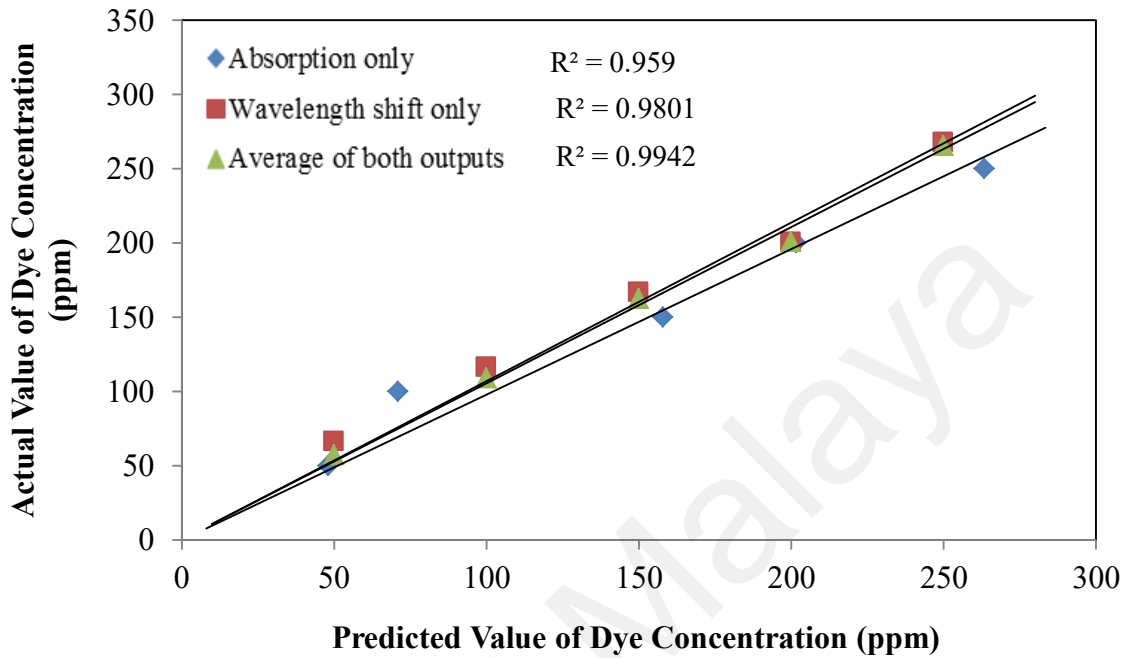


Figure 6.14: Scatter plots of the actual value compared to predicted value for average of both outputs using NATFOS-2.

Table 6.4: Performance indices (R^2 , RMSE and MAPE) for models using two different NATFOS.

Statistic criteria	Predictive Model					
	Absorption only		Wavelength shift only		Average of both outputs	
	NATFOS	NATFOS-2	NATFOS	NATFOS-2	NATFOS	NATFOS-2
R^2	0.9778	0.9590	0.9838	0.9801	0.9875	0.9942
RMSE	11.9680	14.7390	11.1078	19.7689	7.6761	7.9106
MAPE (%)	8.7736	8.8611	7.700	16.7847	4.1257	5.1934

In Section 6.3, the author is mainly interested in introducing a new approach of analyzing the dye concentration of an analyte by combining the two typical responses – absorption and wavelength shift. The hybrid analysis in the optical system presented here was only tested on Remazol Black B in a limited range of concentrations. It is noteworthy to point out that the results can be improved by increasing the range of dye concentrations tested. Besides, it should be noted that the measured spectra shifts and the absorption of light changed slightly when a different sensor is used as each sensor is uniquely fabricated.

6.4 Summary

Cross sensitivity due to temperature variation and the presence of other contaminants in an analyte could affect the accuracy of concentration measurement made by a sensor. A miniaturized non-adiabatic interferometer fibre optic sensor (NATFOS) is used to monitor the Remazol Black B (RBB) dye concentration in the presence of other contaminants, pH adjustment and temperature variation. The objective of this experiment is to investigate the ability and accuracy of the sensor to monitor RBB concentration under the influence of cross-sensitivity from a single spectrum, which is considered as an advantage over traditional sensing techniques. The developed sensor shows a dye concentration sensitivity of 0.0013 nm/ppm between 0 to 800 ppm when conducted room temperature without the presence of other contaminants. The influence of pH, suspended solids in the sample and temperature variation on the accuracy of the measurement is also examined. The results show that the sensor could still provide an accurate measurement if the pH value falls between 3.07 and 10.09 with very low concentration of suspended solids (approximately 1 mg/L). In addition, a corrective measure for temperature bias is carried out by compensating the cross-sensitivity effect and a model for temperature compensation is established. This might

well be the first attempt to establish temperature correction and compensation for optical fibre sensing using non-adiabatic tapered fibre sensor. In extended experiments involving many concentration levels, the results obtained are encouraging.

In the extended experiment, two output variables in the form of absorption and wavelength shift were used to infer the dye concentration of an analyte containing Remazol Black B. The system could measure the dye concentration of the analyte within a range of 50 ppm to 250 ppm with sufficient sensitivity and configurability. A new predictive model was formulated by combining the predicted dye concentrations of absorption and wavelength shift with equal weightings. Then an experiment was performed to measure the accuracy of the models that use absorption, wavelength shift and their combination to predict the concentration of an analyte in the range of 50 ppm to 250 ppm. The differences between the actual and predicted dye concentration values were evaluated. The results show that by combining the two parameters, a better estimate ($R^2=0.9875$, $RMSE=7.6761$, $MAPE=4.1257$) of the dye concentration with higher correlation and lower error can be achieved. Finally, an additional experiment is conducted to validate the accuracy of the sensors.

CHAPTER 7: CONCLUSIONS AND RECOMMENDATIONS FOR FUTURE

WORK

7.1 Conclusion

Tapered fibre is known to be very susceptible to minute change of ambient condition. The current research aimed at investigating the possibility of applying three types of tapered fibre optic sensors, namely the tapered plastic optical fibre, core mismatch tapered fibre and non-adiabatic tapered fibre sensors for measuring Remazol Black B dye concentrations. Since each sensor was uniquely fabricated, they had different working principles and sensing capabilities. The cross sensitivity effects were quantified in order to improve the efficiency and precision of the developed sensors. In this study, the cross sensitivity issues were overcome by compensating the effects or realizing the multi-parameter sensing capability. Furthermore, predictive model was proposed and demonstrated as an efficient tool for improving the efficiency of the sensing system.

The research started with fabrication of tapered plastic optical fibre sensor (TPOF) with different diameters: $d = 0.65$ mm, 0.45 mm, and 0.35 mm, using chemical etching technique. The performance of TPOF of different diameters in measuring the concentration of RBB aqueous solutions was investigated. The sensors were easy to fabricate and easy to handle with a good sensitivity, linearity and reproducibility. Although the sensitivity of the sensors was enhanced when the thickness of the cladding decreased, they became more vulnerable to the influence of the temperature of the analyte. Therefore, three model equations were introduced and validated to make appropriate adjustment to compensate for the temperature bias in the output reading. The POF with $d = 0.45$ mm displayed good sensitivity and adequate stability within the tested temperature range. Knowledge of the optimum diameter of the tapered sensor for

the operating temperature and RBB concentration range is useful for developing an efficient sensor for the target application. Based on the experimental data, Multiple Linear Regression (MLR), Central Composite Design (CCD) and Neuro-fuzzy Inference System (ANFIS) models were developed. The predictive capabilities of the models were evaluated in terms of correlation coefficient, root mean square error, value accounted for and mean absolute percentage error. Given an intensity ratio value, the models were used to predict the concentration of the RBB solution. Then, the discrepancies between the predicted and measured values were calculated and summarized. In general, all models showed fairly high accuracy in estimating the RBB concentrations with ANFIS showing the best performance. The models could be useful at the preliminary stage of designing a wastewater treatment plant.

Mach-Zehnder interferometer fibre optic sensor was fabricated by bridging two single-mode fibre (SMF) with a tapered multimode fibre (MMF), namely core mismatch fibre optic sensor (CMFOS). MMF of three different diameters: 27.7 μm , 23.2 μm and 19.5 μm , were tested to investigate the effect of diameter on the sensitivity of the sensor. The response surface methodology (RSM) results indicated that the sensor with the thinnest MMF diameter produced the strongest evanescent field that interacted with the analytes and thus showed the highest sensitivity. In addition, using RSM, two output variables in the form of intensity ratio and spectral shift were found significant to infer the dye concentration. ANFIS was utilized to evaluate the two output variables in predicting RBB concentrations. The prediction capabilities of the models were evaluated in terms of R^2 , RMSE and MAPE values.

In addition, CMFOS was used for the first time for measuring dye concentration and temperature to resolve the cross-sensitivity effect. One of the unique advantages of the proposed sensor was its capability of measuring multiple parameters by only one sensing element and its simple signal processing method. It was observed that the

wavelength of the interference spectrum was red-shifted against dye concentration increment and blue-shifted against temperature increment. The proposed sensor held a high linearity, good reversibility performance and high accuracy of the forecasted values of dye concentration or temperature measurements. The results revealed that this sensing device worked efficiently and exhibited a great potential for sensing multiple parameters with further research and development. The results indicated the potential of the sensors to be used for online monitoring of wastewater quality in the future.

Furthermore, a non-adiabatic tapered fibre optic sensor (NATFOS) was utilized to measure the concentrations of Remazol Black B (RBB) solutions in the presence of other contaminants, different pH conditions and temperature variations. The experimental results demonstrated that the sensor worked efficiently with a sensitivity of 0.0013 nm/ppm under room temperature. It showed an excellent reversibility and stability under diverse conditions within a wide pH range from 3.0 to 9.4. A temperature compensation model was introduced and applied to overcome the bias caused by temperature cross sensitivity and the accuracy of the predicted results was verified. NATFOS was developed for measuring the change of concentrations of Remazol Black B analytes by monitoring the light absorbance and attenuation wavelength shift of the output. This was the first attempt to combine and analyze the two responses simultaneously in a single setup. The result was positive in the extended experiments with different concentration levels. In reality, most users do not know the actual concentration level of pollutants and the mean of the predicted values is commonly used to estimate the pollutant concentration. The sensor and its hybrid analysis could be useful monitoring tools as they were highly sensitive towards changes in refractive index and absorption. The validity of the reported sensing technique was highly promising.

7.2 Knowledge Contribution to the Field

1. A simple sensing technique was developed to measure dye concentration using tapered fibre optic sensors. Higher sensitivity can be achieved by modifying the configuration of the fibre since the sensitivity of the sensor is heavily influenced by the diameter of the fibre.

2. It was found that the cross sensitivity effects could be quantified and compensated. The study showed that the core mismatch fibre optic sensor was capable of measuring multiple parameters by utilizing the cross-sensitivity approach. The results showed that tapered fibre optic sensors could measure a number of discrete points accurately and precisely over a continuous region.

3. A simple compensation process to resolve the inherent cross-sensitivity problem was realized by applying a simple signal processing method, as shown in the study of tapered plastic fibre optic sensor and non-adiabatic fibre optic sensor. Therefore, the operating cost of the sensors should be considerably less than that of a conventional sensor that requires complex compensation processes.

4. Reliable predictive models were established by using soft computing techniques or dual output approach. The models provide a simple and accurate technique for real time measurement and open up the opportunity of non-invasive monitoring technique to control the dosage of chemicals in a water treatment system.

7.3 Recommendations for Future Work

The application of tapered fibre optic sensors for dye concentration measurement is still in its early stage and further research, development and enhancement are needed before the sensors can be commercialized. The system can be improved in the future by conducting the recommended research below:-

1. Extensive studies in discriminating dyes from different solutions are necessary in order to demonstrate the feasibility and practicability of the fabricated sensors in the sensing application. Coated fibre-optics sensors could enhance the selectivity of measurement and enable better resolution.

2. Data analyses can be conducted by using more powerful signal processing approaches to further improve the accuracy of the measurement. The proposed sensing systems require intensity referencing due to unwanted loss, which may be due to variation in the output power from the light source, temperature, fibre bend loss and ageing of components.

Universiti Malaysia

REFERENCES

- Abbott, L.C., Batchelor, S.N., Smith, J.R.L., & Moore, J.N. (2010). Resonance Raman and UV-visible spectroscopy of black dyes on textiles. *Forensic Science International*, 202(1-3), 54-63. doi: <http://dx.doi.org/10.1016/j.forsciint.2010.04.026>
- Ahmad, A.B.H. (1994). *Development of a Portable Optical Fibre Chemical Sensor Measuring Instrument*. (Doctor of Philosophy), University of Manchester, United Kingdom.
- Alves de Lima, R.O., Bazo, A.P., Salvadori, D.M.F., Rech, C.M., de Palma Oliveira, D., & de Aragao Umbuzeiro, G. (2007). Mutagenic and carcinogenic potential of a textile azo dye processing plant effluent that impacts a drinking water source. *Mutation Research-Genetic Toxicology and Environmental Mutagenesis*, 626(1-2), 53-60. doi: <http://dx.doi.org/10.1016/j.mrgentox.2006.08.002>
- American Public Health Association, A. (1992). *Standard Methods for the Examination of Water and Wastewater* (18th ed.). Washington, DC: American Water Works Association and Water Environment Federation.
- Armbruster, D.A., & Pry, T. (2008). Limit of Blank, Limit of Detection and Limit of Quantitation. *The Clinical Biochemist Reviews*, 29(Suppl 1), S49-S52.
- Armin, A., Soltanolkotabi, M., & Feizollah, P. (2011). On the pH and concentration response of an evanescent field absorption sensor using a coiled-shape plastic optical fiber. *Sensors and Actuators A: Physical*, 165(2), 181-184. doi: <http://dx.doi.org/10.1016/j.sna.2010.10.006>
- Atadashi, I.M., Aroua, M.K., Abdul Aziz, A.R., & Sulaiman, N.M.N. (2012). High quality biodiesel obtained through membrane technology. *Journal of Membrane Science*, 421-422(0), 154-164. doi: <http://dx.doi.org/10.1016/j.memsci.2012.07.006>
- Baroutian, S., Aroua, M.K., Raman, A.A.A., & Sulaiman, N.M.N. (2011). A packed bed membrane reactor for production of biodiesel using activated carbon supported catalyst. *Bioresource Technology*, 102(2), 1095-1102. doi: <http://dx.doi.org/10.1016/j.biortech.2010.08.076>
- Batimalay, M., Harith, Z., Rafaie, H.A., Ahmad, F., Khasanah, M., Harun, S.W., . . . Ahmad, H. (2014). Tapered plastic optical fiber coated with ZnO nanostructures for the measurement of uric acid concentrations and changes in relative humidity. *Sensors and Actuators A: Physical*, 210(0), 190-196. doi: <http://dx.doi.org/10.1016/j.sna.2014.01.035>
- Batimalay, M., Rahman, H.A., Kam, W., Ong, Y.S., Ahmad, F., Zakaria, R., . . . Ahmad, H. (2014). Evaluation of the tapered PMMA fiber sensor response due to the ionic interaction within electrolytic solutions. *Journal of Modern Optics*, 61(2), 154-160. doi: 10.1080/09500340.2013.850541

- Beres, C., de Nazaré, F.V.B., de Souza, N.C.C., Miguel, M.A.L., & Werneck, M.M. (2011). Tapered plastic optical fiber-based biosensor – Tests and application. *Biosensors and Bioelectronics*, 30(1), 328-332. doi: <http://dx.doi.org/10.1016/j.bios.2011.09.024>
- Bilro, L., Alberto, N., Pinto, J.L., & Nogueira, R. (2012). Optical sensors based on plastic fibers. *Sensors*, 12, 12184-12207.
- Blanco, M., Canals, T., Coello, J., Gené, J., Iturriaga, H., & MasPOCH, S. (2000). Direct determination of leather dyes by visible reflectance spectroscopy using partial least-squares regression. *Analytica Chimica Acta*, 419(2), 209-214. doi: [http://dx.doi.org/10.1016/S0003-2670\(00\)00976-4](http://dx.doi.org/10.1016/S0003-2670(00)00976-4)
- Buerck, J., Roth, S., Kraemer, K., Scholz, M., & Klaas, N. (2001). Application of a fiber-optic NIR-EFA sensor system for in situ monitoring of aromatic hydrocarbons in contaminated groundwater. *Journal of Hazardous Materials*, 83(1–2), 11-28. doi: [http://dx.doi.org/10.1016/S0304-3894\(00\)00335-6](http://dx.doi.org/10.1016/S0304-3894(00)00335-6)
- Campbell, C.G., Laycak, D.T., Hoppes, W., Tran, N.T., & Shi, F.G. (2005). High concentration suspended sediment measurements using a continuous fiber optic in-stream transmissometer. *Journal of Hydrology*, 311(1–4), 244-253. doi: <http://dx.doi.org/10.1016/j.jhydrol.2005.01.026>
- Choi, H.Y., Kim, M.J., & Lee, B.H. (2007). All-fiber Mach-Zehnder type interferometers formed in photonic crystal fiber. *Optics Express*, 15(9), 5711-5720.
- D.O.E. (2012). *Malaysia Environmental Quality Report 2011*. Petaling Jaya, Malaysia: Strategic Communications Division.
- D.O.E. (2013). *Malaysia Environmental Quality Report 2012*. Petaling Jaya, Malaysia: Strategic Communications Division.
- De-Jun, F., Guan-Xiu, L., Xi-Lu, L., Ming-Shun, J., & Qing-Mei, S. (2014). Refractive index sensor based on plastic optical fiber with tapered structure. *Applied Optics*, 53(10), 2007-2011. doi: 10.1364/AO.53.002007
- Deboux, B.J.C., Lewis, E., Scully, P.J., & Edwards, R. (1995). A novel technique for optical fiber pH sensing based on methylene blue adsorption. *Journal of Lightwave Technology*, 13(7), 1407-1414. doi: 10.1109/50.400705
- Dong, X., Su, L., Shum, P., Chung, Y., & Chan, C.C. (2006). Wavelength-selective all-fiber filter based on a single long-period fiber grating and a misaligned splicing point. *Optics Communications*, 258(2), 159-163. doi: <http://dx.doi.org/10.1016/j.optcom.2005.07.075>
- El-Kashef, H. (2000). The necessary requirements imposed on polar dielectric laser dye solvents. *Physica B: Condensed Matter*, 279(4), 295-301. doi: [http://dx.doi.org/10.1016/S0921-4526\(99\)00856-X](http://dx.doi.org/10.1016/S0921-4526(99)00856-X)
- Elosua, C., Matias, I.R., Bariain, C., & Arregui, F.J. (2006). Volatile Organic Compound Optical Fiber Sensors: A Review. *Sensors*, 6, 1440-1465.

- Farahi, F., Webb, D.J., Jones, J.D.C., & Jackson, D.A. (1990). Simultaneous measurement of temperature and strain: cross-sensitivity considerations. *Journal of Lightwave Technology*, 8(2), 138-142. doi: 10.1109/50.47862
- Fogg, E.T., Hixson, A.N., & Thompson, A.R. (1955). Densities and Refractive Indexes for Ethylene Glycol-Water Solutions. *Analytical Chemistry*, 27(10), 1609-1611. doi: 10.1021/ac60106a033
- Garcia-Rubio, L.H. (1992). Refractive Index Effects on the Absorption Spectra of Macromolecules. *Macromolecules*, 25, 2608-2613.
- Gardner, J.D., Young, W., Sloan, S., Robinson, M., & Miner, P.B. (2006). The effects of changing temperature correction factors on measures of acidity calculated from gastric and oesophageal pH recordings. *Alimentary Pharmacology & Therapeutics*, 23(5), 629-638. doi: 10.1111/j.1365-2036.2006.02787.x
- Ghafari, S., Aziz, H.A., Isa, M.H., & Zinatizadeh, A.A. (2009). Application of response surface methodology (RSM) to optimize coagulation–flocculation treatment of leachate using poly-aluminum chloride (PAC) and alum. *Journal of Hazardous Materials*, 163(2–3), 650-656. doi: http://dx.doi.org/10.1016/j.jhazmat.2008.07.090
- Ghafari, S., Hasan, M., & Aroua, M.K. (2009). Nitrate remediation in a novel upflow bio-electrochemical reactor (UBER) using palm shell activated carbon as cathode material. *Electrochimica Acta*, 54(17), 4164-4171. doi: http://dx.doi.org/10.1016/j.electacta.2009.02.062
- Ghatak, A., & Thyagarajan, K. (2004). *Introduction to Fiber Optics*. Cambridge, United Kingdom: Cambridge University Press.
- Ghose, D.K., Panda, S.S., & Swain, P.C. (2013). Prediction and optimization of runoff via ANFIS and GA. *Alexandria Engineering Journal*, 52(2), 209-220. doi: http://dx.doi.org/10.1016/j.aej.2013.01.001
- Gong, Y., Yu, C.-B., Wang, T.-T., Liu, X.-P., Wu, Y., Rao, Y.-J., . . . Peng, G.-D. (2014). Highly sensitive force sensor based on optical microfiber asymmetrical Fabry-Perot interferometer. *Optics Express*, 22(3), 3578-3584.
- Gouveia, C., Chesini, G., Cordeiro, C.M.B., Baptista, J.M., & Jorge, P.A.S. (2013). Simultaneous measurement of refractive index and temperature using multimode interference inside a high birefringence fiber loop mirror. *Sensors and Actuators B: Chemical*, 177, 717-723. doi: http://dx.doi.org/10.1016/j.snb.2012.11.095
- Grattan, K.T.V., & Sun, T. (2000). Fiber optic sensor technology: an overview. *Sensors and Actuators A: Physical*, 82(1–3), 40-61. doi: http://dx.doi.org/10.1016/S0924-4247(99)00368-4
- Gulbag, A., & Temurtas, F. (2006). A study on quantitative classification of binary gas mixture using neural networks and adaptive neuro-fuzzy inference systems. *Sensors and Actuators B: Chemical*, 115(1), 252-262. doi: http://dx.doi.org/10.1016/j.snb.2005.09.009

- Güneri, A.F., Ertay, T., & Yücel, A. (2011). An approach based on ANFIS input selection and modeling for supplier selection problem. *Expert Systems with Applications*, 38(12), 14907-14917. doi: <http://dx.doi.org/10.1016/j.eswa.2011.05.056>
- Guo, S., & Albin, S. (2003). Transmission property and evanescent wave absorption of cladded multimode fiber tapers. *Optics Express*, 11(3), 215-223.
- Guwy, A.J., Farley, L.A., Cunnah, P., Hawkes, F.R., Hawkes, D.L., Chase, M., & Buckland, H. (1999). An automated instrument for monitoring oxygen demand in polluted waters. *Water Research*, 33(14), 3142-3148. doi: [http://dx.doi.org/10.1016/S0043-1354\(99\)00202-X](http://dx.doi.org/10.1016/S0043-1354(99)00202-X)
- Hang-Zhou, Y., Xue-Guang, Q., Ali, M.M., Islam, M.R., & Kok-Sing, L. (2014). Optimized Tapered Optical Fiber for Ethanol (C₂H₅OH) Concentration Sensing. *Journal of Lightwave Technology*, 32(9), 1777-1783. doi: 10.1109/JLT.2014.2311175
- Harun, S.W., Jasim, A.A., Rahman, H.A., Muhammad, M.Z., & Ahmad, H. (2013). Micro-ball lensed fiber-based glucose sensor. *IEEE Sensors Journal*, 13(1), 348-350. doi: 10.1109/JSEN.2012.2215958
- Harun, S.W., Lim, K.S., Tio, C.K., Dimiyati, K., & Ahmad, H. (2013). Theoretical analysis and fabrication of tapered fiber. *Optik - International Journal for Light and Electron Optics*, 124(6), 538-543. doi: <http://dx.doi.org/10.1016/j.ijleo.2011.12.054>
- Helseth, L.E. (2012). Simultaneous measurements of absorption spectrum and refractive index in a microfluidic system. *Optics Express*, 20(4), 4653-4662. doi: 10.1364/OE.20.004653
- Hu, S., Zhao, Y., & Hu, H. (2014). Modeling and simulation of tapered fiber-optic oil concentration sensor using negative dielectrophoresis. *Sensors and Actuators B: Chemical*, 199, 70-75. doi: <http://dx.doi.org/10.1016/j.snb.2014.03.066>
- Inaloo, K.D., Naddafi, K., Mesdaghinia, R., Nasser, Nodehi, N., & Rahimi. (2011). Optimization of Operational Parameters For Decolorization and Degradation of C.I. Reactive Blue 29 By Ozone. *Iran. J. Environ. Health. Sci. Eng.*, 8(3), 227-234.
- J. Grochowski, M. Myśliwiec, P. Mikulic, W.J. Bock, & Śmietana, M. (2013). Temperature Cross-Sensitivity for Highly Refractive Index Sensitive Nanocoated Long-Period Gratings. *Acta Physica Polonica A*, 124(3), 421-424.
- Janunts, E.A., Babajanyan, A.J., Margaryan, N.L., & Nerkararyan, K.V. (2004). Opto-chemical sensor on the base of two-channel tapered waveguide. *Sensors and Actuators A: Physical*, 116(1), 91-94. doi: <http://dx.doi.org/10.1016/j.sna.2004.03.041>
- Jha, R., Villatoro, J., & Badenes, G. (2008). Ultrastable in reflection photonic crystal fiber modal interferometer for accurate refractive index sensing. *Applied Physics Letters*, 93(19), 191106. doi: <http://dx.doi.org/10.1063/1.3025576>

- Jinhua, Y., Zhang, A.P., Li-Yang, S., Jin-Fei, D., & Sailing, H. (2007). Simultaneous Measurement of Refractive Index and Temperature by Using Dual Long-Period Gratings With an Etching Process. *IEEE Sensors Journal*, 7(9), 1360-1361. doi: 10.1109/JSEN.2007.905037
- Kamikawachi, R.C., Abe, I., Paterno, A.S., Kalinowski, H.J., Muller, M., Pinto, J.L., & Fabris, J.L. (2008). Determination of thermo-optic coefficient in liquids with fiber Bragg grating refractometer. *Optics Communications*, 281(4), 621-625. doi: <http://dx.doi.org/10.1016/j.optcom.2007.10.023>
- Kao, C.M., Chou, M.S., Fang, W.L., Liu, B.W., & Huang, B.R. (2001). Regulating Colored Textile Wastewater By 3/31 Wavelength ADMI Methods In Taiwan. *Chemosphere*, 44(5), 1055-1063.
- Kao, K.C., & Hockham, G.A. (1966). Dielectric-fibre surface waveguides for optical frequencies. *IEEE Proceedings*, 133(3), 191-198.
- Kermani, B.G. (2007). Modeling oligonucleotide probes for SNP genotyping assays using an adaptive neuro-fuzzy inference system. *Sensors and Actuators B: Chemical*, 121(2), 462-468. doi: <http://dx.doi.org/10.1016/j.snb.2006.04.102>
- Khalil, S., Bansal, L., & El-Sherif, M. (2004). Intrinsic fiber optic chemical sensor for the detection of dimethyl methylphosphonate. *Optical Engineering*, 43(11), 2683-2688. doi: 10.1117/1.1786294
- Kim, Y.H., Park, S.J., Jeon, S.-W., Ju, S., Park, C.-S., Han, W.-T., & Lee, B.H. (2012). Thermo-optic coefficient measurement of liquids based on simultaneous temperature and refractive index sensing capability of a two-mode fiber interferometric probe. *Optics Express*, 20(21), 23744-23754. doi: 10.1364/OE.20.023744
- Kuang, K.S.C., Quek, S.T., & Maalej, M. (2008). Remote flood monitoring system based on plastic optical fibres and wireless motes. *Sensors and Actuators A: Physical*, 147(2), 449-455. doi: <http://dx.doi.org/10.1016/j.sna.2008.05.030>
- Latifi, H., Zibaii, M., Hosseini, S., & Jorge, P. (2012). Nonadiabatic tapered optical fiber for biosensor applications. *Photonic Sensors*, 2(4), 340-356. doi: 10.1007/s13320-012-0086-z
- Latifi, H., Zibaii, M.I., Hosseini, S.M., & Jorge, P. (2012). Nonadiabatic Tapered Optical Fiber for Biosensor Applications. *Photonic Sensors*, 2(4), 340-356.
- Layeghi, A., Latifi, H., & Frazao, O. (2014). Magnetic Field Sensor Based on Nonadiabatic Tapered Optical Fiber With Magnetic Fluid. *IEEE Photonics Technology Letters*, 26(19), 1904-1907. doi: 10.1109/LPT.2014.2341662
- Lee, B.H., Kim, Y.H., Park, K.S., Eom, J.B., Kim, M.J., Rho, B.S., & Choi, H.Y. (2012). Interferometric fiber optic sensors. *Sensors*, 12, 2467-2486.
- Lim, K.-S., Aryanfar, I., Chong, W.-Y., Cheong, Y.-K., Harun, S.W., & Ahmad, H. (2012). Integrated microfibre device for refractive index and temperature sensing. *Sensors*, 12, 11782-11789.

- Loock, H.-P., & Wentzell, P.D. (2012). Detection limits of chemical sensors: Applications and misapplications. *Sensors and Actuators B: Chemical*, 173(0), 157-163. doi: <http://dx.doi.org/10.1016/j.snb.2012.06.071>
- Loukas, Y.L. (2001). Adaptive Neuro-Fuzzy Inference System: An Instant and Architecture-Free Predictor for Improved QSAR Studies. *Journal of Medicinal Chemistry*, 44(17), 2772-2783. doi: 10.1021/jm000226c
- Lu, W.-H., Chen, L.-W., Xie, W.-F., & Chen, Y.-C. (2012). A Sensing Element Based on a Bent and Elongated Grooved Polymer Optical Fiber. *Sensors*, 12, 7485-7495.
- Luna-Moreno, D., Monzon-Hernandez, D., Villatoro, J., & Badenes, G. (2007). Optical fiber hydrogen sensor based on core diameter mismatch and annealed Pd–Au thin films. *Sensors and Actuators B: Chemical*, 125(1), 66-71. doi: <http://dx.doi.org/10.1016/j.snb.2007.01.036>
- Lye, P.G., Boerkamp, M., Ernest, A., & Lamb, D.W. (2005). Investigating the sensitivity of PMMA optical fibres for use as an evanescent field absorption sensor in aqueous solutions. *Journal of Physics: Conference Series*, 15(1), 262.
- Lye, P.G., Boerkamp, M., Ernest, A., & Lamb, D.W. (2005). *Investigating the sensitivity of PMMA optical fibres for use as an evanescent field absorption sensor in aqueous solutions.*
- Merchant, D.F., Scully, P.J., & Schmitt, N.F. (1999). Chemical tapering of polymer optical fibre. *Sensors and Actuators A: Physical*, 76(1–3), 365-371. doi: [http://dx.doi.org/10.1016/S0924-4247\(99\)00008-4](http://dx.doi.org/10.1016/S0924-4247(99)00008-4)
- Minkovich, V.P., Monzón-Hernández, D., Villatoro, J., & Badenes, G. (2006). Microstructured optical fiber coated with thin films for gas and chemical sensing. *Optics Express*, 14(18), 8413-8418. doi: 10.1364/OE.14.008413
- Mook, W.T., Aroua, M.K., Chakrabarti, M.H., Low, C.T.J., Aravind, P.V., & Brandon, N.P. (2013). The application of nano-crystalline PbO₂ as an anode for the simultaneous bio-electrochemical denitrification and organic matter removal in an up-flow undivided reactor. *Electrochimica Acta*, 94(0), 327-335. doi: <http://dx.doi.org/10.1016/j.electacta.2013.02.001>
- Muhammad, M.Z., Jasim, A.A., Ahmad, H., Arof, H., & Harun, S.W. (2013). Non-adiabatic silica microfiber for strain and temperature sensors. *Sensors and Actuators A: Physical*, 192, 130-132.
- Nguyen, L.V., Hwang, D., Moon, S., Moon, D.S., & Chung, Y. (2008). High temperature fiber sensor with high sensitivity based on core diameter mismatch. *Optics Express*, 16(15), 11369-11375.
- Nolan, D.A., Blaszyk, P.E., & Udd, E. (1991). Optical Fibers. In E. Udd (Ed.), *Fiber Optic Sensors: An Introduction for Engineers and Scientists* (pp. 33). United States of America: John Wiley & Sons, Inc.

- Nosrati, S., Jayakumar, N.S., & Hashim, M.A. (2011). Extraction performance of chromium (VI) with emulsion liquid membrane by Cyanex 923 as carrier using response surface methodology. *Desalination*, 266(1-3), 286-290. doi: <http://dx.doi.org/10.1016/j.desal.2010.08.023>
- Ogita, M., Nagai, Y., Mehta, M.A., & Fujinami, T. (2000). Application of the adsorption effect of optical fibres for the determination of critical micelle concentration. *Sensors and Actuators B: Chemical*, 64, 147-151.
- Ohno, Y., & Hardis, J.E. (1997). Four-Color Matrix Method for Correction of Tristimulus Colorimeters [301-305].
- Paleologos, E.K., Prodromidis, M.I., Giokas, D.L., Pappas, A.C., & Karayannis, M.I. (2002). Highly selective spectrophotometric determination of trace cobalt and development of a reagentless fiber-optic sensor. *Analytica Chimica Acta*, 467(1-2), 205-215. doi: [http://dx.doi.org/10.1016/S0003-2670\(02\)00094-6](http://dx.doi.org/10.1016/S0003-2670(02)00094-6)
- Pelaez-Cid, A.-A., Blasco-Sancho, S., & Matysik, F.-M. (2008). Determination Of Textile Dyes By Means of Non-Aqueous Capillary Electrophoresis With Electrochemical Detection. *Talanta*, 75 1362-1368.
- Pereira, D.A., Frazão, O., & Santos, J.L. (2004). Fiber Bragg grating sensing system for simultaneous measurement of salinity and temperature. *Optical Engineering*, 43(2), 299-304. doi: 10.1117/1.1637903
- Peters, K. (2011a). Polymer Optical Fiber Sensors-A Review. *Smart Materials and Structures*, 20, 1-17.
- Peters, K. (2011b). Polymer optical fiber sensors: a review. *Smart Materials and Structures*, 20, 013002-013001-013017.
- Potyrailo, R.A., Hobbs, S.E., & Hieftje, G.M. (1998). Optical waveguide sensors in analytical chemistry: today's instrumentation, applications and trends for future development. *Fresenius' Journal of Analytical Chemistry*, 362(4), 349-373. doi: 10.1007/s002160051086
- Prakash Maran, J., Sivakumar, V., Thirugnanasambandham, K., & Sridhar, R. (2013). Artificial neural network and response surface methodology modeling in mass transfer parameters predictions during osmotic dehydration of Carica papaya L. *Alexandria Engineering Journal*, 52(3), 507-516. doi: <http://dx.doi.org/10.1016/j.aej.2013.06.007>
- Rahman, H.A., Harun, S.W., Yasin, M., Phang, S.W., Damanhuri, S.S.A., Arof, H., & Ahmad, H. (2011). Tapered plastic multimode fiber sensor for salinity detection. *Sensors and Actuators A: Physical*, 171(2), 219-222. doi: <http://dx.doi.org/10.1016/j.sna.2011.09.024>
- Rajendra, M., Jena, P.C., & Raheman, H. (2009). Prediction of optimized pretreatment process parameters for biodiesel production using ANN and GA. *Fuel*, 88(5), 868-875. doi: <http://dx.doi.org/10.1016/j.fuel.2008.12.008>

- Rezaeianzadeh, M., Tabari, H., Arabi Yazdi, A., Isik, S., & Kalin, L. (2014). Flood flow forecasting using ANN, ANFIS and regression models. *Neural Computing and Applications*, 25(1), 25-37. doi: 10.1007/s00521-013-1443-6
- Ribeiro, R.M., Canedo, J.L.P., Werneck, M.M., & Kawase, L.R. (2002). An evanescent-coupling plastic optical fibre refractometer and absorptionmeter based on surface light scattering. *Sensors and Actuators A: Physical*, 101(1-2), 69-76. doi: [http://dx.doi.org/10.1016/S0924-4247\(02\)00185-1](http://dx.doi.org/10.1016/S0924-4247(02)00185-1)
- Ronot-Trioli, C., Trouillet, A., Veillas, C., El-Shaikh, A., & Gagnaire, H. (1996). Fibre optic chemical sensor based on surface plasmon monochromatic excitation. *Analytica Chimica Acta*, 319(1-2), 121-127. doi: [http://dx.doi.org/10.1016/0003-2670\(95\)00494-7](http://dx.doi.org/10.1016/0003-2670(95)00494-7)
- Şahin, U., Ülgen, A., Kekeç, A., & Gökmen, A. (2004). Real-Time Monitoring of Indigo Concentrations in the Dye bath with a Laser Diode Spectrometer. *Textile Research Journal*, 74(3), 193-197. doi: 10.1177/004051750407400302
- Salceda-Delgado, G., Monzon-Hernandez, D., Martinez-Rios, A., Cardenas-Sevilla, G.A., & Villatoro, J. (2012). Optical microfiber mode interferometer for temperature-independent refractometric sensing. *Optics Letters*, 37(11), 1974-1976. doi: 10.1364/OL.37.001974
- Salmasnia, A., Baradaran kazemzadeh, R., & Mohajer Tabrizi, M. (2012). A novel approach for optimization of correlated multiple responses based on desirability function and fuzzy logics. *Neurocomputing*, 91(0), 56-66. doi: <http://dx.doi.org/10.1016/j.neucom.2012.03.001>
- Saratale, R.G., Saratale, G.D., Chang, J.S., & Govindwar, S.P. (2011). Bacterial decolorization and degradation of azo dyes: a review. *Journal of the Taiwan Institute of Chemical Engineers*, 42, 138-157.
- Singh, P., & Deo, M.C. (2007). Suitability of different neural networks in daily flow forecasting. *Applied Soft Computing*, 7(3), 968-978. doi: <http://dx.doi.org/10.1016/j.asoc.2006.05.003>
- Smietana, M., Bock, W.J., & Mikulic, P. (2011). Temperature sensitivity of silicon nitride nanocoated long-period gratings working in various surrounding media. *Measurement Science and Technology*, 22(11), 115203.
- Soldano, L.B., & Pennings, E.C.M. (1995). Optical multi-mode interference devices based on self-imaging : principles and applications. *Journal of Lightwave Technology*, 13(4), 615-627.
- Su, H., & Huang, X.G. (2007). Fresnel-reflection-based fiber sensor for on-line measurement of solute concentration in solutions. *Sensors and Actuators B: Chemical*, 126(2), 579-582. doi: <http://dx.doi.org/10.1016/j.snb.2007.04.008>
- Sun, H., Hu, M., Rong, Q., Du, Y., Yang, H., & Qiao, X. (2014). High sensitivity optical fiber temperature sensor based on the temperature cross-sensitivity feature of RI-sensitive device. *Optics Communications*, 323(0), 28-31. doi: <http://dx.doi.org/10.1016/j.optcom.2014.02.045>

- Tamunaidu, P., & Bhatia, S. (2007). Catalytic cracking of palm oil for the production of biofuels: Optimization studies. *Bioresource Technology*, 98(18), 3593-3601. doi: <http://dx.doi.org/10.1016/j.biortech.2006.11.028>
- Tan, C.-Y., & Huang, Y.-X. (2015). Dependence of Refractive Index on Concentration and Temperature in Electrolyte Solution, Polar Solution, Nonpolar Solution, and Protein Solution. *Journal of Chemical & Engineering Data*. doi: 10.1021/acs.jced.5b00018
- Thyagarajan, K., & Ghatak, A. (2007). *Fiber Optic Essentials*. New Jersey: John Wiley & Sons Inc.
- Tiryaki, S., & Aydın, A. (2014). An artificial neural network model for predicting compression strength of heat treated woods and comparison with a multiple linear regression model. *Construction and Building Materials*, 62(0), 102-108. doi: <http://dx.doi.org/10.1016/j.conbuildmat.2014.03.041>
- Trono, C., Baldini, F., Brenci, M., Chiavaioli, F., & Mugnaini, M. (2011). Flow cell for strain- and temperature-compensated refractive index measurements by means of cascaded optical fibre long period and Bragg gratings. *Measurement Science and Technology*, 22(7), 075204.
- Tsourveloudis, N. (2010). Predictive Modeling of the Ti6Al4V Alloy Surface Roughness. *Journal of Intelligent & Robotic Systems*, 60(3-4), 513-530. doi: 10.1007/s10846-010-9427-6
- Udd, E. (1995). An overview of fiber - optic sensors. *Review of Scientific Instruments*, 66(8), 4015-4030. doi: [doi:http://dx.doi.org/10.1063/1.1145411](http://dx.doi.org/10.1063/1.1145411)
- Udd, E., & Jr, W.B.S. (2011). *Fiber Optic Sensors: An Introduction For Engineers and Scientists* (2nd ed.). Singapore: John Wiley & Sons, Inc.
- Villatoro, J., Finazzi, V., Minkovich, V.P., Pruneri, V., & Badenes, G. (2007). Temperature-insensitive photonic crystal fiber interferometer for absolute strain sensing. *Applied Physics Letters*, 91(9), 091109. doi: [doi:http://dx.doi.org/10.1063/1.2775326](http://dx.doi.org/10.1063/1.2775326)
- Villatoro, J., & Monzon-Hernandez, D. (2006). Low-cost optical fiber refractive-index sensor based on core diameter mismatch. *Journal of Lightwave Technology*, 24(3), 1409-1413.
- Wang, Q., Farrell, G., & Yan, W. (2008). Investigation on single-mode-multimode-single-mode fiber structure. *Journal of Lightwave Technology*, 26(5), 512-519.
- Wen Bin, J., Huan Huan, L., Swee Chuan, T., Kin Kee, C., & Lim, A. (2012). Ultrahigh Sensitivity Refractive Index Sensor Based on Optical Microfiber. *IEEE Photonics Technology Letters*, 24(20), 1872-1874. doi: 10.1109/LPT.2012.2217738
- Wu, Q., Semenova, Y., Wang, P., & Farrell, G. (2011). High sensitivity SMS fiber structure based refractometer – analysis and experiment. *Optics Express*, 19(9), 7937-7944.

- Xiong, R., Meng, H., Yao, Q., Huang, B., Liu, Y., Xue, H., . . . Huang, X. (2014). Simultaneous Measurement of Refractive Index and Temperature Based on Modal Interference. *IEEE Sensors Journal*, 14(8), 2524-2528.
- Xu, B., Li, Y., Sun, M., Zhang, Z.-W., Dong, X.-Y., Zhang, Z.-X., & Jin, S.-Z. (2012). Acoustic vibration sensor based on nonadiabatic tapered fibers. *Optics Letters*, 37(22), 4768-4770. doi: 10.1364/OL.37.004768
- Yeo, T.L., Sun, T., & Grattan, K.T.V. (2008). Fibre-optic sensor technologies for humidity and moisture measurement. *Sensors and Actuators A: Physical*, 144, 280-295.
- Yilmaz, I., & Kaynar, O. (2011). Multiple regression, ANN (RBF, MLP) and ANFIS models for prediction of swell potential of clayey soils. *Expert Systems with Applications*, 38(5), 5958-5966. doi: <http://dx.doi.org/10.1016/j.eswa.2010.11.027>
- Yin, S., Ruffin, P.B., & Yu, F.T.S. (2008). *Fiber Optic Sensors* (2 ed.). Florida, United States: CRC Press.
- Zibaii, M.I., Latifi, H., Karami, M., Gholami, M., Hosseini, S.M., & Ghezelayagh, M.H. (2010). Non-adiabatic tapered optical fiber sensor for measuring the interaction between α -amino acids in aqueous carbohydrate solution. *Measurement Science and Technology*, 21, 105801 (105812pp).
- Zibaii, M.I., Latifi, H., Saeedian, Z., & Chenari, Z. (2014). Nonadiabatic tapered optical fiber sensor for measurement of antimicrobial activity of silver nanoparticles against *Escherichia coli*. *Journal of Photochemistry and Photobiology B: Biology*, 135, 55-64. doi: <http://dx.doi.org/10.1016/j.jphotobiol.2014.03.017>